12-16-2015

An Investigation of Autoxidation and DNA Thermal Cleavage by Polymethine Cyanine Dyes and Analogs in Aqueous Solutions

Ziyi Li
ziyi.lzy@gmail.com

AN INVESTIGATION OF AUTOXIDATION AND DNA THERMAL CLEAVAGE BY POLYMETHINE CYANINE DYES AND ANALOGS IN AQUEOUS SOLUTIONS

by

ZIYI LI

Under the Direction of Kathryn B. Grant, Ph.D.

ABSTRACT

Studies on a series of polymethine cyanine dyes and analogs (**1**-**24**) show that certain near-infrared cyanines are capable of damaging DNA in the absence of light and external reducing agents. Experimental results imply that in this DNA thermal cleavage, the cyanine reduces Cu(II) to Cu(I) which reacts with O_2 to generate the reactive oxygen species (ROS) $O_2^{\cdot-}$ and ·OH. The formation of these ROS is also thought to be responsible for the irreversible bleaching of the dyes in aqueous solutions. A correlation between structural features and DNA thermal cleavage activity as well as dye bleaching is suggested. Long polymethine chains appear to confer instability to cyanines in aqueous solutions and further contribute to undesired thermal DNA cleavage. These drawbacks can be overcome by introducing an electron-withdrawing group to the polymethine bridge of the cyanine dye.

INDEX WORDS: Dark cleavage, Bleaching, Reactive oxygen species, Gel electrophoresis, UV-visible spectroscopy, Colorimetric assay

AN INVESTIGATION OF AUTOXIDATION AND DNA THERMAL CLEAVAGE BY POLYMETHINE CYANINE DYES AND ANALOGS IN AQUEOUS SOLUTIONS

by

ZIYI LI

A Thesis Submitted in Partial Fulfillment of the Requirements for the Degree of

Master of Science

in the College of Arts and Sciences

Georgia State University

2015

AN INVESTIGATION OF AUTOXIDATION AND DNA THERMAL CLEAVAGE BY POLYMETHINE CYANINE DYES AND ANALOGS IN AQUEOUS SOLUTIONS

by

ZIYI LI

Committee Chair: Kathryn B. Grant

Committee: Maged Henary

W. David Wilson

Electronic Version Approved:

Office of Graduate Studies

College of Arts and Sciences

Georgia State University

December 2015

DEDICATION

I dedicate this thesis to my dear mother. It is impossible to thank you adequately for your unending love and all the sacrifices. I love you with all of my heart.

To my aunt and my cousin who have tolerated my selfishness and supported me all the times.

ACKNOWLEDGEMENTS

I would like to acknowledge my advisor Dr. Kathryn B. Grant. Thank you for accepting me to your lab, and your patience, advice, and guidance during these two and a half years. I feel so lucky to have worked for you.

I would like to thank my committee members, Dr. Maged Henary and Dr. W. David Wilson, for their time and attention. Thank Dr. Siming Wang and Dr. Zhenming Du for helping me with MS and NMR respectively.

I would like to thank my lab mates, Cory, and Eduardo, it was a pleasure to meet and work with you all. To Dominique and Khoa, thank you for your help, patience, and advice regarding experiments when I was new to this lab, thank you for teaching me to love this lab. To Sadegh, thank you for your generous help and all the happy, funny chats, thank you for being a nice and positive individual who always brightened a gray day. I hope our foodie adventure with Zahra, Christina, and Chris will continue. To Cory, thank you for your kindness and help, and being always interested in discussing research with me, thank you for reviewing my thesis writing. To Andy and Sarah, thank you for correcting my terrible grammatical errors.

I would like to thank my wonderful family, my mother, aunt, and cousin, thank you for your love, support, and understanding. I would never have gotten to where I am without you.

TABLE OF CONTENTS

ACKNOWLEDGEMENTS ..... **v**

LIST OF TABLES ..... **ix**

LIST OF FIGURES ..... **x**

1 INTRODUCTION **1**

1.1 Polymethine Cyanine Dyes **1**

1.1.1 DNA binding modes ***2***

1.1.2 Aggregation and photostability ***3***

1.1.3 Photodynamic therapy ***4***

1.1.4 Reactive oxygen species (ROS) generation and toxicity ***5***

1.2 Cyanine Dyes of Interest and Thesis Summary **7**

2 EXPERIMENTAL **11**

2.1 Materials **11**

2.2 Instruments **12**

2.3 Methods **13**

2.3.1 Photocleavage of supercoiled plasmid DNA ***13***

2.3.2 Thermal cleavage of supercoiled plasmid DNA ***13***

2.3.3 Colorimetric detection of copper(I) ***14***

2.3.4 Thermal denaturation of calf thymus DNA experiments ***15***

2.3.5 Ethidium bromide displacement assay ***15***

2.3.6 Reagent-induced changes in DNA thermal cleavage 16

2.3.7 Enzymatic religation 17

2.3.8 UV-visible absorption monitoring 17

2.3.9 Mass spectrometry analysis 18

3 RESULTS AND DISCUSSION 18

3.1 PUC19 Plasmid DNA Cleavage Analysis of Cyanine Dye 1 18

3.1.1 DNA photocleavage 18

3.1.2 Temperature-dependent dark cleavage 19

3.1.3 Time course thermal cleavage 20

3.1.4 Evaluating metal ion and iodide anion involvement in DNA thermal cleavage 22

3.2 Colorimetric Detection of Copper(I) 24

3.3 Reagent-Induced Changes in DNA Thermal Cleavage 26

3.4 T4 Ligation Experiment 27

3.5 DNA Thermal Denaturation Experiments 30

3.6 UV-Visible Absorption Analysis of Cyanine Dye 1 31

3.6.1 Time course UV-visible absorption study 31

3.6.2 UV-visible absorption titration 33

3.6.3 H- and J-aggregation study 34

3.6.4 Time course UV-visible absorption in the presence of chemical reagents . 36

3.7 Mass Spectrometry Study of Bleaching 40

3.8 Preliminary Investigation of Cyanine Dye Analogs 42

3.8.1 Time course UV-visible absorption 42

3.8.2 DNA thermal cleavage activity study 43

3.9 Thermal Cleavage Activity Study of Initial versus Bleached Compounds .. 47

3.9.1 DNA thermal cleavage by initial vs. bleached compounds 47

3.9.2 Colorimetric detection of copper(I) 48

3.9.3 Competitive DNA binding assay 49

3.10 Studies of High versus Low Thermal Cleavage Dyes 53

3.10.1 Colorimetric detection of copper(I) 54

3.10.2 Competitive DNA binding assay 55

3.10.3 DNA thermal cleavage of dyes 20 and 3 in the presence of Cu(II) 56

4 CONCLUSIONS 58

REFERENCES 61

APPENDICES 66

Supplementary data 66

LIST OF TABLES

Table 3.1 Percent inhibition of DNA thermal cleavage by ROS scavengers, D_2O, and EDTA 26

LIST OF FIGURES

Figure 1.1 Generic structure of cyanine dyes 2

Figure 1.2 A proposed ROS-mediated degradation process of cyanine dyes..... 4

Figure 1.3 The mechanism of ·OH generation through the Fenton reaction 5

Figure 1.4 Hypothetical Cu(I)-involved generation route of $O_2^{\cdot-}$ and ·OH in the dark..... 6

Figure 1.5 The structure of pentamethine cyanine dye ESS-16 (**1**)..... 8

Figure 1.6 Structures of pentamethine cyanine dyes with benzo[*e*]indolium ring systems (**2-7**)..... 9

Figure 1.7 Structures of polymethine cyanine dyes with phenanthridinium ring systems (**8-10**)..... 9

Figure 1.8 Structures of trimethine cyanine dyes with quinolinium ring systems (**11-12**) 9

Figure 1.9 Structures of pentamethine cyanine dyes with quinolinium ring systems (**16-19**) 10

Figure 1.10 Structures of phenanthridine derivatives with different counter anions (**20-21**) 10

Figure 1.11 The structure of a heptamethine cyanine dye with indolium ring systems (**22**) 10

Figure 1.12 Structures of phenanthridine derivatives (**23-24**)..... 10

Figure 3.1 A photograph of a 1.5 % non-denaturing agarose gel showing DNA photocleavage by cyanine **1** under 765 nm irradiation 19

Figure 3.2 A photograph of a 1.5 % non-denaturing agarose gel showing DNA thermal cleavage by cyanine **1** at 4 ℃ or 37 ℃..... 20

Figure 3.3 Photographs of 1.5 % non-denaturing agarose gels showing DNA thermal cleavage by cyanine **1** in time course at 37 ℃ 21

Figure 3.4 A 1.5 % non-denaturing agarose gel **A)** and corresponding histogram **B)** showing DNA thermal cleavage by cyanine **1** in the presence of metal ions at 37 ℃ for 24 h.... 23

Figure 3.5 A 1.5 % non-denaturing agarose gel **A)** and corresponding histogram **B)** showing DNA thermal cleavage by dye **1** in the presence of Cu^{2+} and/or I^- at 37 ℃ for 24 h..... 24

Figure 3.6 UV-visible absorption spectra to monitor Cu(I)-BCS complex formation by dye **1** 25

Figure 3.7 A 1.5 % non-denaturing agarose gel **A)** and corresponding histogram **B)** showing DNA thermal cleavage by dye **1** at 37 ℃ for 29 h 29

Figure 3.8 Time course UV-visible absorption spectra of cyanine **1** 32

Figure 3.9 Time course UV-visible absorption spectra of dye **1** in the presence of CT DNA 33

Figure 3.10 UV-visible absorption spectra showing binding-induced changes by dye **1**. 34

Figure 3.11 UV-visible absorption spectra of dye **1** in methanol/buffer solutions..... 36

Figure 3.12 Proposed mechanisms causing photofading of dyes (ISC: intersystem crossing) 37

Figure 3.13 Hypothetical mechanism causing bleaching of dyes in the dark..... 38

Figure 3.14 Comparisons of reagent-induced effects on bleaching rates of cyanine dye **1** 39

Figure 3.15 Hypothetic decomposed products of cyanine dye **1** 42

Figure 3.16 A 1.5 % non-denaturing agarose gel **A)** and corresponding histogram **B)** showing percent DNA thermal cleavage by fourteen cyanine analogs at 37 ℃ for 24 h 44

Figure 3.17 A 1.5 % non-denaturing agarose gel **A)** and corresponding histogram **B)** showing percent DNA thermal cleavage by eight cyanine analogs at 37 ℃ for 24 h 45

Figure 3.18 A 1.5 % non-denaturing agarose gel **A)** and corresponding histogram **B)** showing percent DNA thermal cleavage by initial and bleached cyanines **1**, **9**, **13**, and **16** at 37 ℃ for 24 h 48

Figure 3.19 UV-visible absorption spectra to monitor Cu(I)-BCS complex formation by initial vs. bleached compounds 49

Figure 3.20 Line charts showing concentration course ethidium bromide displacement study of initial and bleached compounds. 51

Figure 3.21 A histogram comparing percent ethidium replacement of initial and bleached dyes **1**, **9**, **13**, and **16** at 50 μM 53

Figure 3.22 UV-visible absorption spectra to monitor Cu(I)-BCS complex formation by compounds **20** and **3** 55

Figure 3.23 Percent ethidium replacement of six unbleached dyes 56

Figure 3.24 A 1.5 % non-denaturing agarose gel **A)** and corresponding histogram **B)** showing percent DNA thermal cleavage by **20** or **3** in the absence or presence of Cu(II) at 37 ℃ for 24 h 57

1 INTRODUCTION

1.1 Polymethine Cyanine Dyes

Cyanine dyes were first synthesized by Greville Williams nearly 160 years ago. Though displaying a variety of colors, cyanines were not suitable for general dyeing purposes because of their tendency to discolor upon exposure to light and acid. Instead, they were primarily used in silver halide photography to broaden the range of sensitive wavelengths of panchromatic emulsions. Other applications for cyanine dyes include their use in laser materials, absorbers of solar energy, photo-stimulators of polymer synthesis, and optical recording media.[1] More recently, thanks to the development of stabilizers, the archival lifetimes of cyanine optical disks (CD-R and DVD-R media) have been extended to 75 years or more.[1a] One of the most promising current applications of cyanines is found in the biomedical field as fluorescent probes for biomolecular labeling and imaging, and as photosensitizers in photodynamic therapy.[1a, 2]

The typical structure of a cyanine consists of two terminal heterocyclic ring systems linked by a polymethine bridge (Figure 1.1). Common heterocycles include indole, quinoline, benzoxazole, and benzothiazole.[3] Since the bridge contains an odd number of carbons, the positive charge is delocalized over the two nitrogen atoms *via* conjugation. As cations, cyanines are normally synthesized as halide or perchlorate salts.[1a] The physical and chemical properties of cyanines can be optimized through structural modification. Research mainly focuses on altering the substituents on polymethine chains, aromatic rings, and the scaffold,[2a] in order to improve stability and solubility in water solutions, to reduce aggregation, and more importantly, to bathochromically shift absorption maxima for optimum light penetration through biological tissues.[4]

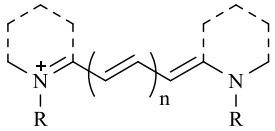

Generic cyanine dye

Figure 1.1 Generic structure of cyanine dyes

R refers to substituents, mainly alkyl groups.

1.1.1 DNA binding modes

The structural features of cyanine dyes enable them to bind with the DNA helix. Depending on the precise structure, dyes can interact with DNA *via* three major binding modes: intercalative, groove, and/or external binding. Primarily, cationic ligands approach the negatively charged phosphodiester groups along DNA backbone through electrostatic attraction. For intercalators, ligands slide planar aromatic components in between the hydrophobic area of the DNA base pairs through π-π stacking effects. To accommodate the insertion, the bases have to have a separation as wide as 3.4 Å, *i.e.* the van der Waals thickness of an aromatic ring. Subsequently, local DNA backbone unwinds to tolerate the base-pair separation, and the perturbation propagates and cumulates throughout the DNA helix. Well-studied drugs in this category include ethidium bromide, acridine orange, and methylene blue.[3, 5] It is more often to find large biomolecules, like protein, than small molecules binding within the major groove.[3] Minor groove binding, on the other hand, requires a certain degree of torsional freedom. Ligands that adopt this binding mode are usually composed of simple aromatic rings connected by flexible bonds. This enables ligands to twist and insert following the curve of the groove on the double helix, and maximizes van der Waals contacts. Therefore, groove binders pose less distortion to DNA compared to intercalators. Classic examples are netropsin and distamycin which possess favorable crescent molecular shape.[3, 5] Armitage has summarized that a positive

charge, curvature, flexibility, and hydrogen bond donors and acceptors are the four critical structural characteristics for a minor groove binder.[3]

1.1.2 Aggregation and photostability

It is well recognized that cyanine dyes are subject to self-aggregation in polar solutions, which plays an important role in their usage as fluorescent probes. This propensity strengthens as the polymethine bridge extends, because of the increasing hydrophobicity and polarizability.[3] The tilting degree of the dye stacking is described by the molecular slippage angle (α). It equals to the angle from the horizontal line to the axis through the center of the monomer column. Depending on the scale of slippage, two types of supramolecular arrangements can be formed, which are the ladder and the staircase arrays, namely *H*-aggregates and *J*-aggregates.[6] The precise aggregation type of a dye is determined by a variety of factors, such as the structure and concentration of the dye, and the polarity, pH value, and ionic strength of the solvent.[6a] Nevertheless, Armitage pointed out that unsubstituted dyes lean to *H*-aggregation for greater π-π stacking and minimum exposure to water molecules; whereas substituted dyes adopt *J*-aggregation to relieve steric resistance.[3]

Degradation is another complication for cyanine dyes with long polymethine linkers. Molecular oxygen and light are the two vital factors contributing to the decomposition. Studies show that cyanine dyes are bleached upon redox reactions with singlet oxygen ($^1O_2$) and/or superoxide anions ($O_2^{\cdot-}$).[7] It was found that the α- and γ-carbon (C_α and C_γ) to the positively charged nitrogen on the terminal ring is relatively electron-deficient and thus liable to the nucleophilic attack by reactive oxygen species (ROS).[8] Oushiki *et al.* have studied the photobleaching of two commercially available cyanine dyes (Cy5 and Cy7) by ROS, including $\cdot OH$, $O_2^{\cdot-}$, and H_2O_2, in phosphate buffer (pH 7.4) similar to our experimental condition. They

observed higher susceptibility of Cy7 with longer methine linker than Cy5. The mechanism of photodegradation was inferred to involve one-electron oxidation of the C_α-C_β bond by ROS followed by a breakup of the polymethine bridge.[9] The major products of the reaction were suggested to be ketone and/or aldehyde species (Figure 1.2).[9-10] It is worth pointing out that Oushiki and coworkers found attaching a strong electron-withdrawing group onto the terminal ring systems of the cyanine dye notably suppressed its reactivity with ROS.[9] A review paper written by Henary and Mojzych has summarized approaches that have been used to improve the stability of cyanine dyes based on introducing rigidity and steric protection to the molecules. For instance, one of the representative ways to stabilize a cyanine dye with a methine chain that is seven carbons or longer is to incorporate part of the bridge into a ring.[7]

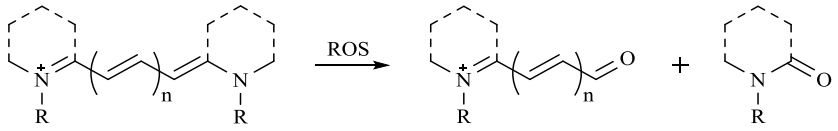

Figure 1.2 A proposed ROS-mediated degradation process of cyanine dyes

1.1.3 Photodynamic therapy

Photodynamic therapy (PDT) is an emerging non-invasive cancer treatment founded on the investigation of natural or synthetic photosensitizing agents. It is currently applied to cure age-related macular degeneration, pre-cancerous conditions, and localized cancers for which surgery is not an option.[4a] During the PDT process, a photosensitizer (PS) is either delivered directly to target tissue or introduced systemically to the human body. Upon light exposure, PS is activated from ground state (^{1}PS) to excited singlet state (^{1}PS*) which rapidly undergoes intersystem crossing (ISC) to a long-lived excited triplet state (^{3}PS*). ^{3}PS* reacts with molecular oxygen and generates reactive oxygen species (ROS) *via* energy or electron transfer.[4a] Due to the *in vivo* background interference from water, hemoglobin, and other endogenous chromophores,

an ideal PDT agent will absorb light within an "optical window" ranging from 700 to 1200 nm for maximum light penetration in biological tissue.[4] Therefore, near-infrared (NIR) polymethine cyanine dyes strongly appeal to clinical PDT drug development for their favorable photophysical properties. Particularly, the absorption maxima of cyanines are related to the length of the central methine chains. With every methylene unit extension, the excitation and emission maxima shift bathochromically by approximately 100 nm. However, this is at the cost of stability in aqueous solutions as discussed above.[2a]

1.1.4 Reactive oxygen species (ROS) generation and toxicity

In PDT process, there are two typical pathways to generate reactive oxygen species (ROS) by photosensitizers. During Type I reaction, ^{3}PS* conducts one-electron transfer to ground state molecular oxygen ($^3O_2$) yielding superoxide anion radicals ($O_2^{\cdot-}$). The product undergoes spontaneous dismutation to form hydrogen peroxide (H_2O_2) which further reacts with redox active metal ions, such as Fe(II) and Cu(I), and produces hydroxyl radicals (·OH) through the Fenton-type reaction (Figure 1.3).[4a, 11] In Type II photosensitization process, singlet oxygen ($^1O_2$) is formed upon energy transfer from ^{3}PS* to $^3O_2$. Although both pathways are applicable to ^{1}PS*, reactions with ^{3}PS* are more efficient.[4a, 11b] More importantly, the diffusion distances of $^1O_2$ and ·OH are exceedingly limited by their short lifetimes, which promises highly localized photo-oxidative damage to target tissues.[12]

$$^3PS^* + {}^3O_2 \rightarrow {}^3PS^{*+} + O_2^{\cdot-}$$

$$Fe^{3+} + O_2^{\cdot-} \rightarrow Fe^{2+} + {}^3O_2$$

$$2O_2^{\cdot-} + 2H^+ \rightarrow H_2O_2 + {}^3O_2$$

$$Fe^{2+} + H_2O_2 \rightarrow Fe^{3+} + \cdot OH + OH^- \quad \text{(Fenton reaction)}$$

Figure 1.3 The mechanism of ·OH generation through the Fenton reaction

Although very little attention has been paid to them, ground state one-electron reduction of $^3O_2$ in the absence of light is an alternative pathway to trigger Fenton-type reactions that subsequently produce ·OH. As Wood suggested, in order to initiate such a reductive step, an electron donor should have a similar or lower redox potential than E° [$O_2/O_2^{\cdot-}$] (-0.33 V at pH 7.0).[13] This implies possibilities of yielding $O_2^{\cdot-}$ from a redox reaction of $^3O_2$ either with an eligible dye directly or, more likely, with adventitious reduced metal ions (Cu(I) in our case) that are produced from the dye/metal ion electron transfer. Based on the findings discussed above, a mechanism of the $O_2^{\cdot-}$ and ·OH formation in the DNA thermal cleavage by NIR cyanine dyes is proposed. The process starts with the formation of Cu(I) from the dye/Cu(II) redox reaction. After that, Cu(I) reacts with $^3O_2$ and generates $O_2^{\cdot-}$ which undergoes the Fenton-type reaction to produce ·OH (Figure 1.4).[4a, 11a, 14]

$$\text{Dye} + Cu^{2+} \rightarrow \text{Dye}^+ + Cu^+$$

$$Cu^+ + {}^3O_2 \rightarrow Cu^{2+} + O_2^{\cdot-}$$

$$2O_2^{\cdot-} + 2H^+ \rightarrow H_2O_2 + {}^3O_2$$

$$Cu^+ + H_2O_2 \rightarrow Cu^{2+} + \cdot OH + OH^- \quad \text{(Fenton-type reaction)}$$

Figure 1.4 Hypothetical Cu(I)-involved generation route of $O_2^{\cdot-}$ and ·OH in the dark

As scientists continually expand the conjugated system to explore novel NIR cyanine dyes for clinical usage, concomitant problems like self-aggregation and decomposition may be raised. Moreover, our research reveals that this progress is even accompanied by another potential severe drawback, namely dark cleavage of nucleic acids which may be accomplished through the alternative pathway mentioned above. Herein, a series of experiments were conducted to identify the mechanism behind the phenomenon. This research would be important for understanding the relationship between the structures of cyanine dyes and their potential dark toxicity, and would provide basic guidelines for near-infrared PDT drug design.

1.2 Cyanine Dyes of Interest and Thesis Summary

With the aim to attain absorption maxima in far-red and near-IR light range, Dr. Maged Henary's lab (GSU) has synthesized twenty polymethine cyanine dyes and two chromophores from four heterocyclic families. Yet, considerable DNA cleavage by some of the cyanines in the absence of light and/or externally added metal ions or reducing agents was observed. To elucidate the mechanism of thermal DNA damage, several experimental techniques have been employed. In particular, UV-visible spectroscopy was utilized to monitor the stability of dyes in various solutions as a function of time. Gel electrophoresis of DNA reactions run under different conditions allowed one to evaluate and compare the thermal cleavage activity of the dyes. In addition, a colorimetric assay was performed to detect the production of Cu(I) when Cu(II) was added to the reactions. While scavenger experiments revealed the critical reactive oxygen species responsible for DNA damage, an ethidium bromide study assessed relative DNA binding affinity.

Since cyanine ESS-16 (**1**) displays distinct physical and chemical attributes of interest, it was studied in the majority of the experiments described in this thesis (Figure 1.5). Section 3.1 consists of a series of DNA cleavage experiments, from which it was discovered that the dark cleavage depends on time and temperature, and is likely to be copper-mediated. In the next four sections (3.2-3.5), the mechanism of thermal cleavage is explored by means of colorimetric detection, scavenger experiments, T4 religation, and DNA melting temperature assays. The results point to oxidative thermal cleavage involving the generation of hydroxyl radicals. Section 3.6 focuses on monitoring the absorbance of dye **1** in buffer solutions under a variety of conditions. It was found that the rigorous dye bleaching is associated with the formation of

reactive oxygen species and probably self-aggregation. In Section 3.7, mass spectroscopy was employed in the hope of determining dye decomposed product(s).

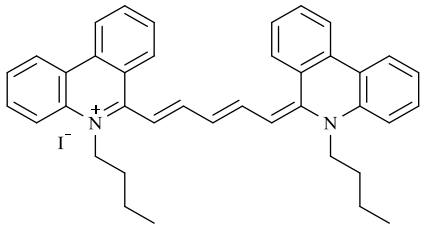

ESS-16 (**1**)

Figure 1.5 The structure of pentamethine cyanine dye ESS-16 (**1**)

In Section 3.8, four cyanine families with respective phenanthridinium, benzo[*e*]indolium, quinolinium, and indolium ring systems were analyzed. Within each family, the structures are varied in three aspects, including the length of the methine bridge, the substituent on the linker, and the ring system (Figures 1.6-1.9 and 1.11, **2-19** and **22**). The photocleavage property of sensitizers **2-7** was studied by Mapp *et al.*.[15] **20**, **21**, and two additional chromophores, 5-methyl-phenanthridine iodide (**23**) and ethidium bromide (**24**), obtained from commercial sources are for studying the thermal cleaving activity of the aryl component (Figure 1.10 and 1.12). The goal in this section was to find out the structural features conferring unwanted physical and chemical properties arising from thermal hydroxyl radical production by certain dyes.

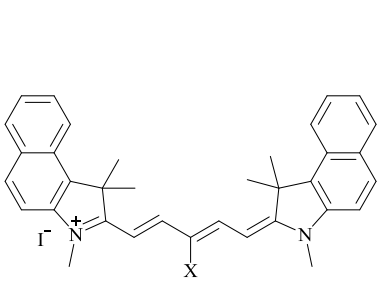

X = H LO-3 (**2**)
X = Cl E-36 (**3**)
X = Br LO-2 (**4**)

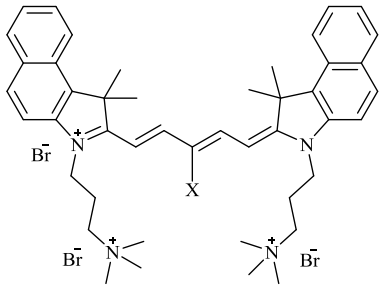

X = H E-70 (**5**)
X = Cl E-71 (**6**)
X = Br E-72 (**7**)

Figure 1.6 Structures of pentamethine cyanine dyes with benzo[*e*]indolium ring systems (**2-7**)

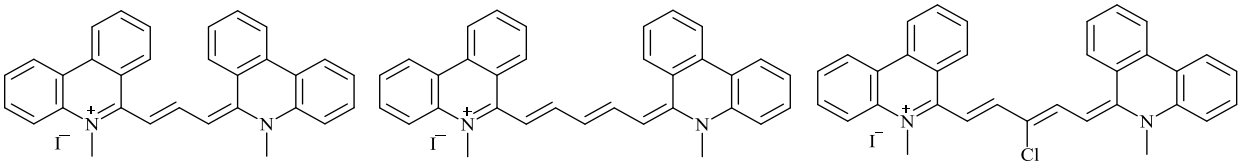

ESS-36 (**8**) ESS-23 (**9**) ESS-44 (**10**)

Figure 1.7 Structures of polymethine cyanine dyes with phenanthridinium ring systems (**8-10**)

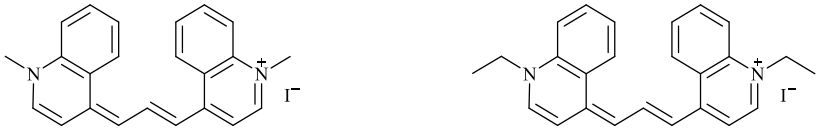

CMH-14 (**11**) CMH-16 (**12**)

Figure 1.8 Structures of trimethine cyanine dyes with quinolinium ring systems (**11-12**)

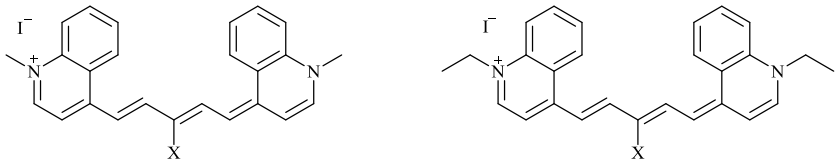

X = H BA-4 (**13**)
X = Cl ESS-2-3 (**14**)
X = Br ESS-2-4 (**15**)

X = H ESS-96 (**16**)
X = Cl ESS-100 (**17**)

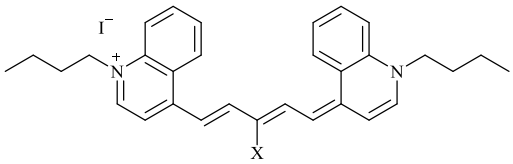

X = Cl ESS-2-11 (**18**)
X = Br ESS-2-12 (**19**)

Figure 1.9 Structures of pentamethine cyanine dyes with quinolinium ring systems (**16-19**)

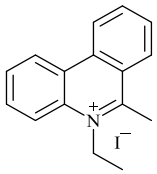

ESS-4 (**20**)

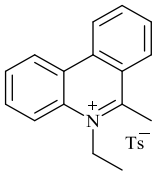

ESS-2-22 (**21**)

Figure 1.10 Structures of phenanthridine derivatives with different counter anions (**20-21**)

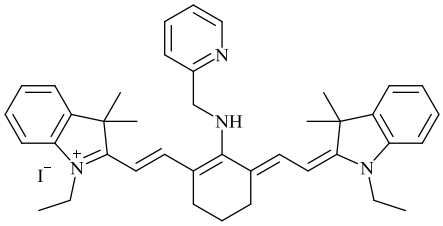

PS-142 (**22**)

Figure 1.11 The structure of a heptamethine cyanine dye with indolium ring systems (**22**)

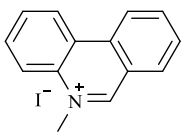

5-methyl-phenanthridinium iodide (**23**)

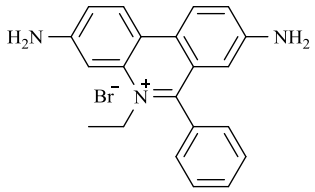

ethidium bromide (**24**)

Figure 1.12 Structures of phenanthridine derivatives (**23-24**)

The behavior of bleached cyanine dyes was examined in Section 3.9. To evaluate the changes in chemical properties upon bleaching, the dark DNA cleavage activity, the capability of reducing Cu(II), and the relative DNA binding propensity between intact and bleached compounds were compared. It was shown that pre-bleaching the cyanine dyes significantly reduced the levels of plasmid scission which was found to be related to a decrease in Cu(II) reduction and a loss of DNA binding affinity. The same research strategy was employed in Section 3.10. With respect to inactive compounds, lower Cu(II) reduction as well as DNA binding affinity were observed compared to highly active dyes. Overall, this investigation has opened up a unique research field of NIR cyanine dyes. Our data have given a preliminary explanation for the unusual activity in the absence of light and the rapid decomposition of the dyes in aqueous solutions. Vast observation suggests some structural modifications to eliminate or at least minimize these undesired properties. We hope that this report can provide information to optimize synthetic design of NIR photosensitizers with the goal of improving dye stability in aqueous solutions and decreasing potential toxic ROS production under dark conditions.

2 EXPERIMENTAL

2.1 Materials

Deionized, distilled water was used in the preparation of all the samples and buffer solutions. All stock chemicals were of the highest available purity and utilized without further purification unless noted. Calf thymus DNA (CT DNA) was obtained from Invitrogen (Cat. No. 15633-019, 10 mg/mL, average size ≥2,000 bp). Sodium phosphate dibasic and sodium phosphate monobasic came from Fisher Scientific (Fairlawn, NJ). Ethylenediaminetetraacetic acid disodium salt (EDTA, ≥99.0%) was purchased from IBI Scientific (Peosta, IA).

Tris(hydroxymethyl)aminomethane (tris base, >99.9%) was from Research Product International (Mt. Prospect, IL). All other chemicals including agarose, ethidium bromide (EtBr, **24**), dimethyl sulfoxide (DMSO, >99.9%), iron(III) chloride hexahydrate (≥99.999%), copper(II) chloride dihydrate (≥99.999%), potassium iodide (≥99.99%), sodium chloride (≥99.999%), sodium bromide (≥99.99%), sodium iodide (≥99.99%), *L*-ascorbic acid sodium salt, sodium azide (≥99.99%), sodium benzoate (99%), deuterium oxide (D_2O), bathocuproinedisulfonic acid (BCS) disodium salt hydrate, catalase from bovine liver, methanol (≥99.8%), and 5-methyl-phenanthridinium iodide (**23**) were purchased from Sigma-Aldrich (St. Louis, MO). T4 DNA ligase (Lot. No. 1091410, 2,000,000 cohesive end units/mL), 10× T4 DNA ligase reaction buffer (Lot. No. 0021501), and 100 bp DNA ladder (Cat. No. N3231L, 42, 500 μg/mL, prepared with restriction enzyme) were purchased from New England Biolabs (Ipswich, MA), while blue/orange 6× loading dye was from Promega (Madison, WI). Compounds **1**-**22** for this research were synthesized by Dr. Henary's group (Georgia State University, Atlanta, GA).

PUC19 plasmid DNA from transfected *E.coli* competent cells (Stratagene, XL-1 blue) was cloned in bacterial cultures following established literature protocols.[16] Purification was accomplished with a QIAfilter Plasmid Mega Kit (Qiagen™, Cat. No. 12263).

2.2 Instruments

The photocleavage reactions were carried out using 765-nm light emitting diodes (LEDs). The non-denaturing agarose gels were electrophoresed in a Wide Mini-sub® Cell GT electrophoresis box (Bio-Rad Laboratories). The temperatures for thermal cleavage reactions were maintained in a standard heat block (VWR Scientific). Gels were stained with ethidium bromide, visualized *via* a transilluminator (VWR Scientific, LM-20E) at 302 nm, and then photographed with a UVP PhotoDoc-It™ imaging system. UV-visible spectra were recorded with

a PerkinElmer Lambda 35 spectrophotometer, and the graphs were plotted using Microsoft Excel software. Gel Quantitative analysis was done by the ImageQuant 5.2 program. A Cary 300 Bio UV-visible spectrophotometer fitted with a Cary temperature controller was utilized for DNA melting temperature determination, while thermal melting curves were plotted with KaleidaGraph 4.0 software. The mass spectra were acquired on a Micromass Q-Tof micro mass spectrometer (MS) with electrospray ionization (ESI).

2.3 Methods

2.3.1 Photocleavage of supercoiled plasmid DNA

A quotient of a 40-μL reaction mixture contained 25 μM bp of pUC19 plasmid DNA in 10 mM sodium phosphate buffer and 0 μM or 10 μM of **1**. Samples were kept in the dark for 1 h at room temperature and then irradiated under 765-nm LEDs for 60 min. After adding 3 μL of electrophoresis loading buffer (15.0% (w/v) Ficoll, 0.025% (w/v) bromophenol blue), a total of 20 μL of each solution was loaded onto 1.5% non-denaturing agarose gels stained with ethidium bromide (0.5 μg/mL). Electrophoresis was carried out at 105 V in 1× TAE (tris-acetate-EDTA) running buffer for about 60 min. Gels were visualized on a transilluminator at 302 nm and photographed with the imaging system.

2.3.2 Thermal cleavage of supercoiled plasmid DNA

To obtain thermal cleavage by cyanine dyes, special black Eppendorf tubes were used to protect reactions from light. Sample transfer if needed was performed in a light-proof paper box. Gel electrophoresis was carried out in a black-walled hood.

In the temperature dependent experiment, 40-μL reactions containing 25 μM bp of pUC19 plasmid DNA in 10 mM sodium phosphate buffer and 0 μM or 10 μM of **1** were

equilibrated at 4 ℃ or 37 ℃ for 24 h. In time course experiments, sufficient amount of reaction solutions were prepared and kept in a 37 ℃ heat block. After every specific time period (hours or days), a 25-μL aliquot of the sample was transferred to another tube with 5 mM EDTA, and was frozen at -20 ℃ immediately in order to halt the reaction. After all the reaction products were collected, the resulting solutions were loaded onto one gel. In metal ion and iodide anion involvement studies, reaction mixtures (40 μL) containing 25 μM bp of pUC19 plasmid DNA in 10 mM sodium phosphate buffer and 0 μM or 10 μM of **1** in the absence or presence of $FeCl_3$, $CuCl_2$, or NaI were incubated at 37 ℃ for 24 h.

In thermal cleavage activity comparison experiments (initial versus bleached dyes), the solutions of bleached compounds were prepared by mixing dyes and sodium phosphate buffer in advance. When the solutions were bleached, 25 μM bp of pUC19 plasmid DNA was added to launch reactions. The experimental condition was 37 ℃ for 24 h.

Resulting solutions were resolved on 1.5% non-denaturing agarose gels as described above. For metal ion and iodide anion involvement, thermal cleavage activity comparison, and some other experiments, gels were quantitated with ImageQuant 5.2 software. Considering the lower binding affinity of ethidium bromide to supercoiled than nicked and linear plasmid forms, the data for supercoiled DNA were multiplied by a correction factor of 1.22. The thermal cleavage yields were calculated according to the following equation:

Percent DNA thermal cleavage (%) = [(nicked + linear DNA) / (linear + nicked + supercoiled DNA)] × 100

2.3.3 Colorimetric detection of copper(I)

A total volume of 600 μL solution was prepared for each sample. Individual tubes consisted of 10 mM sodium phosphate buffer (pH 7.0) and either (1) 30 μM of $CuCl_2$ and 30 μM

of NaI; (2) 30 μM of $CuCl_2$ and 10 μM of an initial or bleached compound; (3) 10 μM of an initial or bleached compound; (4) 30 μM of *L*-ascorbic acid; (5) 10 μM of **1** and 30 μM of *L*-ascorbic acid; (6) 25 μM bp of pUC19 plasmid DNA and 30 μM of *L*-ascorbic acid, or (7) 25 μM bp of pUC19 plasmid DNA and 30 μM of $CuCl_2$. The solutions of bleached compounds were made following the same procedures mentioned above. $CuCl_2$ was not added until the solutions became colorless. All the reactions were warmed in a heat block at 37 ℃ in the dark for 1 h. A positive control had 30 μM of $CuCl_2$ and one molar equivalent of *L*-ascorbic acid, while a negative control contained only the former. The reaction time was 15 min. Thereafter, 42 μM of bathocuproinedisulfornic acid (BCS) disodium salt hydrate was introduced and the systems were equilibrated in the dark for another 30 min at room temperature. The formation of Cu(I)-BCS complex (2:1) was monitored with a UV-visible spectrophotometer at 480 nm.

2.3.4 Thermal denaturation of calf thymus DNA experiments

Reference sample consisted of 10 mM sterilized sodium phosphate buffer (pH 7.0); whereas the other samples contained 25 μM bp of CT DNA in 10 mM sodium phosphate buffer (pH 7.0) in the presence of 0, 1.25, 2.5, 10, 20, 30, 40, or 45 μM compound **1**. 1000 μL of each solution were transferred to and equilibrated in a 1.5 mL Starna quartz cuvette at room temperature for 90 – 100 min. The absorbance at 260 nm was then recorded as a function of temperature from 25 to 95 ℃ at a heating rate of 0.5 ℃/min. The best fit curves for the first derivative of $\delta Abs_{260\ nm}/\delta T$ versus temperature were obtained through KaleidaGraph 4.0 software where the reflection points indicated the melting temperatures (T_m) of CT DNA.

2.3.5 Ethidium bromide displacement assay

To rule out the influence from light, special black Eppendorf tubes were utilized. Gel electrophoresis was carried out in a black-walled hood.

Bleached compound solutions were prepared as demonstrated above. In the concentration-titration assay, individual reactions with 0, 10, 50, or 75 μM of compound were equilibrated in the dark for 15 min, and then mixed with 3-μL electrophoresis loading buffer. A total of 20 μL of each reaction product was loaded onto 1.7% non-denaturing agarose gels without staining. Gels were electrophoresed at 80 V in 1× TAE running buffer for about 3 h 30 min in the absence of ethidium bromide. After that they were stained in 0.5 μg/mL concentrated ethidium bromide buffer for 30 min followed by 10- to 15-min de-staining in 1× TAE running buffer. In the DNA binding study of initial versus bleached compounds, similar experimentation was employed, except the duration of gel electrophoresis was reduced to 30 min, and the de-staining process was elongated to 30 min. The results were visualized on a transilluminator at 302 nm and photographed with the imaging system.

The gel images were quantitated with ImageQuant 5.2 software. The quantities of supercoiled DNA bands in the presence of dyes were individually compared with their corresponding negative controls to obtain percent ethidium replacement:

Percent ethidium replacement (%) = (volume of supercoiled DNA band $_{\text{with compound}}$ / volume of supercoiled DNA band $_{\text{without compound}}$) × 100

2.3.6 Reagent-induced changes in DNA thermal cleavage

Reactions (40 μL total volume) containing 25 μM bp of pUC19 plasmid DNA in 10 mM sodium phosphate buffer (pH 7.0) and 10 μM of **1** were incubated in a heat block at 37 ℃ for 24 h in the presence of one of the following reagents: 100 mM sodium benzoate, 50 mM potassium iodide, 4 μL DMSO, 100 mM sodium azide, 84% (v/v) D_2O, and 50 mM EDTA. A total of 20 μL of each sample was loaded onto 1.5% non-denaturing agarose gels stained with ethidium bromide (0.5 μg/mL). Gels were electrophoresed and visualized as described above. The

influence from light was eliminated by using special black Eppendorf tubes and running electrophoresis in a black-walled hood.

The results were quantitated with ImageQuant 5.2 software. Average % changes in thermal cleavage were acquired according to the following equation:

Percent thermal cleavage inhibition (%) = [(linear + nicked DNA $_{\text{without scavenger}}$) – (linear + nicked DNA $_{\text{with scavenger}}$)] / (linear + nicked DNA $_{\text{without scavenger}}$) × 100

2.3.7 Enzymatic religation

Samples were protected from light during the whole process. The reaction (40 μL) containing 25 μM bp of pUC19 plasmid DNA in 10 mM sterilized sodium phosphate buffer and 12.7 μM of **1** was incubated at 37 ℃ for 29 h to generate linearized pUC19 plasmid DNA. In the meanwhile, 25 μg/mL of 100 bp DNA ladder sample (40 μL) was prepared and allowed to equilibrate for 10-15 min at room temperature. Then the DNA ladder sample and the reaction solutions were treated with 2 μL of 10× T4 DNA ligase reaction buffer and 3.3 units/μL of T4 ligase, and incubated overnight at 4 ℃.[16] After adding 6-μL blue/orange 6× loading dye, a total of 20 μL of each solution was loaded onto a 1.5% non-denaturing agarose gel stained with ethidium bromide (0.5 μg/mL). The procedures of gel electrophoresis and quantitation were same as prior description.

2.3.8 UV-visible absorption monitoring

In the time course UV-visible spectra measurement, the absorbance of sample cuvettes was recorded by a UV-vis spectrophotometer at intervals of 10 to 30 min within the wavelength region from 1000 to 200 nm or 1100 to 200 nm up to 60 min or when the changes in absorbance were negligible. Each sample contained 10 μM of compound in either 10 mM sodium phosphate

buffer (pH 7.0) or DMSO in the absence or presence of CT DNA, $CuCl_2$, radical scavengers, or chelating agents.

In the *H*- and *J*-aggregation study, sample cuvettes were prepared by adding 10 μM cyanine dye **1** into a series of methanol-phosphate buffer solutions with different volume ratios. After 2-hour equilibration in the dark at room temperature, they were scanned sequentially.

2.3.9 Mass spectrometry analysis

Individual samples were respectively prepared with following components and experimental conditions: (1) 20 μM of **1** in ddH_2O was equilibrated for 2 h before mixing with methanol in a 1:1 volume ratio; (2) 10 μM of **1** in methanol; (3) 10 μM of **1** and 20 μM of Cu(II) were dissolved in chelexed ddH_2O and then mixed with ddH2O (0.1% formic acid) in the ratio of 2:1. Each solution (~5 μL) was injected into a Micromass Q-Tof micro mass spectrometer with a syringe. In the time course measurement, 10 μM of **1** in ACN was monitored first. After that, half of the sample was left in the transparent syringe for 60 min at room temperature, while the other half was stored in the dark. Mass spectra were acquired for both solutions. Lastly, the latter half was kept in the dark for a further testing two days later.

3 RESULTS AND DISCUSSION

3.1 PUC19 Plasmid DNA Cleavage Analysis of Cyanine Dye 1

3.1.1 DNA photocleavage

In spite of the potential for DNA photocleavage by cyanine dye **1** within the "optical window" of photodynamic cancer therapy (PDT), a significant amount of supercoiled DNA was damaged in dark control reactions in photocleavage experiments (Lane 4 in Figure 3.1). This abnormal situation was not ameliorated even when quencher (*e.g.* EDTA or EtBr) was added to

reactions to help minimize oxidation by ambient light during the electrophoresis process. The cleavage in the absence of light and/or reducing agents raises concern for dark toxicity of this cyanine dye family for *in vivo* applications. The study suggests that factors other than light have induced the unusual appearance of nicked plasmid DNA, and it is highly worthy to investigate the mechanism behind this.

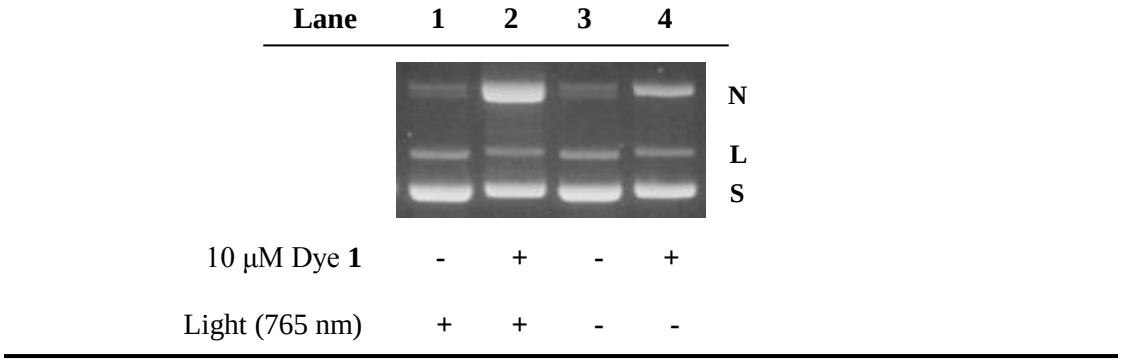

Figure 3.1 A photograph of a 1.5 % non-denaturing agarose gel showing DNA photocleavage by cyanine **1** under 765 nm irradiation

Samples contained 10 mM of sodium phosphate buffer (pH 7.0) and 25 μM bp of pUC19 plasmid DNA. Lanes 1 and 3: in the absence of **1**. Lanes 2 and 4: in the presence of 10 μM of **1**. Reactions in Lanes 1 and 2 were irradiated at 765 nm for 60 min. Reactions in Lanes 3 and 4 were kept in the dark for 60 min. Abbreviations: N = nicked; L = linear; S = supercoiled.

3.1.2 Temperature-dependent dark cleavage

It was speculated that heat was the primary exogenetic energy source of the dark reaction. Indeed, an experiment run at two distinct temperatures revealed that this dark cleavage by cyanine dye **1** is temperature-dependent. In Figure 3.2, an intense nicked DNA band is observed in reactions at 37 ℃ (Lane 4). Moreover, compared to the parallel control (Lane 1), cleavage was even triggered at a temperature as low as 4 ℃ without light exposure (Lane 2) suggesting that the reaction requires a very low activation energy.

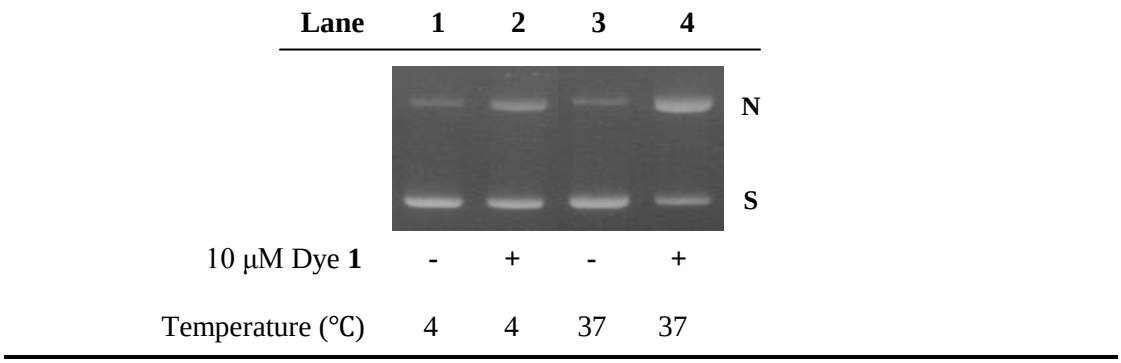

Figure 3.2 A photograph of a 1.5 % non-denaturing agarose gel showing DNA thermal cleavage by cyanine **1** at 4 ℃ or 37 ℃

Reactions were carried out in darkness. Samples contained 10 mM of sodium phosphate buffer (pH 7.0) and 25 μM bp of pUC19 plasmid DNA. Lanes 1 and 3: in the absence of **1**. Lanes 2 and 4: in the presence of 10 μM of **1**. Abbreviations: N = nicked; S = supercoiled.

3.1.3 Time course thermal cleavage

Considering that cyanine dyes have been extensively investigated for *in vivo* use as fluorescent probes and photosensitizers, it would be more meaningful to study their behavior at physiological temperature (37 ℃). Our previous experiments have shown that at this temperature, an appropriate amount of nicked DNA was generated by **1**. Thereafter, 37 ℃ was set as the reaction temperature for the following DNA thermal cleavage experiments.

Our next goal was to monitor the extent of DNA scission as a function of time. This was done in order to find an optimal reaction time for future mechanistic studies. Figure 3.3A illustrates continuous activity of cyanine dye **1** up to 24 hours at 37 ℃ in which large amounts of nicked and even linear plasmid were produced. Moreover, a gradual decrease in supercoiled plasmid was observed over four days (Figure 3.3B). Altogether, 24 hours seems to be the best reaction time for thermal cleavage activity evaluation because of its practical duration and the distinct DNA cleaving pattern produced.

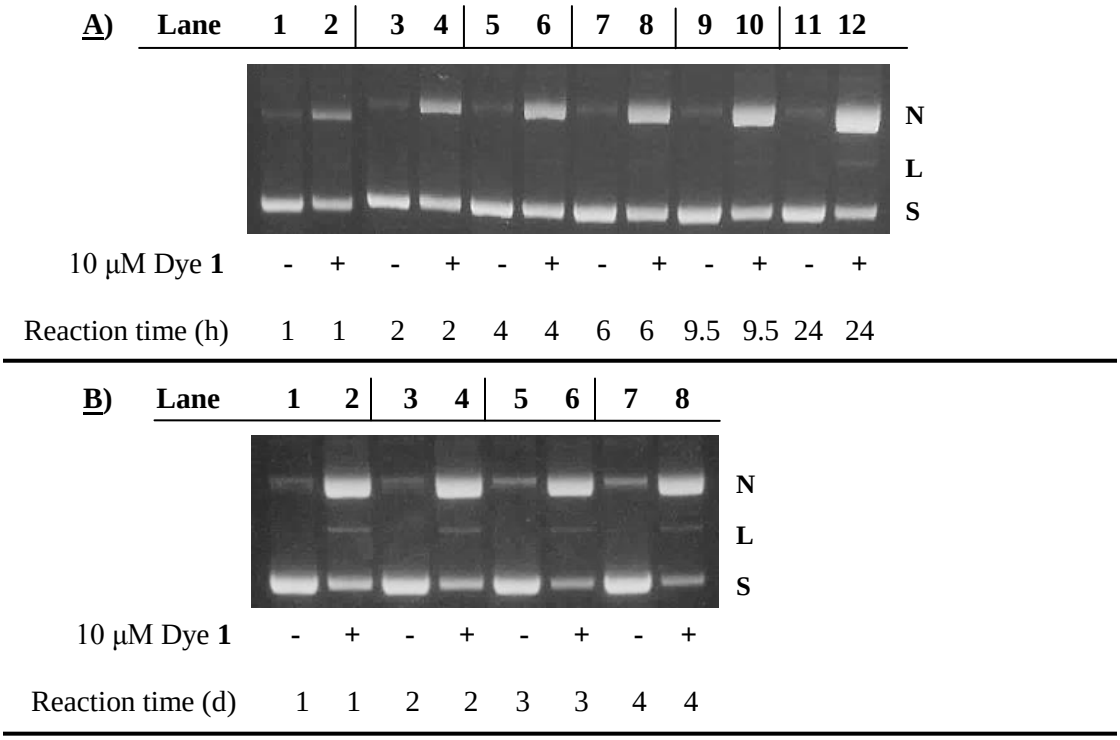

Figure 3.3 Photographs of 1.5 % non-denaturing agarose gels showing DNA thermal cleavage by cyanine **1** in time course at 37 ℃

Reactions were carried out in darkness. Samples contained 10 mM of sodium phosphate buffer (pH 7.0) and 25 μM bp of pUC19 plasmid DNA. **A)** Lanes 1, 3, 5, 7, 9, and 11: in the absence of **1**. Lanes 2, 4, 6, 8, 10, and 12: in the presence of 10 μM of **1**. Reaction time increased from 1 to 24 hours. **B)** Lanes 1, 3, 5, and 7: in the absence of **1**. Lanes 2, 4, 6, and 8: in the presence of 10 μM of **1**. Reaction time increased from 1 to 4 days. Abbreviations: N = nicked; L = linear; S = supercoiled.

It is worth noticing that this DNA dark cleavage is unlikely to be caused by water contamination. This is substantiated by a DNA thermal cleavage analysis of samples prepared with water (81.5%, v/v) from various sources which include tap water, and water filtered by Chelex 100 chelating ion exchange resin (Bio-Rad), Solution 2000 (Aqua solutions), PURELAB Classic DI (ELGA), Barnstead NANOpure Diamond (Thermo Scientific), and Milli-Q Advantage A10 (EMD Millipore) water purification systems. (The water used for our research was purified with Solution 2000 water purification system.) The results show no differences in DNA thermal damage among these samples, suggesting that the water source does not play a role in the thermally induced DNA-cyanine **1** reaction (Figure 3.S21).

3.1.4 Evaluating metal ion and iodide anion involvement in DNA thermal cleavage

As bioessential trace elements, iron and copper are broadly distributed throughout the body and mediate vital redox reactions in a variety of metalloenzymes such as superoxide dismutase, tyrosinase, and cytochrome oxidase. The levels of iron and copper ions in serum sometimes can be a physiological sign of a pathological condition.[17] More importantly, Fe(II) and Cu(I) are known as the two competent metal ions initiating reactive oxygen species (ROS) formation *in vitro* and *in vivo* through a Fenton-type redox cycle (Figures 1.3 and 1.4).[4a, 11a, 14a, 18]

Studies showed that the apparent dissociation constants for Cu(II)- and Fe(III)-DNA complexes were measured at micro molar levels, but the concentration of Fe(III) was 4- to 7-fold higher than Cu(II).[19] It suggests direct binding of copper and iron ions to DNA duplex in solutions. In this research, the possible involvement of adventitious redox active metal ions in the thermal cleavage process was tested by adding 10 μM of $FeCl_3$ or $CuCl_2$ to the reaction system. As can be seen in Figure 3.4A below, when the DNA-dye **1** solution is metal free (Lane 4) and in the presence of Fe(III) (Lane 5), they exhibit a very similar DNA cleaving pattern. This was verified with gel quantitation which reported a only 2% increase in nicked plasmid and no change in linear plasmid with the addition of Fe(III) (Figure 3.4B). In contrast, the histogram clearly shows that the addition of Cu(II) has promoted the conversion from supercoiled to nicked DNA, as well as a small amount of linear plasmid (4%) was generated (Lane 6 in Figure 3.4B).

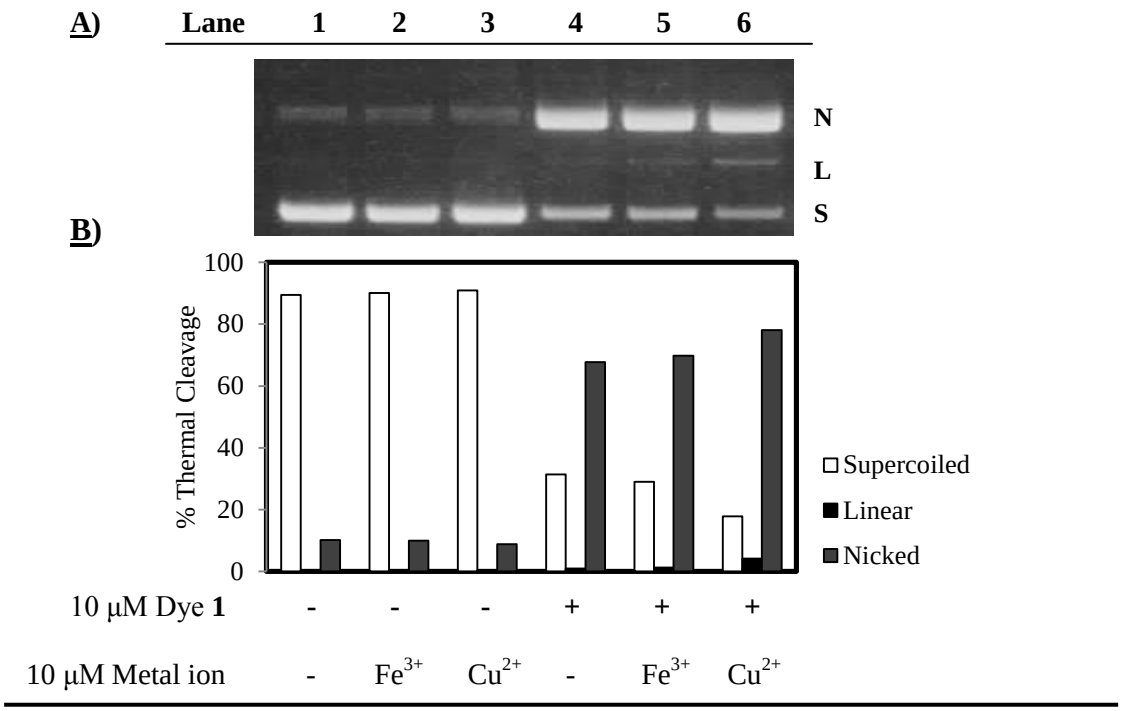

Figure 3.4 A 1.5 % non-denaturing agarose gel **A)** and corresponding histogram **B)** showing DNA thermal cleavage by cyanine **1** in the presence of metal ions at 37 ℃ for 24 h

Reactions were carried out in darkness. Samples contained 10 mM of sodium phosphate buffer (pH 7.0) and 25 μM bp of pUC19 plasmid DNA. Lanes 1 and 4: 0 and 10 μM of **1** in the absence of metal ions; lanes 2 and 5: 0 and 10 μM of **1** in the presence of 10 μM $FeCl_3$; lanes 3 and 6: 0 and 10 μM of **1** in the presence of 10 μM $CuCl_2$. Abbreviations: N = nicked; L = linear; S = supercoiled.

Chromophore **1** was synthesized with iodide counter anion. It is suspected that in the dark cleavage, the iodide anion, rather than the sensitizer, acted as the reducing agent in Figure 1.4 and reduced Cu(II) to Cu(I) according to the known reaction shown in Eq. 1 below:[20]

$$2Cu^{2+} + 2I^- \rightarrow 2Cu^+ + I_2 \quad (1)$$

As a result, an iodide salt was introduced to the reaction system. Gel quantitation in Figure 3.5B illustrates a nearly identical distribution of the three DNA conformations between the sample with iodide anions (Lane 4) and the positive control (Lane 2), suggesting that iodide anions might not have an effect on the dark cleavage in the absence of Cu(II). Interestingly, the histogram shows a small increase in nicked DNA compared to the reaction with only Cu(II)

(Lane 3) when both NaI and Cu(II) were present (Lane 5). A probable interpretation for that would be the simultaneous addition of Cu(II) and I^- elevated the formation of Cu(I).

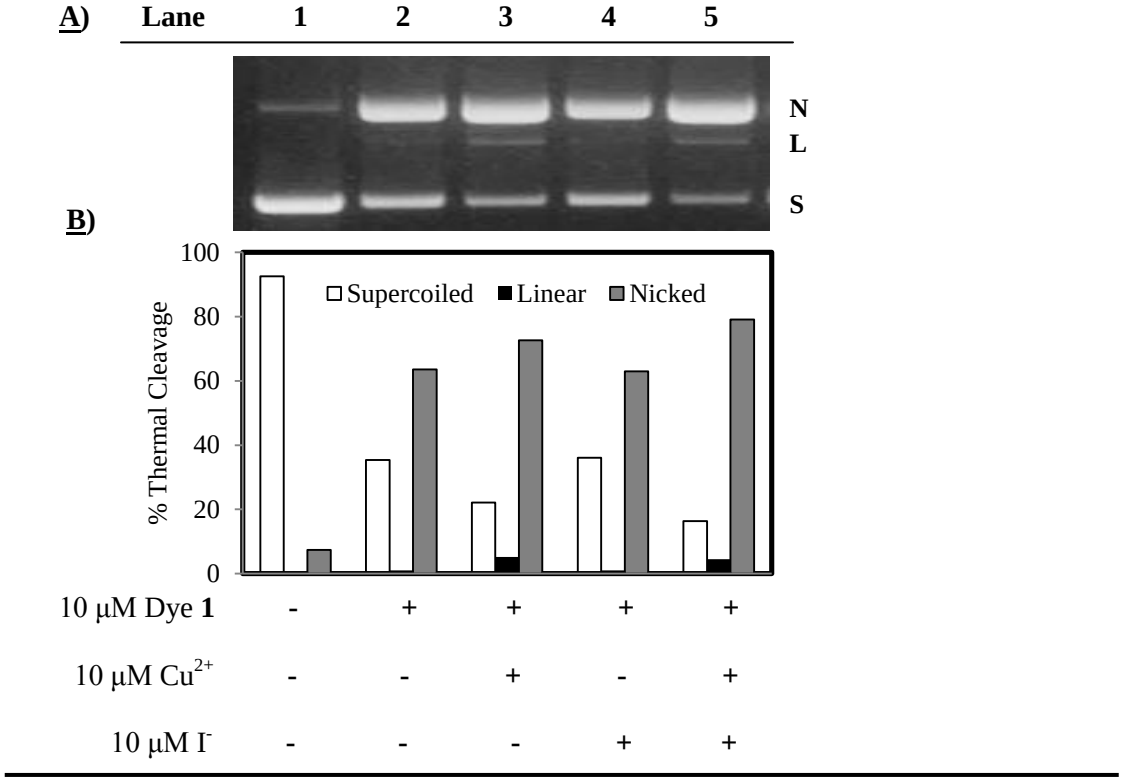

Figure 3.5 A 1.5 % non-denaturing agarose gel **A)** and corresponding histogram **B)** showing DNA thermal cleavage by dye **1** in the presence of Cu^{2+} and/or I^- at 37 ℃ for 24 h

Reactions were carried out in darkness. Samples contained 10 mM sodium phosphate buffer (pH 7.0) and 25 μM bp of pUC19 plasmid DNA. Lane 2: 10 μM of **1** in the absence of $CuCl_2$ or NaI; lanes 3 and 5: 10 μM of **1** in the presence of 10 μM $CuCl_2$; lanes 4 and 5: 10 μM of **1** in the presence of 10 μM NaI. Abbreviations: N = nicked; L = linear; S = supercoiled.

3.2 Colorimetric Detection of Copper(I)

We hypothesized that trace levels of Cu(II) must be present in out laboratory solutions and/or plasmid DNA preparation. The reaction of the Cu(II) with the cyanine dyes might contribute to DNA thermal cleavage. Our next goal was to determine if cyanine dyes (or I^-) could indeed reduce Cu(II) to Cu(I). Colorimetric detection of Cu(I) is achieved based on the fact that bathocuproinedisulfonic acid (BCS) disodium salt hydrate, a chromophore that forms a 2:1,

bright orange-colored complex with Cu(I) (λ_{max} = 480 nm; ε = 13,500 $M^{-1}cm^{-1}$).[21] This assay could provide direct experimental evidence for determining the involvement of Cu(II)/Cu(I) redox cycling in reactions. As expected, a Cu(II) and *L*-ascorbic acid positive control (red line in Figure 3.6A) gave a signature absorption band at 480 nm, while a Cu(II) negative control (blue line in Figure 3.6A) did not. A Cu(II) + I^- sample was prepared to test for Cu(I) generated by the Cu(II)/I^- redox reaction in Eq. 1. Yet, the spectrum in Figure 3.6A reveals that I^- could not reduce Cu(II) to Cu(I) (green line), ruling against its participation in ROS production. This fails to explain the mild enhancement of thermal cleavage in the presence of Cu(II) and I^- (Figure 3.5). Likewise, none of the controls in Figure 3.6B present evidence for Cu(I)-BCS complex formation. On the other hand, the strong absorption band at 480 nm from the sample containing cyanine **1** and Cu(II) (purple line in Figure 3.6A) indicates that the dye is capable of reducing Cu(II) to Cu(I) in the absence of light and that DNA is not necessary for the reduction reaction.

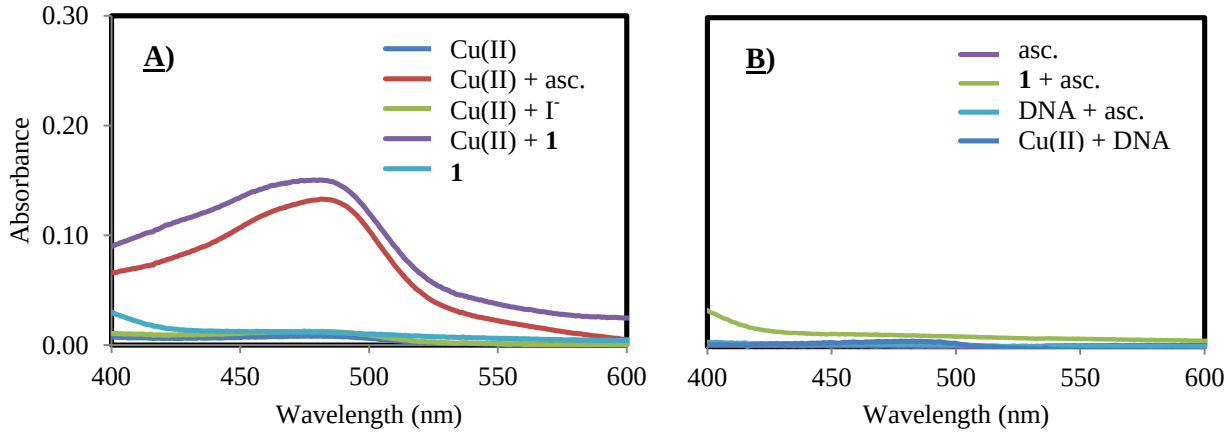

Figure 3.6 UV-visible absorption spectra to monitor Cu(I)-BCS complex formation by dye **1**

Reactions containing 10 mM of sodium phosphate buffer (pH 7.0) and one or more of the following reagents were carried out at 37 ℃ for 60 min in the dark: 30 μM of $CuCl_2$; 30 μM of *L*-ascorbic acid; 30 μM of NaI; 10 μM of **1**; 25 μM bp of pUC19 plasmid DNA. Samples were equilibrated with 42 μM BCS for an additional 30 min prior to absorbance scanning. The spectrum of DNA + Cu(II) sample (blue line) was taken from ref. 21.[22] Abbreviation: asc. = *L*-ascorbic acid.

3.3 Reagent-Induced Changes in DNA Thermal Cleavage

Table 3.1 Percent inhibition of DNA thermal cleavage by ROS scavengers, D_2O, and EDTA

Reagent	Species targeted	% inhibition of thermal cleavage[a]
Sodium benzoate (100 mM)	·OH	52 ± 4
Potassium iodide (50 mM)	·OH	43 ± 4
DMSO (4 μL)	·OH	44 ± 4
Sodium azide (100 mM)	$^1O_2$	26 ± 11
D_2O (84% v/v)	$^1O_2$ / hydrolysis	29 ± 1
EDTA[b] (50 mM)	Cu(II)	58

[a]Data are averaged over three trials and standard deviation is reported.
[b]21% and 95 ± 4% inhibition of thermal cleavage were observed in the presence of 5 mM and 100 mM of EDTA.
[c]Gel photographs are shown in Figure 3.S1, Supplementary data.

The effects of the chemical reagents on the thermal cleavage of DNA by dye **1** shed light on the essential species contributing to the reaction. According to the results shown in Table 3.1, the hydroxyl radical (·OH) scavengers, sodium benzoate[23], potassium iodide[24], and DMSO[25] all inhibited DNA damage in darkness. Specifically, ·OH radicals react with benzoate anions through two possible paths, addition and H-atom abstraction. It was found that among the positions (*i.e.* ipso, ortho, meta, and para) on the benzene ring, the ortho-carbon seemed to be favored based on kinetics and thermochemistry analyses.[26] Our results suggest formation of ·OH during the reactions causing DNA damage. In agreement with the colorimetric findings indicating metal ion involvement in DNA thermal cleavage, 50 mM of EDTA led to an around 60% quenching of the reactions. On the other hand, singlet oxygen ($^1O_2$), whose formation normally relies on the photon transfer from the excited state of photosensitizers to the ground state, would not be a concern, as reactions were excluded from light. Accordingly, the singlet oxygen ($^1O_2$) quencher, sodium azide, prevented strand breaking to a very small extent, which is most likely due to the interaction of azide anions with Cu(II).[27] D_2O solvent is often used to confirm the involvement of $^1O_2$ reflected in increased DNA scission, as it prolongs the $^1O_2$ lifetime by a factor of 9-10.[28] To the contrary, D_2O was found to decrease the cleavage by around

30%, indicating a deuterium effect on the reaction. This unusual phenomenon implies a rate-limiting step associated with H_2O and a possible mechanism of hydrolysis in DNA thermal cleavage. As a reference, in a mechanistic study of cerium(IV)-induced DNA hydrolysis, Komiyama *et al.* reported a D_2O solvent isotope effect (k_{H_2O}/k_{D_2O}) of 2.2-2.4 on the rate-limiting proton transfer process.[29]

3.4 T4 Ligation Experiment

To answer the question raised by the inhibitory effect of D_2O on cleavage, a DNA ligation experiment was performed to test for DNA hydrolysis, a reaction that refers to the breaking of phosphodiester bonds in the DNA backbone by water. The existence of Lewis acids, generally metal ions, can mediate DNA hydrolysis by facilitating the nucleophilic attack at phosphate groups by water or hydroxide.[30] T4 DNA ligase, using ATP as a cofactor, connects juxtaposed 5'-phosphate with 3'-hydroxyl termini in duplex DNA *via* phosphodiester bond formation. It is capable of joining duplex DNA restriction fragments with either blunt or cohesive ends.[31] For nicked and linear plasmid DNA cut through hydrolysis, T4 ligase treatment can convert them to closed circular form by direct reconnection of individual plasmid ends. Elongated linear plasmid is observed when more than one individual linear plasmid lines up. Yet, closed circular and nicked conformations cannot be separated on an agarose gel due to their similar migration rates.[32] Hence, the indication of ligation reaction relies on the disappearance or reduction of linear DNA bands, the brightening at nicked band positions, and the emergence of the elongated form. The positive results of T4 ligation experiments in Schnaith *et al.*[33] and Qian *et al.*[33b] studies showed smearing bands above nicked DNA under T4 ligase treatment. These characteristic bands most likely represent the elongated linear plasmid as the extended structure hinders its mobility on agarose gels.

In our experiment, gel quantitation reported no differences in the distributions of supercoiled, nicked, and linear DNA forms between trials with and without T4 ligase treatment (Figure 3.7B). Additionally, no suspicious bands of elongated linear form appeared above the nicked DNA bands in T4 ligase trials. The DNA ladder hydrolyzed by restriction enzymes served as a reference to evaluate the performance of T4 ligase which, in this case, exhibited potent religation competence (Figure 3.7C). Consequently, the experiment provides no evidence to suggest that the hydrolytic pathway is involved in the DNA thermal cleavage by **1**. Combined with the D_2O effect in the scavenger experiment, the data instead indicate that H_2O is associated with a rate-determining step in hydroxyl radical generation. As the deuterium ion is heavier than the hydrogen ion, the substitution of water by deuterium oxide would slow down the cleavage process, and thus, partially inhibit the DNA strand scission.[34]

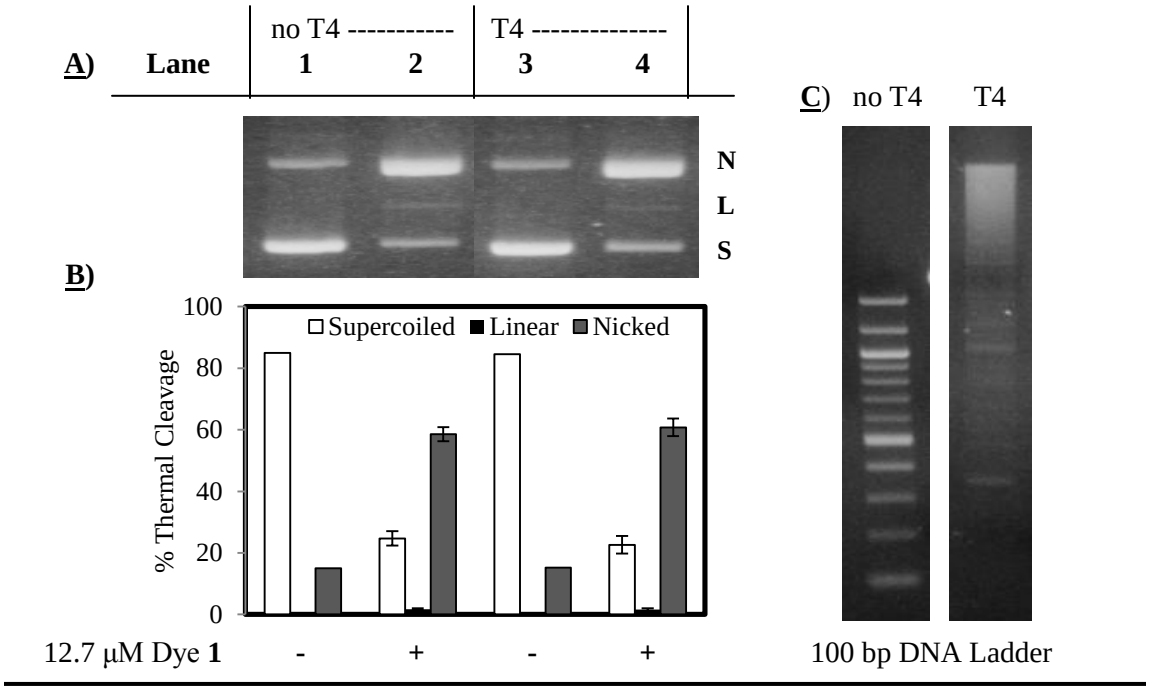

Figure 3.7 A 1.5 % non-denaturing agarose gel **A)** and corresponding histogram **B)** showing DNA thermal cleavage by dye **1** at 37 ℃ for 29 h

Reactions were carried out in darkness. Samples contained 10 mM of sodium phosphate buffer (pH 7.0) and 25 μM bp of pUC19 plasmid DNA. Lanes 1 and 2: without T4 ligase treatment; lanes 3 and 4: with 3.3 units/μL of T4 ligase treatment. Data in **B)** are averaged over three trials and error bars represent standard deviation. Pictures **C**) show 100 bp DNA ladder with and without T4 ligase treatment run on the same gel. Abbreviations: N = nicked; L = linear; S = supercoiled.

Taken together, three experimental results point to a copper-mediated Fenton-type mechanism of ROS generation in pUC19 DNA thermal cleavage by cyanine **1**. The specific evidence is: (1) enhanced plasmid scission upon the addition of Cu(II), (2) the significant amount of Cu(I) generated when dye **1** is reacted with Cu(II), and (3) the strong quenching of the DNA cleavage reaction by EDTA. As evidence implies direct complexation of copper and iron ions with DNA duplex in solutions,[19] we again stress our opinion that the DNA thermal cleavage occurring in the absence of externally added copper points to the presence of adventitious Cu(II) in the plasmid DNA and/or in laboratory solutions.[35] The introduction of hydroxyl radical scavengers reduced the damage of supercoiled DNA, indicating the involvement of ·OH. The T4

ligation experiment does not support the possibility of hydrolytic cleavage and suggests that the inhibitory effect of deuterium oxide is attained by substituting D_2O for H_2O in the rate-limiting step of ·OH production.

3.5 DNA Thermal Denaturation Experiments

Melting temperature (T_m) refers to the midpoint when half of the nucleic acid becomes single-stranded, while the other half remains helical. DNA melting temperature trends reflect the dynamic interaction between drugs and DNA. In general, ligands tend to have greater binding affinity toward helical nucleic acids than single-stranded ones. This stabilizes the helical state and thus raises the T_m of helical nucleic acids. Alternatively, drugs that favor binding to single-stranded nucleic acids over double-stranded lower the T_m values of nucleic acids.[36] For instance, classical intercalators, such as ethidium bromide and diazaphenanthrene, dramatically increase the T_m by a range of 4-22 ℃. Groove-binding compounds, like distamycin, also affect the T_m but to a lesser extent.[37] Biver *et al.* suggested a 10 ℃- and 8 ℃-increase of T_m for intercalative and a mixed binding modes in their study on interactions of poly[d(A-T)] DNA with two cyanine dyes, CCyan2 and Cyan40 respectively.[38]

Dye-to-DNA bp molar ratio (**r**) values ranging from 0.05 to 1.8 were tested in our DNA thermal melting experiments (Figure 3.S2, Supplementary data). Because cyanine dye **1** degrades in buffer solution and damages DNA thermally, the results display relatively inconsistent ΔT_m values as a function of increasing **r** value. Nonetheless, a general 2-5 ℃ rise in T_m was observed upon the addition of **1** and a saturation point was reached at around **r** = 1.6. An interaction between dye **1** and DNA is highly indicated, though the precise binding mode remains uncertain.

3.6 UV-Visible Absorption Analysis of Cyanine Dye 1

3.6.1 Time course UV-visible absorption study

Time based UV-visible spectroscopy was utilized to assess the stability of dye **1** in organic and aqueous solvents. Spectra in Figure 3.8A illustrates that compound **1** was relatively stable in DMSO. However, when it was diluted in sodium phosphate buffer (pH 7.0), the absorption dropped over 80% within one hour at the absorption maximum (λ_{max}) (Figure 3.8B). It is well known that many cyanine dyes are subjected to photooxidation or photodegradation.[2a, 7-10, 39] In order to rule out the impact from light, 10 μM of **1** in 10 mM sodium phosphate buffer was stored in a dark area for 60 min before scanning. The peak intensity at 60 min was found to be slightly higher in Figure 3.8C than the one shown in Figure 3.8B. The absorbance at λ_{max} took an additional 90 min to reach equilibrium (Figure 3.8C). This implies that the absorbance attenuation of the chromophore in protic solvent may be assisted by light to a small degree, as the absorbance continued decreasing remarkably in the absence of light. There may therefore be other factors that have an effect on the apparent instability of **1**.

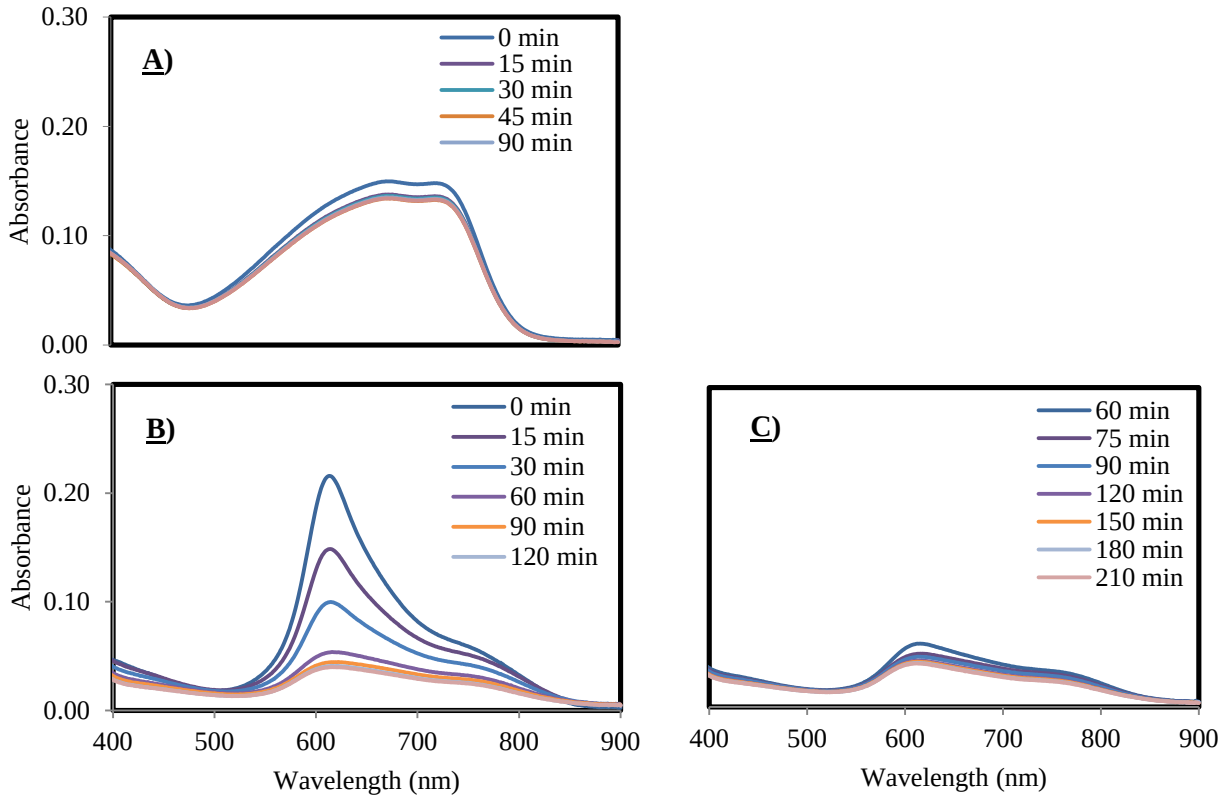

Figure 3.8 Time course UV-visible absorption spectra of cyanine **1**

Spectra were recorded when 10 μM of cyanine **1**was dissolved in **A**) DMSO, **B**) 10 mM sodium phosphate buffer (pH 7.0), and **C**) 10 mM sodium phosphate buffer (pH 7.0) and stocked in the dark for 60 min. The absorbance was collected at intervals of 15 or 30 min until the changes in absorbance were negligible.

Despite such a high speed of absorption degradation, cyanine **1** shows considerable DNA cleaving activity (see Section 3.1). It was suspected that **1** was structurally stabilized upon binding with the DNA helix. To verify this hypothesis, dye **1** was added to a high concentration of calf thymus (CT) DNA (300 μM bp). However, as the spectra in Figure 3.9 suggests, the opposite phenomenon occurred in which the intensity at λ_{max} plunged almost 80% in 15 minutes when the dye was bound to DNA. It seems DNA binding enhances degradation of the cyanine dye.

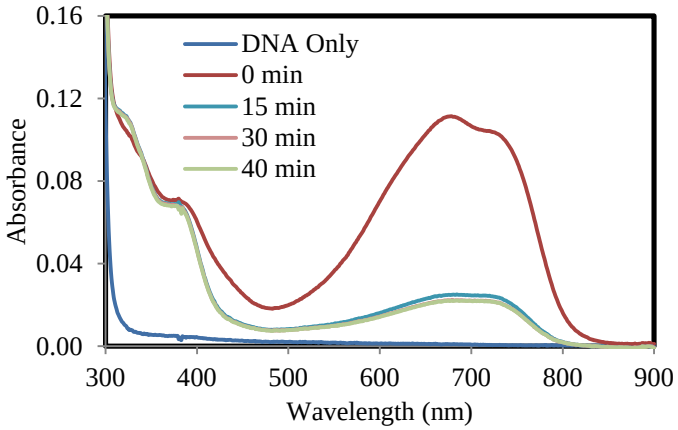

Figure 3.9 Time course UV-visible absorption spectra of dye **1** in the presence of CT DNA

10 μM of dye **1** was dissolved in 10 mM sodium phosphate buffer containing 300 μM bp CT DNA. The absorbance was recorded at intervals of 10 to 15 min until the changes in absorbance were negligible.

3.6.2 UV-visible absorption titration

Equilibrium binding titrations with UV-visible spectroscopy have been broadly employed for DNA-drug interaction studies due to their fast and easy operation. The technique essentially measures progressive optical changes in absorbance of a chromophore upon serial titrations with DNA. If the absorbance obeys the Beer-Lambert Law, it will reflect the concentrations of the free and the DNA-bound states.[40] Typical DNA binding through intercalation results in strong hypochromic and bathochromic shifts at absorption maxima. This is produced by potent π-π stacking and dipole-dipole interactions between the aromatic system of the chromophore and the DNA base pairs. Furthermore, since the strength of electrostatic force is inversely proportional to the cube of the distance from the ligands to the DNA bases, significant hypochromism normally points to a close approach of dyes toward DNA double strands.[1a, 41] In the case of anthracene and some other chromophores, groove-binding is more likely to exhibit moderate hypochromic shifts with less red shifting.[41]

When 10 μM of **1** was directly titrated into a cuvette containing a large amount of CT DNA (300 μM bp), the absorption peak recorded immediately after mixing displayed clear

hypochromism accompanied by a large bathochromic shift (Figure 3.10). Although the trend suggests a strong DNA-dye interaction, it is not sufficient to assign specific binding mode(s) to cyanine **1** as both intercalation and/or groove-binding are capable of generating similar patterns.[15]

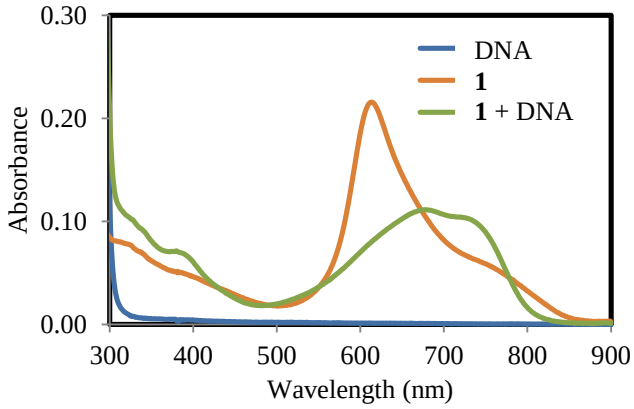

Figure 3.10 UV-visible absorption spectra showing binding-induced changes by dye **1**

Individual samples were prepared in 10 mM sodium phosphate buffer solution The blue line represents the absorbance curve of CT DNA only; whereas, the green and the red lines are absorbance curves of 10 μM of dye **1** in the absence and presence of CT DNA (300 μM bp), respectively..

3.6.3 H- and J-aggregation study

Symmetric and asymmetric cyanine dyes are prone to undergo self-stacking, especially at high concentrations. This tendency results from the hydrophobic attraction involving the planar π-π conjugation systems of chromophores. Depending on the slippage angle (α), there are two types of molecular arrangements, commonly referred to as *H*-aggregates and *J*-aggregates. They can be initially identified on the spectra according to the fact that *H*-aggregates are hypsochromic while *J*-aggregates are bathochromic with respect to cyanine monomers.[3, 6a] Beckford and coworkers have monitored the absorbance of indolium cyanine dyes as a function of solvent hydrophobicity. As the volume percent of methanol to phosphate buffer varied from 1 to 100%, they observed a gradual increase in the peak intensity ratio of monomer (*M*-band) to aggregates

(*H*-band). They believed that the hydrophobic solvent disrupted the highly organized π-π stacking array and shifted the molecules from aggregates to a monomer state.[42]

An aggregation study was employed on **1** in accordance with the concept of Beckford *et al.*'s experiment. Cyanine dye **1** was dissolved in seven methanol-phosphate buffer mixtures with different volume ratios. As learned from previous experiments that **1** degrades rapidly in protic solutions, it is expected after equilibrating in the dark for 2 hours at room temperature that solvents composed of higher amounts of methanol maintain much stronger absorption than those with less methanol. Indeed, Figure 3.11 demonstrates a progressive attenuation of absorbance in high to low volume percentages of methanol, except for a sudden sink between 40% and 20% (v/v). Moreover, as the solvent hydrophobicity increased from 0 to 100% (% v/v, methanol/buffer), a rise in peak height ratio of *M*-band (around 710 nm) to *H*-band (around 635 nm) was observed. The trend was in company with small red shifts of both peaks (Figure 3.11). These spectral characteristics provide evidence sustaining the occurrence of aggregation of dye **1** in aqueous solutions. Nevertheless, it is worth noting that after bleaching, the color of the chromophore **1** buffer solution was not restored upon methanol addition. This means that the loss of absorption was essentially irreversible, and therefore, a more appropriate conclusion should be that both self-aggregation and decomposition contributed to the spectral trends exhibited in Figure 3.11.

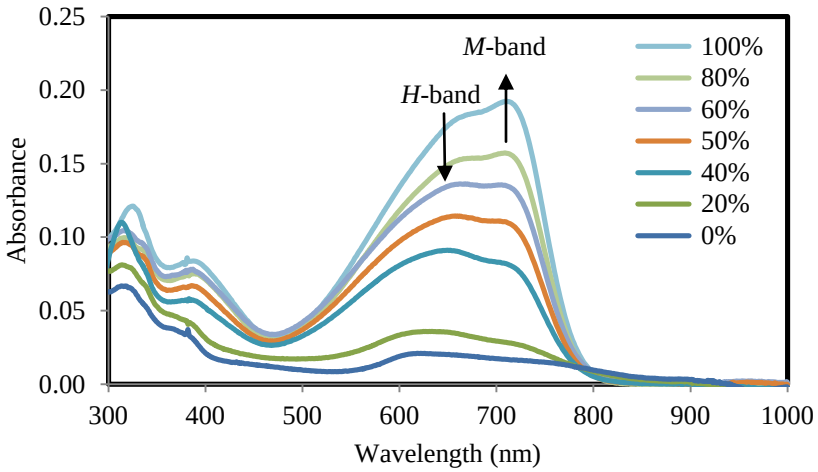

Figure 3.11 UV-visible absorption spectra of dye **1** in methanol/buffer solutions

10 μM of cyanine **1** was dissolved in a series of methanol solutions with varying volume percentages. Scanning was conducted after a 2-h dark equilibration at room temperature. Lines from top to bottom represent the absorbance in 100%, 80%, 60%, 40%, 20%, and 0% (v/v) methanol, respectively.

3.6.4 Time course UV-visible absorption in the presence of chemical reagents

In an early spectroscopic study conducted in 1988, Vlaskin *et al.* stated that the bleaching of some cyanine dyes at low concentrations was associated with protonation of methine chains in protic solutions, resulting in an interruption of the π-electron resonance across the two aromatic ring systems. They reported that the colors of the dyes were retained in basic or proton-accepting solvents, but were immediately lost with the addition of acid (100 μM). Moreover, they added that if UV irradiation was applied then, an irreversible decomposition of the methine bridge would be initiated.[43] Yet, in our case, 100 μM NaOH did not stabilize the color of cyanine **1** solution; Nor did the addition of 100 μM HCl instantly discolor the solution. The disagreement implies that cyanine **1** may not follow the decomposition scheme proposed by Vlaskin *et al.*.

On the other hand, Oushiki *et al.* stated that autoxidation was the main reason causing photobleaching of cyanine dyes.[9] It is believed that the singlet oxygen ($^1O_2$) and the superoxide ($O_2^{\cdot -}$) species, which are formed by the self-sensitizing of dyes under illumination, oxidatively break the polymethine chains, and thus, perturb the chromophoric cores.[9-10] Two proposed

mechanisms were described in the research papers of Chen *et al.*[10] and Chen *et al.*[2a] (Figure 3.12). Nevertheless, these two mechanisms cannot fully explain the phenomenon of dye **1** because its buffer solutions continue losing color even in the absence of light.

Mechanism 1 – Energy transfer:

$$\text{Dye} + h\nu \rightarrow {}^1\text{Dye}^* \xrightarrow{ISC} {}^3\text{Dye}^*$$

$${}^3\text{Dye}^* + {}^3\text{O}_2 \rightarrow \text{Dye} + {}^1\text{O}_2$$

$$\text{Dye} + {}^1\text{O}_2 \rightarrow \text{Dye-O}_2 \text{ (photofading)}$$

Mechanism 2 – Electron transfer:

$$\text{Dye} + h\nu \rightarrow {}^1\text{Dye}^*$$

$${}^1\text{Dye}^* + \text{O}_2 \rightarrow \text{Dye}^+ + \text{O}_2^{\cdot -}$$

$$\text{O}_2^{\cdot -} + \text{Dye} \rightarrow \text{photofading}$$

Figure 3.12 Proposed mechanisms causing photofading of dyes (ISC: intersystem crossing)

As described in the introduction, there is an alternative dark pathway yielding $O_2^{\cdot -}$ through a one-electron reduction of $^3O_2$. Particularly, the standard redox potential for molecular oxygen/superoxide couple, E° [$O_2/O_2^{\cdot -}$], is equal to -0.33 V. To attain this reduction, the donor undergoing oxidation must have a similar or lower redox potential.[13] Thus in theory $^3O_2$ could be converted to $O_2^{\cdot -}$ (1) if the dye possesses electron donors with redox potentials smaller than -0.33 V, or more likely (2) if a sufficient amount of Cu(I) is produced *via* dye/Cu(II) redox reaction (Figure 1.4). As a result, dye bleaching is also possible in darkness as long as ROS are introduced or generated. A paper of Barros *et al.* has reported the reactive positions for electrophilic and nucleophilic reactions along the heptamethine chains of two cyanine dyes through quantum chemical calculations. By individually analyzing the relative overlap or delocalization magnitudes of their HOMO and LUMO energy profiles, it was found that the electronic distribution of these two dyes was markedly distorted particularly in water (even when the chain was incorporated into a ring). Namely, the side containing cationic nitrogen was

electron-deficient, while the opposite side was electron-rich.[8] Likewise, Bouit and coworkers pointed out that the symmetric electronic distribution is progressively lost for longer methine bridges, and finally collapses to an asymmetric form in which one side of the chain holds more electrons than the other side.[44] Therefore, as Barros *et al.* concluded, if oxidants were present, nucleophilic attack would be more likely to occur on the C_α and C_γ to the cationic nitrogen atom (*i.e.* C1 and C3 from N^+), while electrophilic attack on the C_β to the neutral nitrogen (*i.e.* C2 from N).[8] The hypothetical mechanism of dye bleaching in darkness by $O_2^{\cdot-}$ and ·OH shown in Figure 3.13 is inferred from Figures 1.4 and 3.12.[2a, 4a, 10-11, 14a] The mechanism was tested with radical scavengers and chelating agents which were intended to quench any formation of ROS and prevent bleaching of **1**.

$$\text{Dye} + Cu^{2+} \rightarrow \text{Dye}^+ + Cu^+$$

$$Cu^+ + {}^3O_2 \rightarrow Cu^{2+} + O_2^{\cdot-} \rightarrow H_2O_2 \rightarrow \cdot OH$$

$$O_2^{\cdot-}/\cdot OH + \text{Dye} \rightarrow \text{bleaching}$$

Figure 3.13 Hypothetical mechanism causing bleaching of dyes in the dark

The line chart in Figure 3.14 has summarized the final data of the experiments, where the dashed line labeled as “10 mM Buffer” is a control without addition of reagents. The absorbance of cyanine **1** buffer solution was stabilized in the presence of 100 μM BCS (green line) or 50 mM KI (orange line). The addition of 25 U/μL of catalase (purple solid line) also significantly slowed down cyanine **1** bleaching. A weaker stabilization effect was observed with 50 mM EDTA (red line) or 100 mM sodium benzoate (dark blue line). To the contrary, CT DNA appeared to promote the absorbance attenuation of cyanine **1** (light blue line).

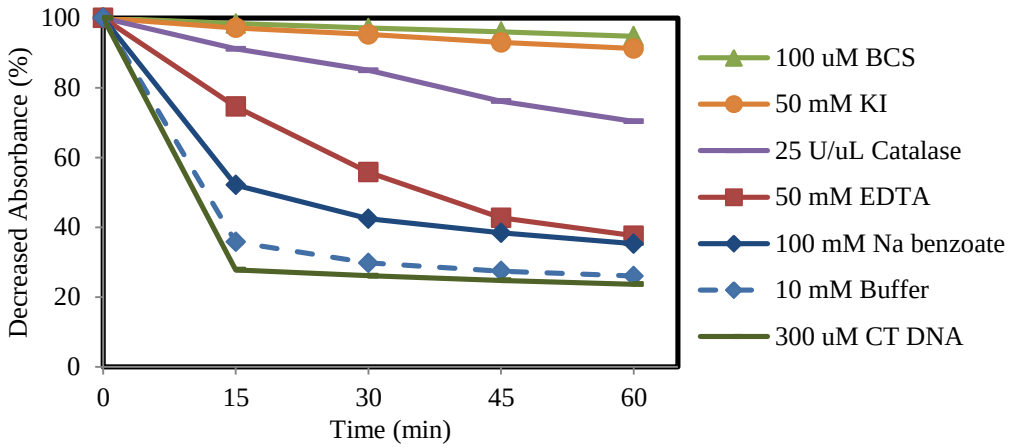

Figure 3.14 Comparisons of reagent-induced effects on bleaching rates of cyanine dye **1**

A line chart summaries the bleaching rates of cyanine dye **1** in the presence of radical scavengers, chelating agents, and CT DNA (solid lines). Individual samples were prepared in 100 mM sodium phosphate buffer. The dashed line ("100 mM Buffer") refers to the control in the absence of reagents. Spectra are shown in Figures 3.S7-3.S8, Supplementary data. Abbreviations: BCS = bathocuproinedisulfonic acid disodium salt; KI = potassium iodide; EDTA = ethylenediaminetetraacetic acid disodium salt.

The concentrations of KI, sodium benzoate, and EDTA were kept the same as those used in the reagent-induced changes in DNA thermal cleavage experiments previously described (Section 3.3). The results seem to agree with the bleaching mechanism proposed in Figure 3.13. Particularly, BCS has high stability constants (logβ) with Cu(I) and Cu(II) (20.8 and 12.4, respectively).[45] It is expected to chelate Cu(I) and Cu(II) in the solution and quench the generation of $O_2^{\cdot-}$ and ·OH (Figure 1.4).[4a, 11a, 14a] KI is known to scavenge H_2O_2 and ·OH.[24] Similarly, the formation of H_2O_2 can be quenched by catalase. Thus, they stabilized cyanine **1** aqueous solution as expected. On the other hand, EDTA has a stability constant (logβ) of 25.1 with Fe(III), but 7.45 and 18.8 with Cu(I) and Cu(II) respectively.[46] The preference for iron over copper may explain the weaker stabilization effect on the absorption attenuation of cyanine **1** compared to BCS. The solution with the ·OH scavenger sodium benzoate also exhibited a reduced degradation speed. On the other hand, the bleaching process was promoted in the presence of DNA. It is believed that this was not attributed to the typical hypochromic and

bathochromic shifts from DNA-drug binding described in Subsection 3.6.2. Since the sample contained a high level of CT DNA, it was assumed that the equilibrium of DNA-drug binding was reached rapidly after thorough mixing. In addition, Figure 3.10 implies that the characteristic spectral shifts of DNA-drug binding have been accomplished before the first UV-visible scan. Therefore, we considered any attenuation afterwards resulted from dye bleaching. It is likely that the ROS were rapidly consumed by reacting with nucleic acids, which pulled the Fenton-type reaction towards the product side of the equilibrium. One other reason might be that the dye becomes more ready to be targeted for ROS attack upon binding with the DNA helix.

3.7 Mass Spectrometry Study of Bleaching

Based on the results discussed to date, a preliminary idea about the rapid fading of cyanine **1** in aqueous solutions has been proposed. Herein, we tried to identify the decomposed product(s) of **1** with the help of mass spectrometry for its robust ability to identify analytes by measuring abundance versus mass-to-charge ratios (m/z). First of all, regardless of the types of solvents (*i.e.* methanol, 50% (v/v) methanol/ddH_2O, and acetonitrile (ACN)) or the length of the equilibration time, the major peaks of the spectra were always bands with a m/z of 535.5, which should be the positively charged chromophore, *i.e.* $[C_{39}H_{39}N_2]^+$ (Figures 3.S3-3.S5, Supplementary data). In a time based trial, 10 μM of **1** was dissolved in ACN and tested at 0 min, 60 min, and after two days. However, the mass spectra showed no differences even though the color of the solution had paled as a function of time and with no color observed by the naked eye two days later (Figure 3.S5, Supplementary data). An internal standard is recommended to have an analogous structure and molecular weight to the analyte such that they demonstrate similar behaviors and fragmentation (if any) during ionization. However, eligible compounds were not found because the mass spectra of similar pentamethine cyanines suffering from such

instability problems were not solved. In the absence of a standard, the quantitative information of the base peaks was not attainable. The molecular ion could be gradually destructed to certain neutral products that could not be detected by the mass spectrometer. Moreover, cyanine **1** dissolved in chelexed water did not generate any mass spectral signal either in the absence or presence of Cu(II). After adding 0.1% formic acid, several new peaks emerged at m/z 149, 268.3, and 549.5 (Figure 3.S6, Supplementary data). The band of m/z 268.3 with two positive charges is thought to be transformed from m/z 535.5 through one-proton addition, *i.e.* $[C_{39}H_{40}N_2]^{2+}$.

The majority of the research on the stability of cyanine dyes is limited to considering the consequence of light exposure. Nevertheless, all of the studies agree that the decisive step contributing to the irreversible dye bleaching is an addition reaction of reactive oxygen species, resulting in fragmentation on the methine bridge (Figure 1.2).[2a, 7-10, 43] As discussed in the previous section, this is because the electronic distribution along the polymethine chain becomes unsymmetrical when it is over elongated or stored in water medium.[8, 44] Theoretically, dark decomposition is equally as achievable as photodegradation, as long as ROS are generated in the solutions or provided externally. In fact, studies have provided convincing evidence substantiating this hypothesis. Though no schemes of structural alteration were proposed, Nakagawa and coworkers showed that cyanine dyes were rapidly bleached in the absence of light upon reacting with $O_2^{\cdot -}$ and/or ·OH which were formed in a controlled Fenton reaction (Fe(II)/H_2O_2 at pH 3.5).[47] More recently, Nani, *et al.* analyzed the reactivity of a heptamethine cyanine with various ROS and corresponding decomposed products in a similar condition (Fe(II)/H_2O_2 at pH 6) with HPLC/MS. They reported a 96.6% damage of the dye by ·OH, but were not able identify any major species form during the reaction.[48] Consulting the articles of

Chen *et al.*[10] and Vlaskin, V. I. & Zakhidov, U.[43], we anticipated three main decomposition products of cyanine **1**: (1) 5-butylphenanthridinone, (2) an ionic aldehyde, which might be further oxidized in water to (3) a carboxylic acid (Figure 3.15). However, none of the m/z values representing these proposed fragments were observed in the mass spectra.

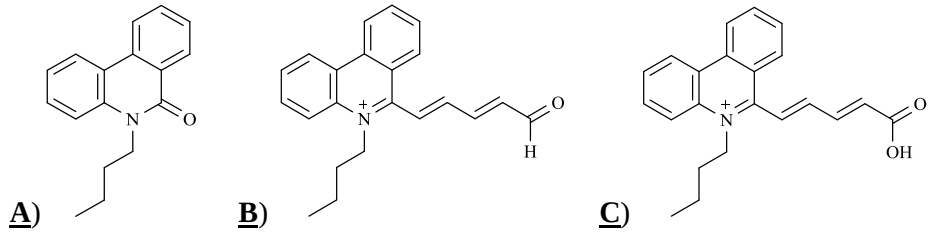

Figure 3.15 Hypothetic decomposed products of cyanine dye **1**

3.8 Preliminary Investigation of Cyanine Dye Analogs

3.8.1 Time course UV-visible absorption

In addition to **1**, we recorded time course UV-visible absorption spectra of twenty-one additional cyanine analogs (**2-22**, Figures 1.6-1.11) in 10 mM sodium phosphate buffer and in DMSO, individually. With the exception of compounds **5**, **6**, and **7**, every cyanine dye experienced some absorption attenuation in buffer solution (Figures 3.S9-3.S12, Supplementary data). This could be caused by self-aggregation and/or by decomposition. Sensitizers **11-13**, **16**, and **17** displayed intense absorption bands in the visible red to near-infrared wavelength range. Conversely, absorbance of nineteen out of the twenty-one dyes was relatively stable in DMSO (Figures 3.S13-3.S16, Supplementary data). The absorption maximum of chromophore **3** at 670 nm decreased in DMSO accompanied by an increase within the 380-460 nm region. Similar for cyanine **5**, the absorption peaks at 680 nm and 260 nm decreased in DMSO along with a slow buildup between 340 and 440 nm wavelengths. Technically compounds **20** and **21** are not

cyanine dyes due to the lack of polymethine chains. Their buffer solutions showed stable absorption from the phenanthridine ring structure in the 230-360 nm wavelength range.[49]

3.8.2 DNA thermal cleavage activity study

The goal of this section was to preliminarily evaluate the thermal cleavage activity of twenty-three target compounds (**1-24**, Figures 1.5-1.12). By studying these cyanine dyes, we were hoping to identify structural features that might give rise to DNA thermal cleavage and possible dark toxicity in *in vivo* experiments. This knowledge would greatly facilitate the design and screening of cyanine dyes for clinical applications. According to the data shown in Figures 3.16 and 3.17, compounds **1-22** produce variable levels of DNA thermal cleavage. For instance, dyes **2**, **5**, **8**, **10**, **18**, and **22** yielded ~10% of nicked and linear plasmid DNA. Higher levels of DNA thermal cleavage were attained in the presence of **1**, **9**, **13**, **16**, **17**, and **19** (39% – 82%). Cyanine dyes with phenanthridinium and quinolinium ring systems produce high cleaving activity. In contrast, non-cyanine chromophores **20** and **21** along with **23** and **24** (Figure 3.S17, Supplementary data) exhibited no activity at all.

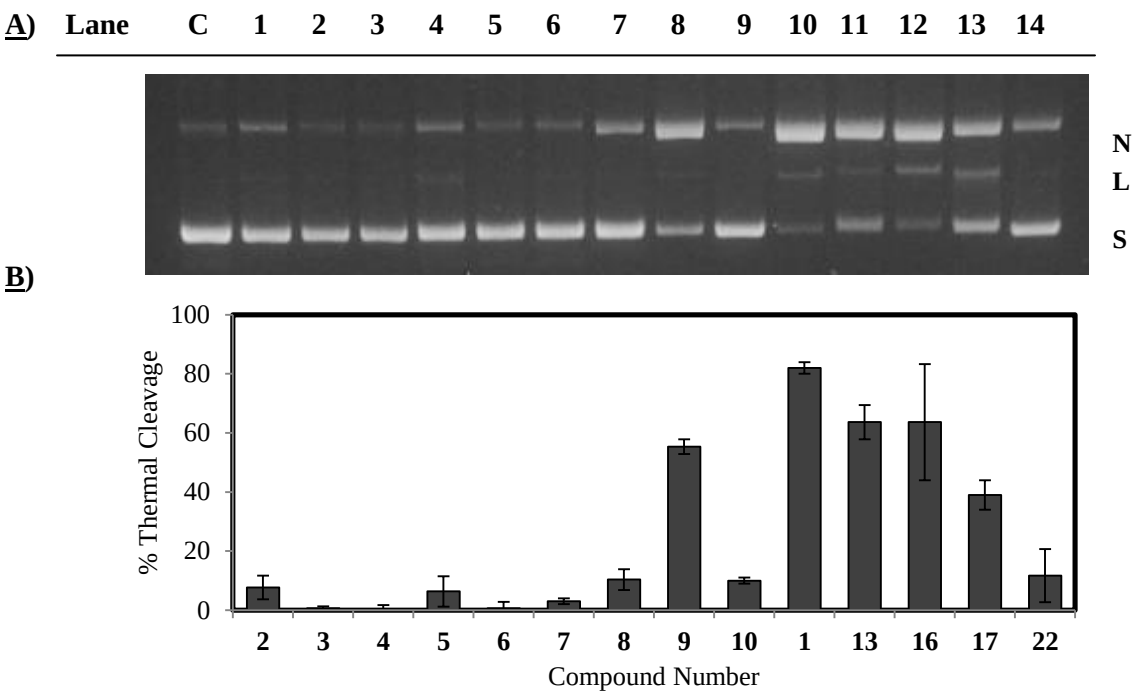

Figure 3.16 A 1.5 % non-denaturing agarose gel **A**) and corresponding histogram **B**) showing percent DNA thermal cleavage by fourteen cyanine analogs at 37 ℃ for 24 h

Reactions were carried out in darkness. Samples contained 10 mM of sodium phosphate buffer (pH 7.0) and 25 μM bp of pUC19 plasmid DNA. Lane C: in the absence of dyes. Lanes 1 to 14: in the presence of different dyes with names labeled on the x axis of **B**). Data in **B)** are averaged over three trials and error bars represent standard deviation. Abbreviations: N = nicked; L = linear; S = supercoiled.

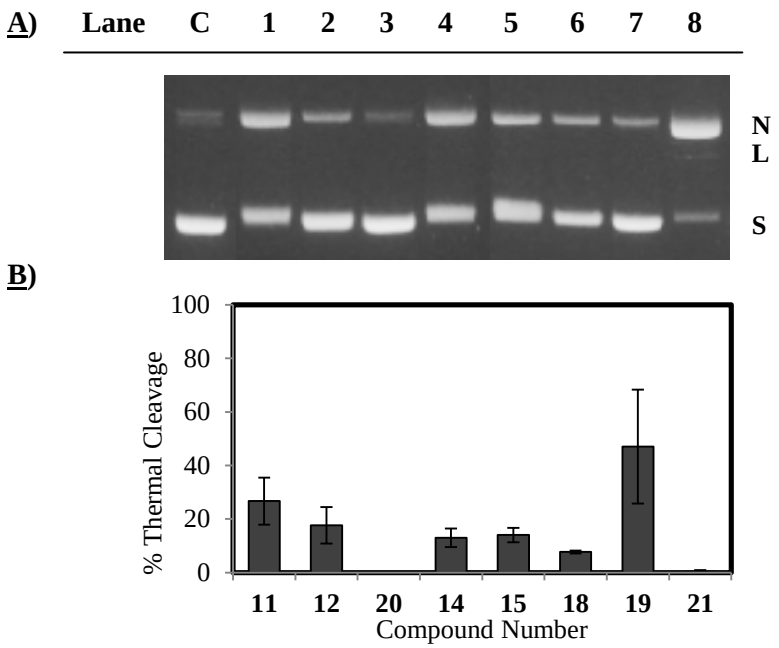

Figure 3.17 A 1.5 % non-denaturing agarose gel **A**) and corresponding histogram **B**) showing percent DNA thermal cleavage by eight cyanine analogs at 37 ℃ for 24 h

Reactions were carried out in darkness. Samples contained 10 mM of sodium phosphate buffer (pH 7.0) and 25 μM bp of pUC19 plasmid DNA. Lane C: in the absence of dye. Lanes 1 to 8: in the presence of different dyes with names labeled on the x axis of **B**). Data in **B)** are averaged over three trials and error bars represent standard deviation. Abbreviations: N = nicked; L = linear; S = supercoiled.

As was discussed in Subsection 3.6.4, Barros and coworkers reported that the electronic distribution of a NIR cyanine dye could be significantly distorted in aqueous medium, in which one side of the polymethine linker was more nucleophilic while the other side more electrophilic.[8] Similarly, Bouit's group stated that the symmetric electron resonance of a symmetric cyanine is progressively lost as the methine bridge lengthens, and is eventually converted to an asymmetric status in which electrons incline towards one side of the bridge.[44] It is suspected the asymmetric profile might confer a relatively lower redox potential on the electron-rich carbons adjacent to the neutral nitrogen. Thus, the cyanine would be able to reduce the trace amount of adventitious Cu(II) in the plasmid DNA and/or in laboratory solutions to Cu(I) which triggers the ROS generation pathway in the absence of light. In the comparisons

within each cyanine family, introducing an electron-withdrawing group (EWG) such as a halogen substituent (Cl or Br) in the middle of the methine bridge seems to partially suppress DNA thermal damage and dye attenuation. For example, dyes **3** and **4**, **6** and **7**, **10**, **14** and **15**, and **17** possess only one-half or less of the thermal cleavage activity of their unsubstituted counterparts (*i.e.* **2**, **5**, **9**, **13** and **16**, respectively). This is achieved perhaps by pulling the electrons toward the electron -poor side and balancing the electronic distribution along the polymethine chain. Following this prospective, a Cl-substituted methine bridge is likely to have weaker dark cleavage than its Br-substituted counterpart, as Cl is a stronger EWG. Two pairs of favorable examples (**3** vs. **4**; **6** vs. **7**) are available in this study (Figure 3.16). However, their percent DNA thermal cleavage is close to zero, which hinders pronounced comparisons. Moreover, as a short methine linker is more likely to retain a symmetric distribution of electrons and avoid the buildup of electron density on one side of the bridge, the trimethine cyanine dyes that were tested, **8**, **11**, and **12**, tended to have lower thermo-induced DNA cleaving property as compared with their pentamethine analogs, **9**, **13**, and **16**. In contrast, simple phenanthridine compounds (*e.g.* **20**, **21**, **23**, and **24**) are exempted from all the influence, and thus were completely inactive under dark conditions. Though we did not test dyes with polymethine bridges composed of ≥ 7 carbons, based on the literature references cited above, it is suspected that they would exert higher levels of thermo-induced DNA scission and exhibit poorer stability in protic solutions.

As it is assumed that the formation of ·OH is responsible for DNA dark cleavage as well as dye bleaching, the absorbance attenuation rate of dyes in buffer solution should follow the same structure-reactivity trend observed in this section. According to Figure 3.S9 and 3.S12, dyes **5-7** and **20-21** are stable in sodium phosphate buffer and thermally inactive to DNA.

Similarly, the decreases in absorption maxima of low cleavage compounds **2-4** and **22** are more likely due to self-aggregation. For those thermally cleave DNA (Figure 3.S10 and 3.S11), trimethine cyanines (**8**, **11**, and **12**) experienced a slower bleaching rate than their pentamethine analogs (**9**, **13**, and **16**). Moreover, with an electron-withdrawing substituent on the methine linker, the absorbance attenuation of the chromophores (**10**, **14-15**, and **17**) seems to slower down compared to their unsubstituted counterparts (**9**, **13** and **16**).

3.9 Thermal Cleavage Activity Study of Initial versus Bleached Compounds

3.9.1 DNA thermal cleavage by initial vs. bleached compounds

Time course UV-visible absorption studies in Subsection 3.8.1 have shown that most of the cyanine dyes (**1-4**, **8-19**) underwent aggregation and/or degradation in sodium phosphate buffer solution. Hence, we were interested in assessing the differences in their thermal nuclease activity before and after bleaching. Four compounds, **1**, **9**, **13**, and **16**, were picked for further studies because of their relatively higher percent thermal cleavage (Figures 3.16 and 3.17). The data in Figure 3.18 demonstrate that bleached compounds exhibited much weaker DNA damaging ability than their initial counterparts. The loss of reactivity along with the discoloration could be caused by self-aggregation and/or some structural transformation (*i.e.* decomposition).

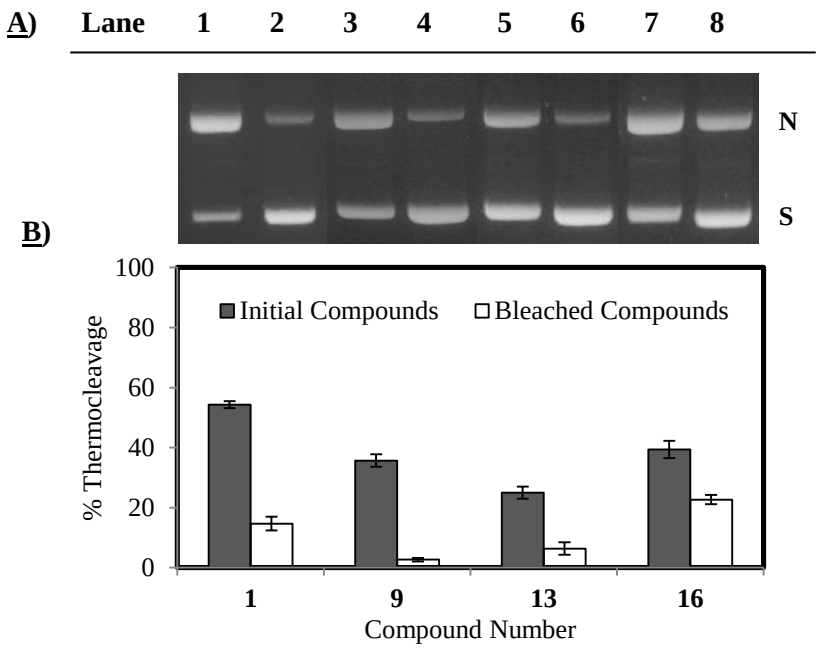

Figure 3.18 A 1.5 % non-denaturing agarose gel **A)** and corresponding histogram **B)** showing percent DNA thermal cleavage by initial and bleached cyanines **1**, **9**, **13**, and **16** at 37 ℃ for 24 h

Reactions were carried out in darkness. Samples contained 10 mM of sodium phosphate buffer (pH 7.0) and 25 μM bp of pUC19 plasmid DNA. Lanes 1, 3, 5, and 7: in the presence of initial dyes. Lanes 2, 4, 6, and 8: in the presence of bleached dyes. Names of dyes are labeled on the x axis of **B)**. Data in **B)** are averaged over three trials and error bars represent standard deviation. Abbreviations: N = nicked; S = supercoiled.

3.9.2 Colorimetric detection of copper(I)

As discussed in Section 3.3, the appearance of Cu(I) provides additional experimental evidence supporting the involvement of Cu(II)/Cu(I) redox cycling in the thermal cleavage process. We therefore attempted to evaluate the reducing ability of bleached compounds versus initial ones to identify the reason for the drastic decrease in DNA thermal cleavage. It was hypothesized that the bleached product(s) might not be able to reduce Cu(II) to Cu(I) to form DNA damaging ROS. The Cu(II) and *L*-ascorbic acid positive control and the Cu(II) negative control are shown as red and blue lines in Figure 3.6A. To eliminate the influence from the background, the absorbance of initial and bleached compounds (blue and orange lines) were subtracted from the signals in the presence of Cu(II) (green and purple lines) respectively. The

spectra show that bleached compounds displayed about one-half to two-third of the Cu(I)-BCS complex absorption signals of their unbleached counterparts (Figure 3.19). This may partially explain the drop in DNA thermal cleavage upon bleaching.

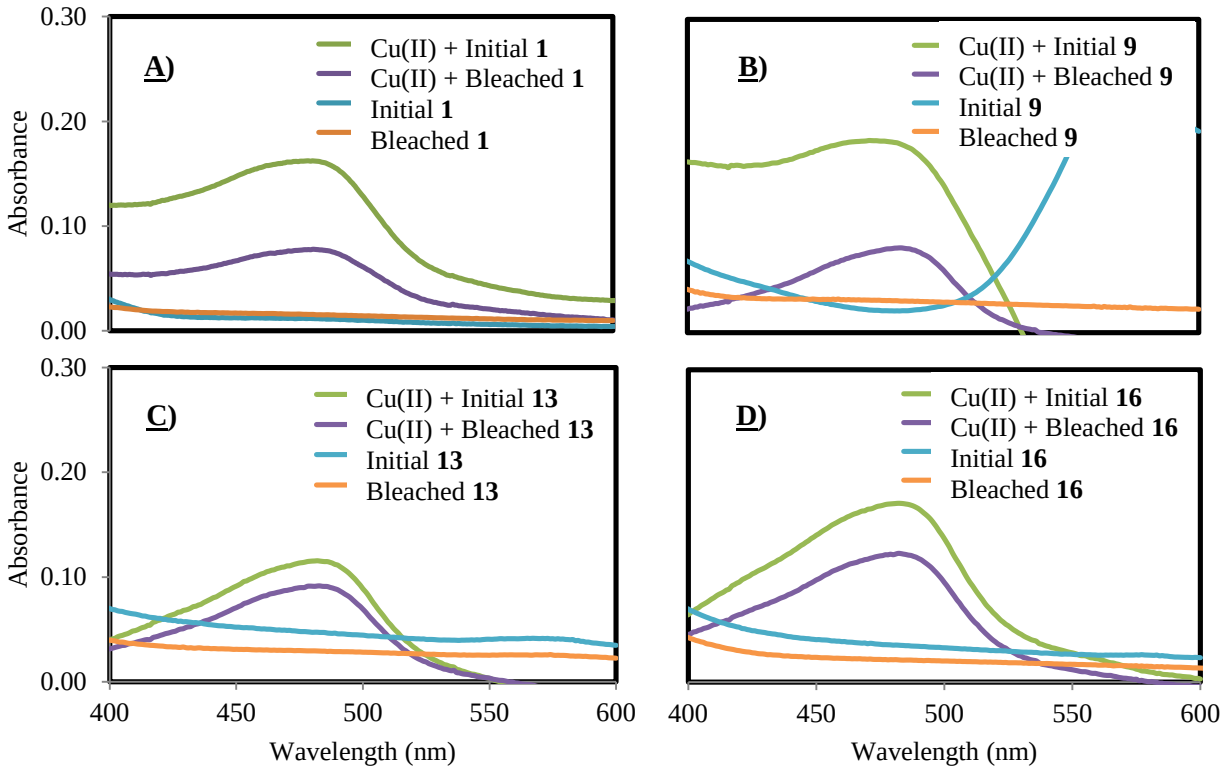

Figure 3.19 UV-visible absorption spectra to monitor Cu(I)-BCS complex formation by initial vs. bleached compounds

Reactions containing 10 mM of sodium phosphate buffer (pH 7.0) and one or more of the following reagents were carried out at 37 ℃ for 60 min in the dark: 30 µM of $CuCl_2$; 30 µM of *L*-ascorbic acid; 10 µM of initial or bleached cyanine dye **A) 1**, **B) 9**, **C) 13**, or **D) 16**. Samples were equilibrated with 42 µM BCS for an additional 30 min prior to absorbance scanning. Individual initial and bleached dye absorbance were subtracted from their absorbance in the presence of Cu(II) respectively.

3.9.3 Competitive DNA binding assay

Going back to the basic perspective of the structural strategy for a good DNA sensitizer, successful plasmid cleavage is premised on efficient interactions between the DNA double helix and ligands. After learning that the results from the colorimetric assay failed to fully explain the low DNA thermal cleavage produced by the bleached dyes, competitive binding experiments

were conducted to compare the DNA binding affinity of initial dyes with that of bleached ones. Ethidium bromide (EtBr), as a non-specific intercalator, has been widely utilized in fluorescence-based displacement competition assays. This technique provides a quick and flexible way to rank relative binding affinity toward the DNA helix within a drug family.[40] In our case, ligands were allowed to equilibrate with pUC19 plasmid in the absence of EtBr, and were resolved on 1.7% non-denaturing agarose gels. After electrophoresis, the gels were stained in EtBr buffer in which ethidium competed with the ligands for DNA binding positions. For those drugs with poor binding propensities, they are more liable to be replaced by ethidium, while, for those that display strong interactions, only limited ethidium replacement is expected. Since ethidium fluoresces under illumination at 302 nm, the former situation will give brighter DNA bands on agarose gels, while the latter one will display dimmer bands. A precise comparison can be achieved through quantitation of the gel image.

In the concentration based ethidium bromide displacement experiment, three concentrations (10, 50, and 75 μM) of two cyanine dyes (**1** and **13**) were studied. The aim was to find an optimum concentration which clearly distinguishes the differences in % ethidium replacement between initial and bleached dyes. For the ease of comparison, the % ethidium replacement of the DNA controls was normalized to 100%. According to the line charts plotted in Figure 3.20, bleached compounds tended to have higher % ethidium replacement than unbleached compounds at all concentrations. In addition, as the concentration increased, the % ethidium replacement decreased. Drugs with concentrations higher than or equal to 75 μM were found to overdamage the plasmid causing smearing bands or precipitation in loading wells. The opposite was seen with 10 μM which was not sufficient to provide a distinct indication of the

ethidium replacement efficiency. Consequently, 50 μM was chosen as the dye concentration for subsequent studies in this section and Section 3.10.2.

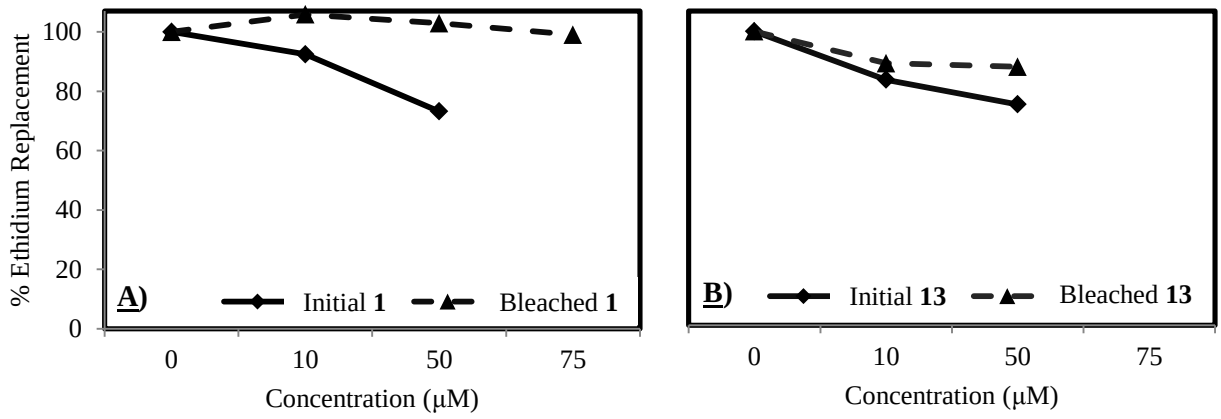

Figure 3.20 Line charts showing concentration course ethidium bromide displacement study of initial and bleached compounds.

Line charts show the trends of percent ethidium displacement of initial (solid lines) and bleached (dash lines) cyanine dyes **A) 1** and **B) 13** from 25 μM bp of pUC19 plasmid DNA (10 mM sodium phosphate buffer, pH 7.0, room temperature) from 0 to 75 μM. Each sample was equilibrated in the dark for 15 min before gel electrophoresis. Data points at 75 min of initial **1**, and initial and bleached **13** were omitted due to DNA precipitation. Representative gel photographs appear in Figure 3.S18, Supplementary data.

In the following experiment, the % ethidium replacement of **1**, **9**, **13**, and **16** in their initial and bleached states at 50 μM were tested. It was found that after gel staining, almost all bleached compounds exhibited low binding to the DNA double helix, but the fresh dyes remained bound, showing lower levels of ethidium fluorescence (Figure 3.21). Dye bleaching may have altered the structures of the cyanine dyes resulting in a gradual loss of DNA binding affinity. Yet, Pasternack *et al.* questioned the reliability of the ethidium displacement assay based on their finding that porphyrins could quench the fluorescence of ethidium bromide. They argued that the simultaneous binding of ethidium and porphyrins with DNA helix can result in Förster resonance energy transfer (FRET) from the former (donor) to the latter (acceptor) at a distance of 25-30 Å because of the spectral overlap of ethidium emission and porphyrin excitation bands. The binding mode seemed to have little effect on the quenching efficiency.[50] Although in our

case some of the dyes monitored display absorption bands overlapping with the ethidium fluorescence, it is believed that the data obtained in this study is still meaningful. The rationale is that the occurrence of FRET requires both the acceptor and the donor to be bound to helical DNA. To have an ethidium replacement percent as high as 95-100%, bleached compounds must be displaced by ethidium from the plasmid because if both remained bound, FRET quenching would have brought down the percentages. Additionally, dyes have lost visible absorbance when bleached, which makes them unqualified acceptors for FRET. Thus, the data regarding bleached dyes should be reliable. However, this might be a concern for unbleached compounds because the 30% drop-off in ethidium replacement of initial compounds may be attributed to the replacement of ethidium and/or the FRET quenching effect. Again, DNA-facilitated FRET quenching is premised on the concurrent binding of cyanine dyes and ethidium. This still indicates that initial ligands remained associated with DNA, though the percent differences between bleached and unbleached compounds might have been inflated. Furthermore, as noted in Figure 3.9, the presence of DNA could remarkably accelerate the absorption degradation of these cyanines. It is assumed that the extinction coefficients (ε) of acceptors may have already dropped to an insignificant level at the point of gel staining. Thus, the quenching efficiency would be reduced accordingly. All in all, our data shows evidence that intact cyanines bind with nucleic acids to a greater degree than their decomposed product(s).

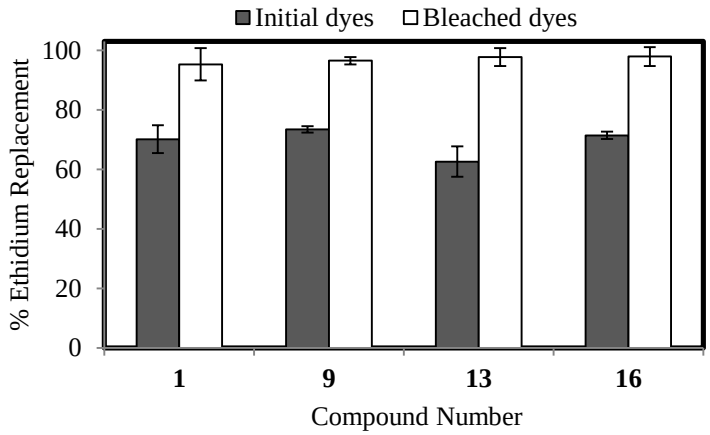

Figure 3.21 A histogram comparing percent ethidium replacement of initial and bleached dyes **1**, **9**, **13**, and **16** at 50 μM

Individual samples were prepared in 10 mM of sodium phosphate buffer (pH 7.0) and 25 μM bp of pUC19 plasmid DNA, and equilibrated in the dark for about 15 min before gel electrophoresis. Representative gel photographs appear in Figure 3.S19, Supplementary data. Data are averaged over three trials and error bars represent standard deviation.

The data suggest that the decrease in thermal cleavage activity of bleached dyes does not depend on a sole factor. It is more likely to be the consequence of combined contributions from the lower dye reducing capacity and lower DNA binding affinity. As Cu(I) is the key contributor to the Fenton-type reaction (Figure 1.4), less Cu(I) formation would lead to lower levels of ROS generation. More importantly, since ROS have short lifetimes, the distance between drugs and plasmid becomes very critical to the cleavage efficiency. Therefore, the failure of a dye to bind could cause inefficient thermal cleavage.

3.10 Studies of High versus Low Thermal Cleavage Dyes

Following the same experimental strategy employed in Section 3.9, two thermally inactive compounds, **20** and **3**, were studied to serve as negative controls (Figures 3.16 and 3.17 respectively). Chromophore **20** contains a phenanthridine heterocycle but lacks a polymethine linker. For dye **3**, a long scaffold is appended from the two benzo[*e*]indole conjugated systems

that are connected by a pentamethine chain. Dye **3** was chosen because it has a pentamethine bridge that does not exert thermo-induced DNA damaging activity. Since both compounds are relatively stable in aqueous solutions (Figures 3.S12 and 3.S9, Supplementary data), herein, only the initial states of **20** and **3** were considered.

3.10.1 Colorimetric detection of copper(I)

The amounts of Cu(I) reduced from Cu(II) by inactive dyes **20** and **3** were monitored. In Figure 3.22, Cu(II) and *L*-ascorbic acid positive controls (red lines) gave a signature absorption band at 480 nm while negative controls in the absence of *L*-ascorbic acid (blue lines) did not. In order to rule out the background interference, the absorbance of Cu(II) + dye samples (purple lines) was corrected by subtracting the absorbance of the dye only (green lines). To our surprise, both dyes exerted reducing capacity comparable to *L*-ascorbic acid upon thermal treatment, as their Cu(I)-BCS complex signals (purple lines) are as intense as the positive controls. The Beer-Lambert Law, that absorbance at a specific wavelength is proportional to the concentration of the analyte (expressed as $A = \varepsilon cl$),[51] allows a rough spectral comparison between Figure 3.22 and Figure 3.19. Compounds **20** and **3** generated lower levels of Cu(I)-BCS complex bands compared to high cleavage compounds (**1**, **9**, **13**, and **16**), which means they have relatively weak copper reducing capacity. Even then, the fact that these two chromophores can reduce Cu(II) to Cu(I) at physiological temperature (37 ℃) in the absence of light is in conflict with their inert behavior toward DNA upon thermal treatment.

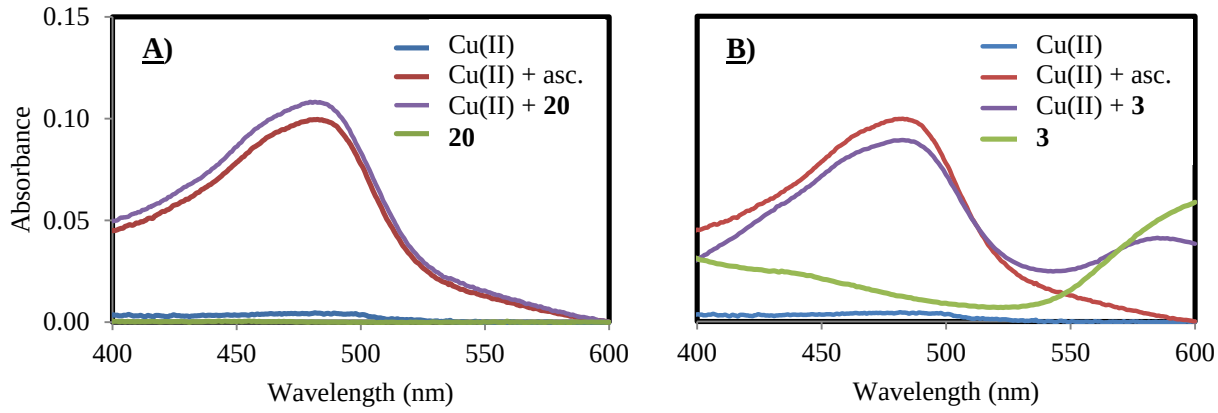

Figure 3.22 UV-visible absorption spectra to monitor Cu(I)-BCS complex formation by compounds **20** and **3**

Reactions containing 10 mM of sodium phosphate buffer (pH 7.0) and one or more of the following reagents were carried out at 37 ℃ for 60 min: 30 μM of $CuCl_2$; 30 μM of *L*-ascorbic acid; 10 μM of dye **A) 20**, or **B) 3**. Samples were equilibrated with 42 μM BCS for an additional 30 min prior to absorbance scanning. Individual dye absorbance was subtracted from its absorbance in the presence of Cu(II). Abbreviation: asc. = *L*-ascorbic acid.

3.10.2 Competitive DNA binding assay

Based on the EtBr displacement study in Subsection 3.9.3, we continued using 50 μM as the dye concentration to evaluate relative DNA binding affinity. In Figure 3.23, we found that over 90% of dyes **20** and **3** were replaced by ethidium, while less than 80% of the highly active dyes (**1**, **9**, **13**, and **16**) were removed from the DNA helical structure. This gives a partial explanation for the inactivity of **20** and **3** in DNA thermal scission. Again, similar to the findings of the bleached dyes, it seems that the lower Cu(II) reduction and the weaker DNA binding are responsible for their negligible DNA damage in the dark at 37 ℃. As we explained in Subsection 3.9.3 regarding to the argument of Pasternack *et al.*, even though FRET between ethidium and cyanines is plausible with DNA helix serving as a scaffold,[50] the lessening of % ethidium replacement suggested higher levels of active cyanines were bound with DNA, compared to

inactive compounds. Besides, energy transfer is not applied to dye **20** because it does not absorb at 590 nm where ethidium fluoresces.

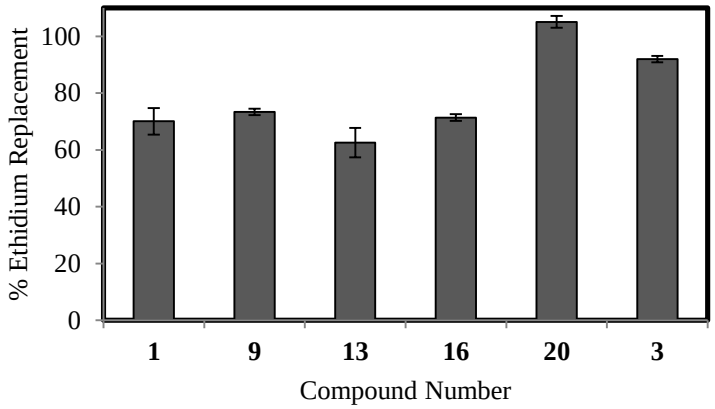

Figure 3.23 Percent ethidium replacement of six unbleached dyes

A histogram compares percent ethidium displacement of unbleached dyes **1**, **9**, **13**, **16**, **20**, and **3** at 50 μM. Individual samples were prepared in 10 mM of sodium phosphate buffer (pH 7.0) and 25 μM bp of pUC19 plasmid DNA, and equilibrated in the dark for about 15 min before gel electrophoresis. Representative gel photographs appear in Figures 3.S19 and 3.S20, Supplementary data. Data are averaged over three trials and error bars represent standard deviation.

3.10.3 DNA thermal cleavage of dyes 20 and 3 in the presence of Cu(II)

As learned from the previous subsections, inactive dyes **20** and **3** exhibited notable Cu(II) reduction capacity but poor nucleic acid binding. It was assumed that increasing the levels of copper in the reaction system might enable dark cleavage by **20** and **3** by compensating their relatively low binding propensity. Hence, one further step was taken in this subsection, in which additional Cu(II) was introduced to the reaction system. The quantitation of the gel images clearly demonstrated that the existence of external Cu(II) activated the potential dark toxicity of dyes **20** and **3** toward plasmid DNA at physiological temperature. The percent thermal cleavage by **20** increased from 2% to 32%, while from 1% to 16% in the case of **3** (Figure 3.24B). This indicates that raising the concentration of Cu(II) may help **20** and **3** overriding the inefficiency in binding with DNA helix and initiate their thermal cleavage activity. The normal level of copper in human tissues varies from around 13 to 55 μM depending on the types of organs[52] and could

be elevated in certain pathological conditions.[17] As a result, it might be harmful if such chromophores were to be approved for clinical studies simply according to their absolute negative dark cleavage at physiological temperature because the hidden toxicity (if any) might be triggered by sufficient copper levels in *in vivo* condition. This study points to the importance to examine the potential dark toxicity of cyanines at physiological levels of metal ions, especially iron and copper.

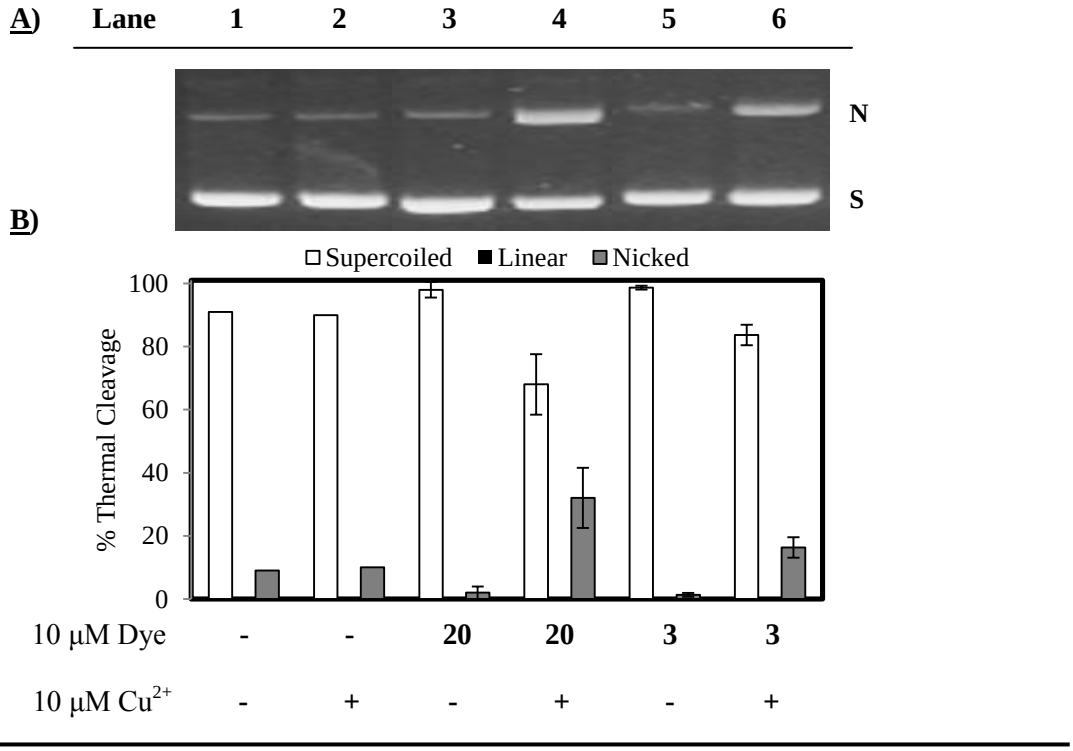

Figure 3.24 A 1.5 % non-denaturing agarose gel **A)** and corresponding histogram **B)** showing percent DNA thermal cleavage by **20** or **3** in the absence or presence of Cu(II) at 37 ℃ for 24 h

Reactions were carried out in darkness. Samples contained 10 mM of sodium phosphate buffer (pH 7.0) and 25 μM bp of pUC19 plasmid DNA. Lanes 1, 3, and 5: in the absence of $CuCl_2$; lanes 2, 4, and 6: in the presence of 10 μM $CuCl_2$. Data (except for controls) are averaged over three trials and error bars represent standard deviation. Abbreviations: N = nicked; S = supercoiled.

4 CONCLUSIONS

Here, we firstly report an investigation of the pentamethine cyanine **1**. The pUC19 plasmid DNA thermal cleavage by **1** depends on the reaction temperature and duration. Mechanistic studies suggest an involvement of copper ions and the formation of hydroxyl radicals. Cleavage through a hydrolytic pathway is unlikely because T4 DNA ligase had no apparent effect on the reaction products. Time course UV-visible absorbance analyses show that most of the cyanines are unstable in aqueous buffer systems. Although the exact cause of dye bleaching is not fully understood, experimental studies suggest the phenomenon is related to a combined process of self-aggregation and autoxidation by reactive oxygen species.

Taken together, the bleaching tendency in protic solvents and DNA thermal cleavage by **1** seem to associate with the spontaneous generation of reactive oxygen species in the dark. We found evidence consistent with the hypothesis.[8, 44, 47] It is said that the elongation of the polymethine chain evokes a distortion of electronic distribution along the bridge and establishes reactive positions for nucleophilic reactions on the side of the cationic nitrogen.[8, 41] If the redox potential of a cyanine reaches to a point lower than that of Cu(II) (E° [Cu(II)/Cu(I)] = 0.161 V at pH 7.0),[46a] it will be able to reduce Cu(II) to Cu(I) which generates $O_2^{\cdot -}$ upon a reaction with $^3O_2$.[4a, 11a, 14] (For example, the standard reduction potential of the well-studied indocyanine green (ICG) is -0.59 V.[8]) Eventually, hydroxyl radicals (·OH) are formed through a Fenton-type reaction (Figure 1.4).[4a, 11a] Plasmid DNA is damaged upon exposure to ·OH.[30] According to relevant literature, $O_2^{\cdot -}$ and ·OH could fragment the polymethine bridge by a one-electron oxidation pathway and thus perturb the π-π conjugation system.[2a, 9-10, 43] This might account for the rapid dye absorbance attenuation in certain polymethine buffer solutions. It should be emphasized that the process can be achieved in the absence of light and that trace amounts of

adventitious Cu(II) in the plasmid DNA and/or in laboratory solutions may be sufficient to trigger the reaction.[35] This strongly implies increasing the wavelength of absorption maxima, or apparently lengthening the polymethine chain could, in darkness, elicit plasmid damage and dye decomposition in aqueous solutions. Nonetheless, from our research, these drawbacks may be overcome by stabilizing dyes with an electron-withdrawing group (EWG) in the center of the methine bridge. It is presumed that the EWG may draw the electron density towards the bridge side bearing a positive charge and partially correct the asymmetric electronic distribution status.

The results of the study on DNA thermal cleavage by twenty-four cyanine analogs (**1**-**24**) at physiological temperature (37 ℃) in the absence of light and external reducing agents are consistent with the hypothesis discussed above. It is found that introducing a halogen substituent at the center position of a polymethine bridge dramatically reduced the thermal cleavage activity of the dye (*e.g.* **10**, **14**, and **15**). A stronger EWG seems to have a higher inhibitory effect on the DNA thermal cleavage activity. As shorter methine linkers are more likely to maintain a balanced distribution of electrons, trimethine cyanines (**8**, **11**, and **12**) appear to have lower thermo-induced DNA cleaving property. Simple phenanthridine dyes (**20**-**21** and **23**-**24**) without polymethine components are inert compounds in the dark. Furthermore, the dye bleaching rates in buffer solution seem to favor the assumption. Thermally inactive dyes (**5**-**7** and **20**-**21**) are stable in sodium phosphate buffer, while the small absorption attenuation of low cleavage dyes (**2**-**4** and **22**) are mainly related to self-aggregation. Trimethine (**8**, **11**, and **12**) and halogen-substituted pentamethine dyes (**10**, **14**-**15**, and **17**) appear to be more stable in comparison with the unsubstituted pentamethine analogs (**9**, **13**, and **16**). The effects of longer polymethine chains and counter anions other than iodide are still in need of more analysis. Yet, based on what is

understood to date, it is assumed that methine linkers with equal or more than seven carbons will have higher dark cleavage activity and lower stability in aqueous solutions.

Lastly, we have compared the differences of chemical properties between intact and bleached dyes, as well as between highly active and inactive compounds. We have observed much lower thermo-induced DNA damage in the cases of bleached compounds. The phenomenon is most likely caused by a decreased capability of reducing Cu(II) to Cu(I) and the weaker DNA binding affinity of bleached and inactive cyanines.

Overall, this report has provided new insights into the reactivity of NIR cyanine dyes in aqueous solutions. A mechanism for thermally induced DNA cleavage by cyanine dyes is proposed. We investigated the rationale behind the decrease in thermal cleavage activity of bleached and inactive compounds in terms of Cu(II) reduction and relative levels of DNA binding. We believe that our findings will benefit future NIR photosensitizer design, by enabling chemists to synthesize dyes that are stable in aqueous solutions with minimal potential toxicity under dark conditions.

REFERENCES

1. (a) Jedrzejewska, B.; Bajorek, A.; Moraczewska, J., Interaction of carbocyanine dyes with DNA: synthesis and spectroscopic studies. *Appl. Spectrosc.* **2013,** *67* (6), 672-680; (b) Mishra, A.; Behera, R. K.; Behera, P. K.; Mishra, B. K.; Behera, G. B., Cyanines during the 1990s: a review. *Chem. Rev.* **2000,** *100*, 1973-2011.

2. (a) Chen, X.; Peng, X.; Cui, A.; Wang, B.; Wang, L.; Zhang, R., Photostabilities of novel heptamethine 3H-indolenine cyanine dyes with different N-substituents. *J. Photochem. Photobiol. A: Chem.* **2006,** *181*, 79-85; (b) Ormond, A. B.; Freeman, H. S., Dye sensitizers for photodynamic therapy. *Materials* **2013,** *6*, 817-840; (c) Pandey, R. K.; James, N.; Chen, Y.; Dobhal, M. P., Cyanine dye-based compounds for tumor imaging with and without photodynamic therapy. *Top Heterocycl. Chem.* **2008,** *14*, 41-74.

3. Armitage, B. A., Cyanine dye-DNA interactions: intercalation, groove binding, and aggregation. *Top Curr. Chem.* **2005,** *253*, 55-76.

4. (a) Castano, A. P.; Demidova, T. N.; Hamblin, M. R., Mechanisms in photodynamic therapy: part one—photosensitizers, photochemistry and cellular localization. *Photodiagnosis Photodyn. Ther.* **2004,** *1*, 279-293; (b) Yoon, I.; Li, J. Z.; Shim, Y. K., Advance in photosensitizers and light delivery for photodynamic therapy. *Clin. Endosc.* **2013,** *46* (1), 7-23.

5. Reversible small molecule–nucleic acid interactions. In *Nucleic Acids in Chemistry and Biology*, 3 ed.; Blackburn, G. M.; Gait, M. J.; Loakes, D.; Williams, D. M., Eds. RSC: Cambridge, UK, 2006; pp 341-382.

6. (a) Kim, J. S.; Kodagahally, R.; Strekowski, L.; Patonay, G., A study of intramolecular H-complexes of novel bis(heptamethine cyanine) dyes. *Talanta* **2005,** *67*, 947-954; (b) Shang, Q.; Xiang, J.; Yang, Q.; Tang, Y., Interaction between aggregates of cyanine dyes and biomolecules. In *J-Aggregates*, Kobayashi, T., Ed. World Scientific: Hackensack, NJ, 2012; Vol. 2.

7. Henary, M.; Mojzych, M., Stability and reactivity of polymethine dyes in solution. *Top Heterocycl. Chem.* **2008,** *14*, 221-238.

8. Barros, T. C.; Toma, S. H.; Toma, H. E.; Bastos, E. L.; Baptista, M. S., Polymethine cyanine dyes in β-cyclodextrin solution: multiple equilibria and chemical oxidation. *J. Phys. Org. Chem.* **2010,** *23*, 893-903.

9. Oushiki, D.; Kojima, H.; Terai, T.; Arita, M.; Hanaoka, K.; Urano, Y.; Nagano, T., Development and application of a near-infrared fluorescence probe for oxidative stress based on differential reactivity of linked cyanine dyes. *J. Am. Chem. Soc.* **2010,** *132*, 2795-2801.

10. Chen, P.; Li, J.; Qian, Z.; Zheng, D.; Okasaki, T.; Hayami, M., Study on the photooxidation of a near-infrared-absorbing benxothiazolone cyanine dye. *Dyes Pigments* **1998,** *37* (3), 213-222.

11. (a) Qian, S. Y.; Buettner, G. R., Iron and dioxygen chemistry is an important route to initiation of biologic free radical oxidations: An electron paramagnetic resonance spin trapping study. *Free Radical Biol. Med.* **1999,** *26*, 1447-1456; (b) Ros, T. D.; Spalluto, G.; Boutorine, A. S.; Bensasson, R. V.; Prato, M., DNA-photocleavage agents. *Curr. Pharm. Des.* **2001,** *7*, 1781-1821.

12. (a) Hatz, S.; Poulsen, L.; Ogilby, P. R., Time-resolved singlet oxygen phosphorescence measurements from photosensitized experiments in single cells: effects of oxygen diffusion and oxygen concentration. *Photoch. Photobiol.* **2008,** *84*, 1284-1290; (b) Makrigiorgos, G. M., Detection of chromatin-associated hydroxyl radicals generated by DNA-bound metal compounds and antitumor antibiotics. In *Metal ions in biological systems*, Sigel, A.; Sigel, H., Eds. CRC Press: Boca Raton, 1999; pp 521-545; (c) Moan, J.; Berg, K., The photodegradation of porphyrins in cells can be used to estimate the lifetime of singlet oxygen. *Photoch. Photobiol.* **1991,** *53*, 549-553.

13. Wood, P. M., The potential diagram for oxygen at pH 7. *Biochemistry* **1988,** *253*, 287-289.

14. (a) Flowers, L.; Ohnishi, S. T.; Penning, T. M., DNA strand scission by polycyclic aromatic hydrocarbon o-quinones: role of reactive oxygen species, Cu(II)/Cu(I) redox cycling, and o-semiquinone anion radicals. *Biochemistry* **1997,** *36*, 8640-8648; (b) Rahman, A.; Shahabuddin; Hadi, S. M.; Parish, J. H.; Ainley, K., Strand scission in DNA induced by quercetin and Cu(II): role of Cu(I) and oxygen free radicals. *Carcinogenesis* **1989,** *10* (10), 1833-1839.

15. Mapp, C. T.; Owens, E. A.; Henary, M.; Grant, K. B., Oxidative cleavage of DNA by pentamethine carbocyanine dyes irradiated with long-wavelength visible light. *Bioorg. Med. Chem. Lett.* **2013,** *24*, 214-219.

16. Sambrook, J.; Fritsch, E. F.; Maniatis, T., *Molecular Cloning: A Laboratory Manual*. 2nd ed.; Cold Spring Harbor Laboratory: Cold Spring Harbor, NY, 1989.

17. Sinha, B. K.; Leinisch, F.; Bhattacharjee, S.; Mason, R. P., DNA cleavage and detection of DNA radicals formed from hydralazine and copper (ii) by ESR and immuno-spin trapping. *Chem. Res. Toxicol.* **2014,** *27*, 674-682.

18. (a) Oikawa, S.; Kawanishi, S., Distinct mechanisms of site-specific DNA damage induced by endogenous reductants in the presence of iron(III) and copper(II). *Biochim. Biophys. Acta* **1998,** *1399*, 19-30; (b) Valko, M.; Izakovic, M.; Mazur, M.; Rhodes, C. J.; Telser, J., Role of oxygen radicals in DNA damage and cancer incidence. *Mol. Cell Biochem.* **2004,** *266*, 37-56.

19. (a) Netto, L. E. S.; Da Costa Ferreira, A. M.; Augusto, O., Iron(III) binding in DNA solutions: Complex formation and catalytic activity in the oxidation of hydrazine derivatives. *Chem. Biol. Interactions* **1991,** *79*, 1-14; (b) Sagripanti, J.-L.; Goering, P. L.; Lamanna, A., Interaction of copper with DNA and antagonism by other metals. *Toxicol. Appl. Pharm.* **1991,** *110*, 477-485.

20. Prakash, S.; Tuli, G. D.; Basu, S. K.; Madan, R. D., Halides and oxy-halides of main group elements. In *Advanced Inorganic Chemistry*, S. Chand & Company Ltd.: New Delhi, India, 2000; Vol. 1, p 940.

21. Wong, A.; Huang, C.-H.; Crooke, S. T., Mechanism of deoxyribonucleic acid breakage induced by 4'-(9-acridiny1amino)methanesulfon-m-anisidide and copper: Role for cuprous ion and oxygen free radicals. *Biochemistry* **1984,** *23*, 2946-2952.

22. Williams, D. E.; Kassai, M.; Gude, L.; Fernandez, M.-J.; Lorente, A.; Grant, K. B. An remarkable DNA photocleaving agent: a photo-active tri-nuclear Cu(II) complex based on hexaazatriphenylene. Georgia State University, Atlanta, GA, 2014.

23. Hullar, T.; Anastasio, C., Yields of hydrogen peroxide from the reaction of hydroxyl radical with organic compounds in solution and ice. *Atmos. Chem. Phys.* **2011,** *11*, 7209-7222.

24. Prasad Naidu, D. V.; Rajan, R.; Kumar, R.; Gandhi, K. S.; Arakeri, V. H.; Chandrasekaran, S., Modelling of a batch sonochemical reactor. *Chem. Eng. Sci.* **1994,** *49* (6), 877-888.

25. Eberhardt, M. K.; Colina, R., The reaction of OH radicals with dimethyl sulfoxide. A comparative study of Fenton's reagent and the radiolysis of aqueous dimethyl sulfoxide solutions. *J. Org. Chem.* **1988,** *53*, 1071-1074.

26. Tanaka, N.; Itoh, S., Density functional theory studies on the addition and abstraction reactions of OH radical with benzoate anion. *Open J. Phys. Chem.* **2013,** *3*, 7-13.

27. (a) Juda, G. A.; Shepard, E. M.; Elmore, B. O.; Dooley, D. M., A comparative study of the binding and inhibition of four copper-containing amine oxidases by azide: implications for the role of copper during the oxidative half-reaction. *Biochemistry* **2006,** *45*, 8788-8800; (b) Schwartz, B.; Olgin, A. K.; Klinman, J. P., The role of copper in topa quinone biogenesis and catalysis, as probed by azide inhibition of a copper amine oxidase from yeast. *Biochemistry* **2001,** *40*, 2954-2963.

28. Merkel, P. B.; Nilsson, R.; Kearns, D. R., Deuterium effects on singlet oxygen lifetimes in solutions. A new test of singlet oxygen reactions. *J. Am. Chem. Soc.* **1971,** *94* (3), 1030-1031.

29. (a) Komiyama, M.; Takeda, N.; Shigekawa, H., Hydrolysis of DNA and RNA by lanthanide ions: Mechanistic studies leading to new applicaitons. *Chem. Commun.* **1999**, 1443-1451; (b) Komiyama, M.; Takeda, N.; Takahashi, Y.; Uchida, H.; Shiiba, T.; Kodama, T.; Yashiro, M., Efficient and oxygen-independent hydrolysis of single-stranded DNA by cerium(IV) ion. *J. Chem. Soc. Perkin Trans.* **1995,** *2*, 269-274.

30. Gowda K. R., S.; Mathew, B. B.; Sudhamani, C. N.; Bhojya Naik, H. S., Mechanism of DNA binding and cleavage. *Biomed. Biotecch.* **2014,** *2* (1), 1-9.

31. Tabor, S., Enzymatic manipulation of DNA and RNA. In *Current Protocols in Molecular Biology*, Ausubel, F. M.; Brent, R.; Kingston, R. E.; Moore, D. D.; Seidman, J. G.; Smith, J. A.; Struhl, K., Eds. John Wiley & Sons: New York, NY, 1995; Vol. 1, p 3.14.1.

32. Hegyi, G.; Kardos, J.; Kovacs, M.; Malnasi-Csizmadia, A.; Nyitray, L.; Pal, G.; Radnai, L.; Remenyi, A.; Venekei, I., Analysis of plasmid DNA by gel electrophoresis. In *Introduction to Practical Biochemistry*, Eötvös Loránd University: 2013; p 149.

33. (a) Schnaith, L. M. T.; Hanson, R. S.; Que, L. J., Double-stranded cleavage of pBR322 by a diiron complex via a "hydrolytic" mechanism. *Proc. Natl. Acad. Sci.* **1994,** *91*, 569-573; (b) Qian, J.; Ma, X.; Tian, J.; Gu, W.; Shang, J.; Liu, X.; Yan, S., Hydrolytic cleavage of double-strand DNA by the water-soluble dicobalt(III) complexes of 1,4,7-Triazacyclononane-N-acetate. *J. Inorg. Biochem.* **2010,** *104*, 993-999.

34. Burch, P. E. DNA damage and cell lethality by photodynamically produced oxygen radicals. Doctor of Philosophy thesis, Rice University, Houston, TX, 1989.

35. (a) Rongoni, E.; Scafati, A.; Matzeu, M.; Belli, M.; Onori, G.; Reale, A.; Balerna, A.; Bianconi, A.; Bernieri, E., UV-induced reduction of Cu(II) in DNA complex studied by Cu-K-edge XANES. *Biopolymers* **1986,** *25*, 217-221; (b) Wacker, W. E. C.; Vallee, B. L., Nucleic acids and metals: I. Chromium, manganese, nickel, iron, and other metals in ribonucleic acid from diverse biological sources. *J. Biol. Chem.* **1959,** *234*, 3257-3262; (c) Zimmer, C.; Luck, G.; Fritzsche, H.; Triebel, H., DNA-copper(II) complex and the DNA conformation. *Biopolymers* **1971,** *10*, 441-463; (d) Hutchinson, F., Published data on mutagenesis by ionizing radiation of plasmids in solution probably reflect in part the specificity of adventitious transition metal ions complexed to the DNA. *Mutat. Res.* **1990,** *281*, 261-266.

36. Wilson, W. D.; Tanious, F. A.; Fernandez-Saiz, M.; Rigl, C. T., Evaluation of drug-nucleic acid interactions by thermal melting curves. In *Methods in Molecular Biology, Vol. 90: Drug-DNA Interaction Protocols*, Fox, K. R., Ed. Human Press: Clifton, NJ, 1997; pp 219-240.

37. Wilson, W. D.; Ratmeyer, L.; Zhao, M.; Strekowski, L.; Boykin, D., The search for structure-specific nucleic acid-interactivedrugs: effects of compound structure on RNA versus DNA interaction strength. *Biochemistry* **1993,** *32*, 4098-4104.

38. Biver, T.; Biasi, A. D.; Secco, F.; Venturini, M.; Yarmoluk, S., Cyanine dyes as intercalating agents: kinetic and thermodynamic studies on the DNA/Cyan40 and DNA/CCyan2 systems. *Biophysical* **2005,** *89*, 374-383.

39. Ishihara, M.; Fujisawa, S., Photooxygenation, photodegradation and antioxidative activity of platonin, a cyanine photosensitizing dye. *in vivo* **2007,** *21*, 163-174.

40. Jenkins, T. C., Optical absorbance and fluorescence techniques for measuring DNA-drug interactions. In *Methods in Molecular Biology, Vol. 90: Drug-DNA Interaction Protocols*, Fox, K. R., Ed. Human Press: Clifton, NJ, 1997; pp 195-218.

41. Terry, C. A.; Fernandez, M.-J.; Gude, L.; Lorente, A.; Grant, K. B., Physiologically relevant concentrations of NaCl and KCl increase dna photocleavage by an N-substituted 9-aminomethylanthracene dye. *Biochemistry* **2011,** *50,* 10375-10389.

42. Beckford, G.; Owens, E.; Henary, M.; Patonay, G., The solvatochromic effects of side chain substitution on the binding interaction of novel tricarbocyanine dyes with human serum albumin. *Talanta* **2012,** *92,* 45-52.

43. Vlaskin, V. I.; Zakhidov, U.; Nizamov, N., Spectroscopic study of bleaching of some cyanine dyes in solution and in polyvinyl alcohol films. *Appl. Spectrosc.* **1988,** *48* (4), 404-406.

44. Bouit, P.-A. A., C.; Toupet, L.; Guennic, B. L.; Andraud, C.; Maury, O., Continuous symmetry breaking induced by ion pairing effect in heptamethine cyanine dyes: beyond the cyanine limit. *J. Am. Chem. Soc.* **2010,** *132,* 4328-4335.

45. Bagchi, P.; Morgan, M. T.; Bacsa, J.; Fahrni, C. J., Robust affinity standards for Cu(I) biochemistry. *J. Am. Chem. Soc.* **2013,** *135* (49), 18549-18559.

46. (a) Harris, D. C., *Quantitative Chemical Analysis*. 8 ed.; W. H. Freeman and Company: New York, NY, 2010; (b) Srinivasan, K., Polarographic and redox potential studies on copper(I) and copper(II) and their complexes. *J. Electroanal. Chem. Interfac.* **1971,** *31* (1), 257-263.

47. Nakagawa, Y.; Hori, H.; Yamamoto, I.; Terada, H., Characteristic bleaching profiles of cyanine dyes depending on active oxygen species in the controlled Fenton reaction. *Biol. Pharm. Bull.* **1993,** *16* (11), 1061-1064.

48. Nani, R. R.; Kelley, J. A.; Ivanic, J.; Schnermann, M. J., Reactive species involved in the regioselective photooxidation of heptamethine cyanines. *Chem. Sci.* **2015,** *6,* 6556-6563.

49. Talrose, V.; Stern, E. B.; Goncharova, A. A.; Messineva, N. A.; Trusova, N. V.; Efimkina, M. V., UV/Visible spectra. In *NIST Chemistry WebBook*, Linstrom, P. J.; Mallard, W. G., Eds. National Institute of Standards and Technology: Gaithersburg, MD, 2015; p 69.

50. Pasternack, R. F.; Caccam, M.; Keogh, B.; Stephenson, T. A.; Williams, A. P.; Gibbs, E. J., Long-range fluorescence quenching of ethidium ion by cationic porphyrins in the presence of DNA. *J. Am. Chem. Soc.* **1991,** *113,* 6835-6840.

51. Campbell, I. D.; Dwek, R. A., Ultraviolet and visible absorption spectroscopy. In *Biological Spectroscopy*, Benjamin/Cummings: 1984; pp 61-88.

52. Lech, T.; Sadlik, J. K., Copper concentration in body tissues and fluids in normal subjects of southern poland. *Biol. Trace. Elem. Res.* **2007,** *118* (1), 10-15.

APPENDICES

Supplementary data

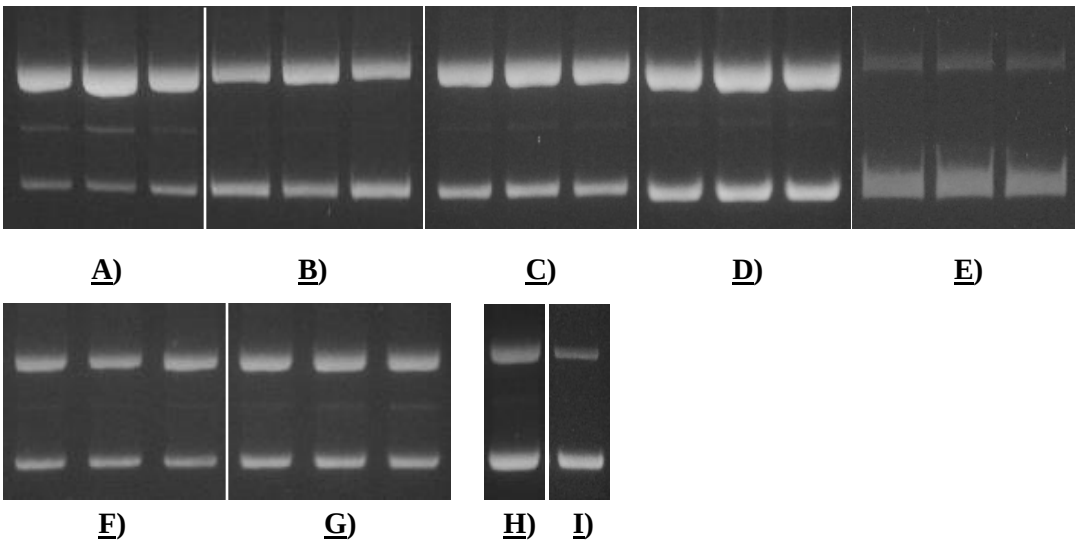

Figure 3.S1 Photographs of representative 1.5% non-denaturing agarose gels showing thermal cleavage of 25 μM bp pUC19 plasmid DNA by 10 μM of **1**. Reactions were run in darkness at 37℃ for 24 h. **A)** in the absence of added chemical reagents, and in the presence of **B)** 100 mM sodium benzoate, **C)** 100 mM sodium azide, **D)** 84% (v/v) D_2O, **E)** 100 mM EDTA, **F)** 50 mM KI, **G)** 4 μL DMSO, **H)** 5 mM EDTA, and **I)** 50 mM EDTA.

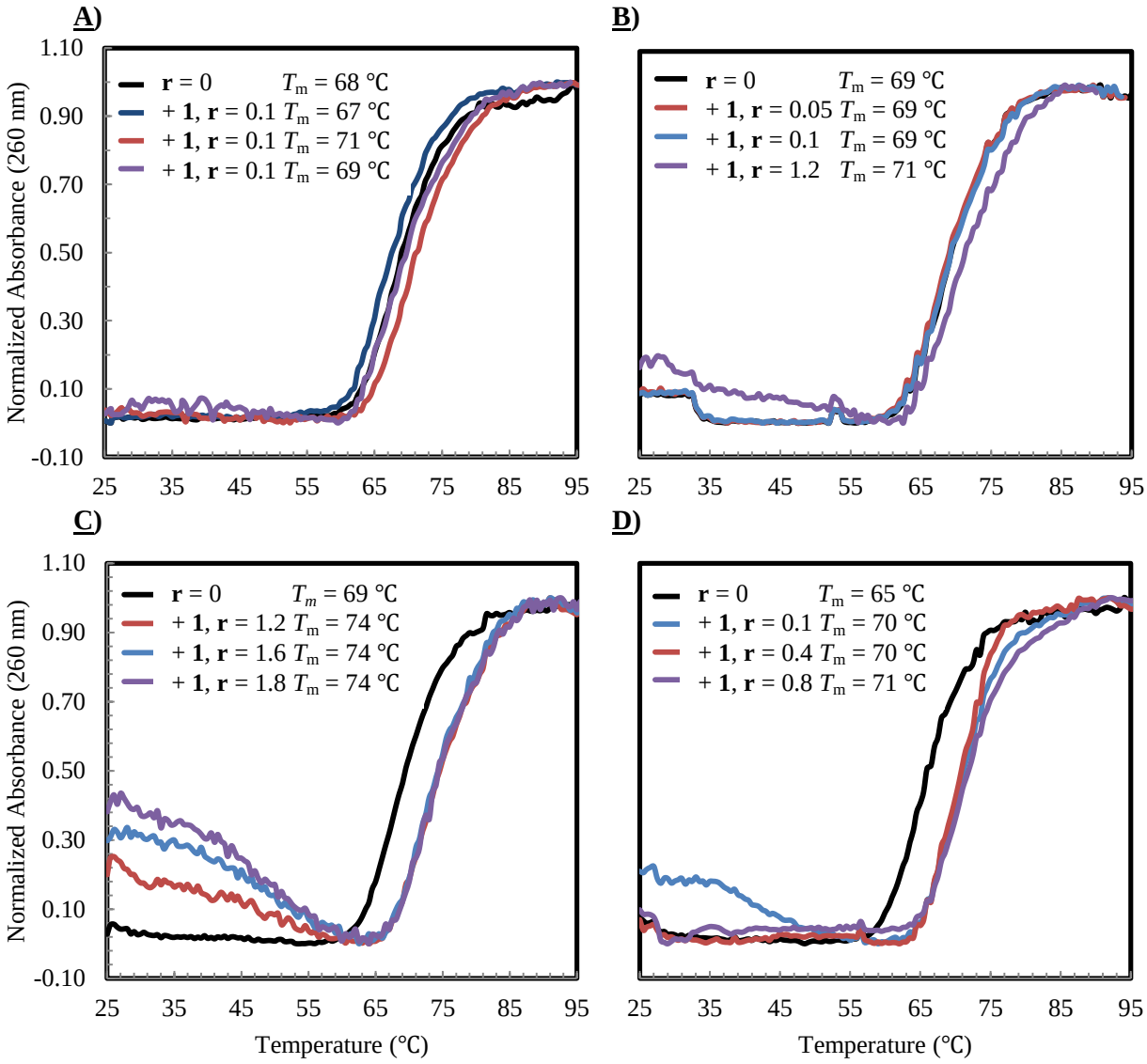

Figure 3.S2 Normalized thermal melting curves of 25 μM bp CT DNA in the absence and presence of 1.25 to 45 μM of **1**. Abbreviations: **r** = compound **1** to DNA bp molar ratio = [**1**] / [DNA bp]; T_m = DNA melting temperature.

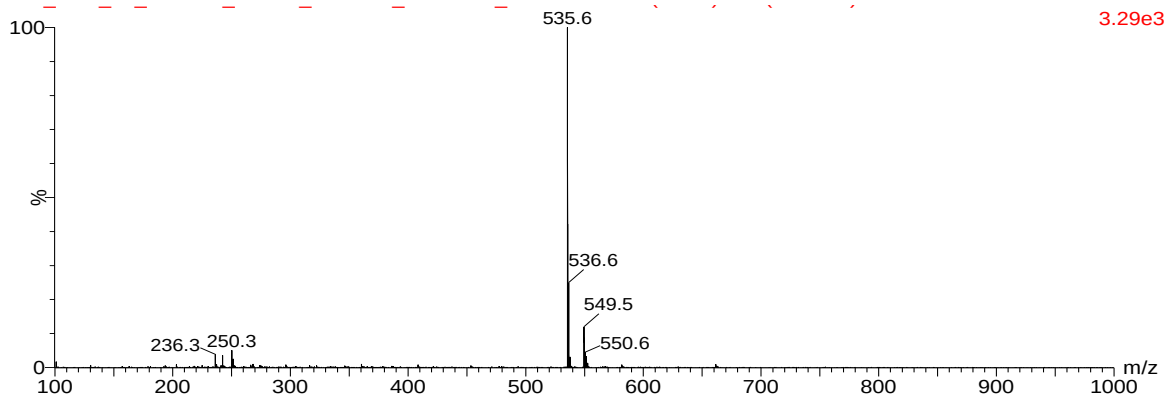

Figure 3.S3 Mass spectrum of 10 μM cyanine dye **1** in 50% MeOH/H_2O (v/v) after over 1 h equilibration in the dark.

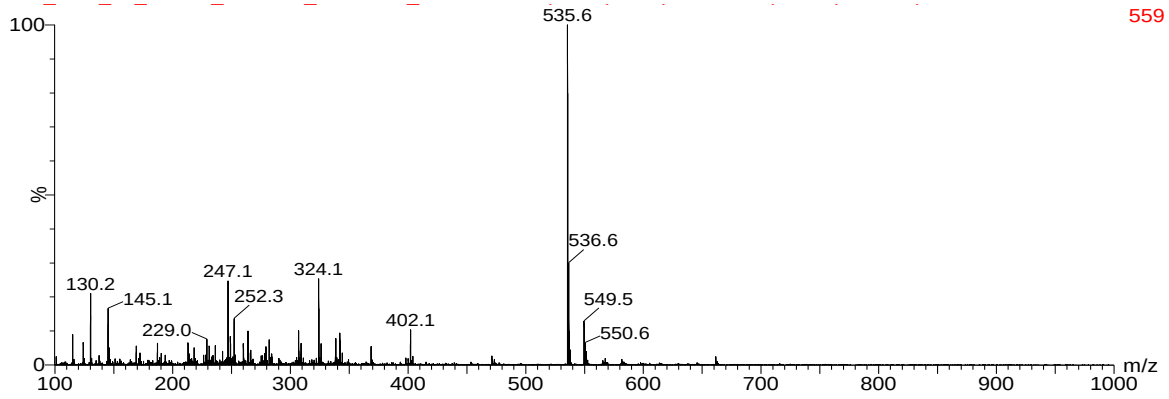

Figure 3.S4 Mass spectrum of 10 μM cyanine dye **1** in MeOH with no equilibration time.

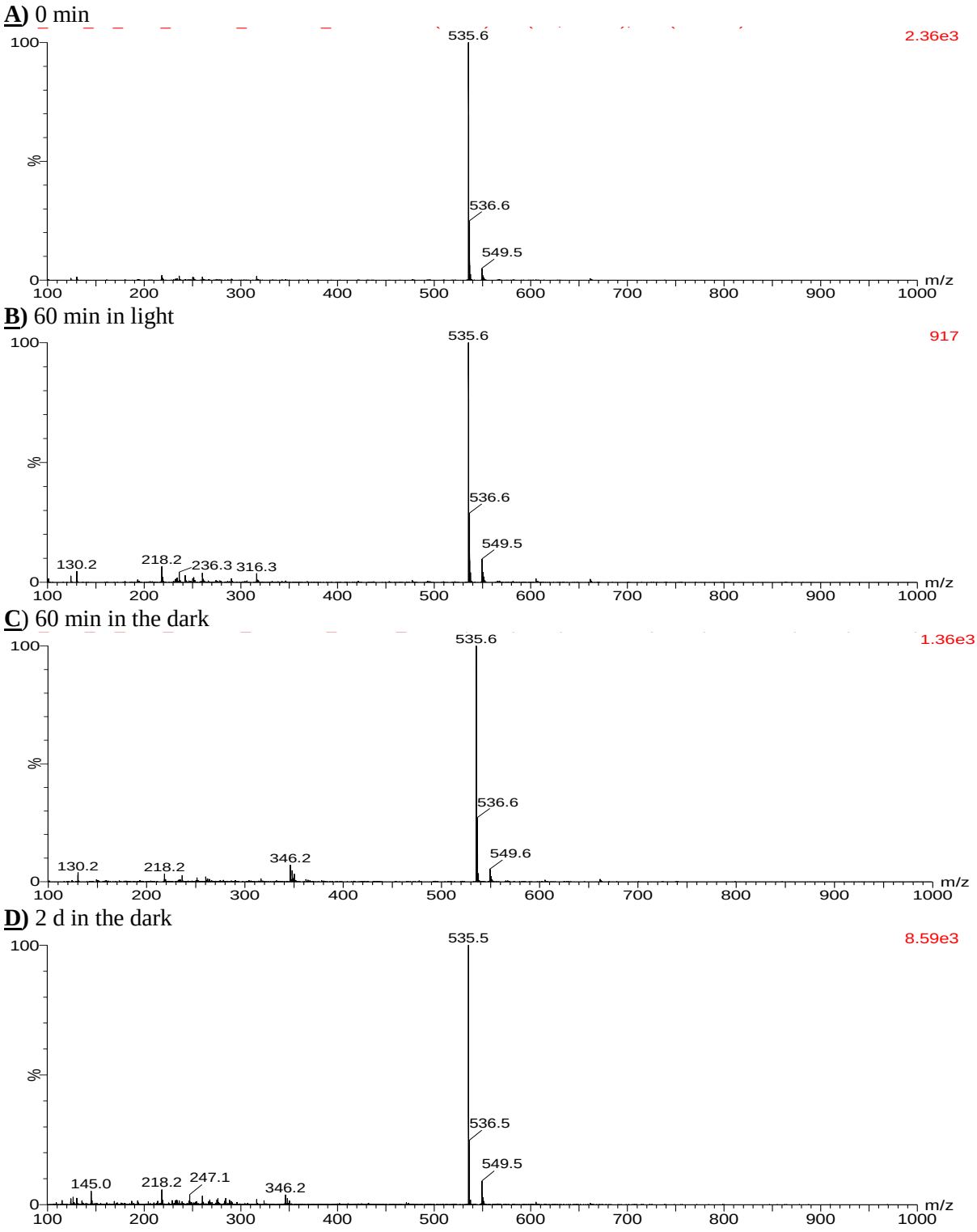

Figure 3.S5 Mass spectra of 10 μM cyanine dye **1** in ACN **A)** with no equilibration time, **B)** after 60-min equilibration time in light, **C)** after 60-min equilibration time in the dark, and **D)** after two-day dark equilibration at room temperature.

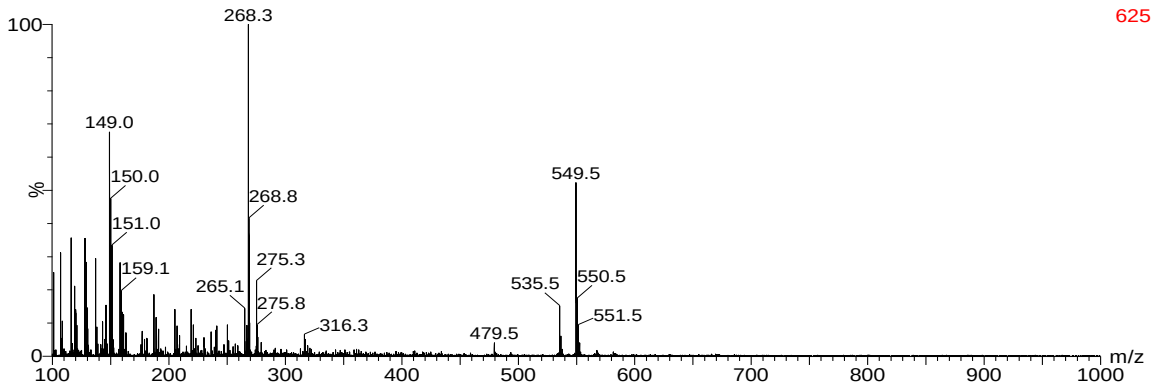

Figure 3.S6 Mass spectrum of 10 μM cyanine dye **1** in 50% MeOH/H_2O (v/v) with 20 μM Cu(II) and 0.1% formic acid after over 1-h equilibration in the dark.

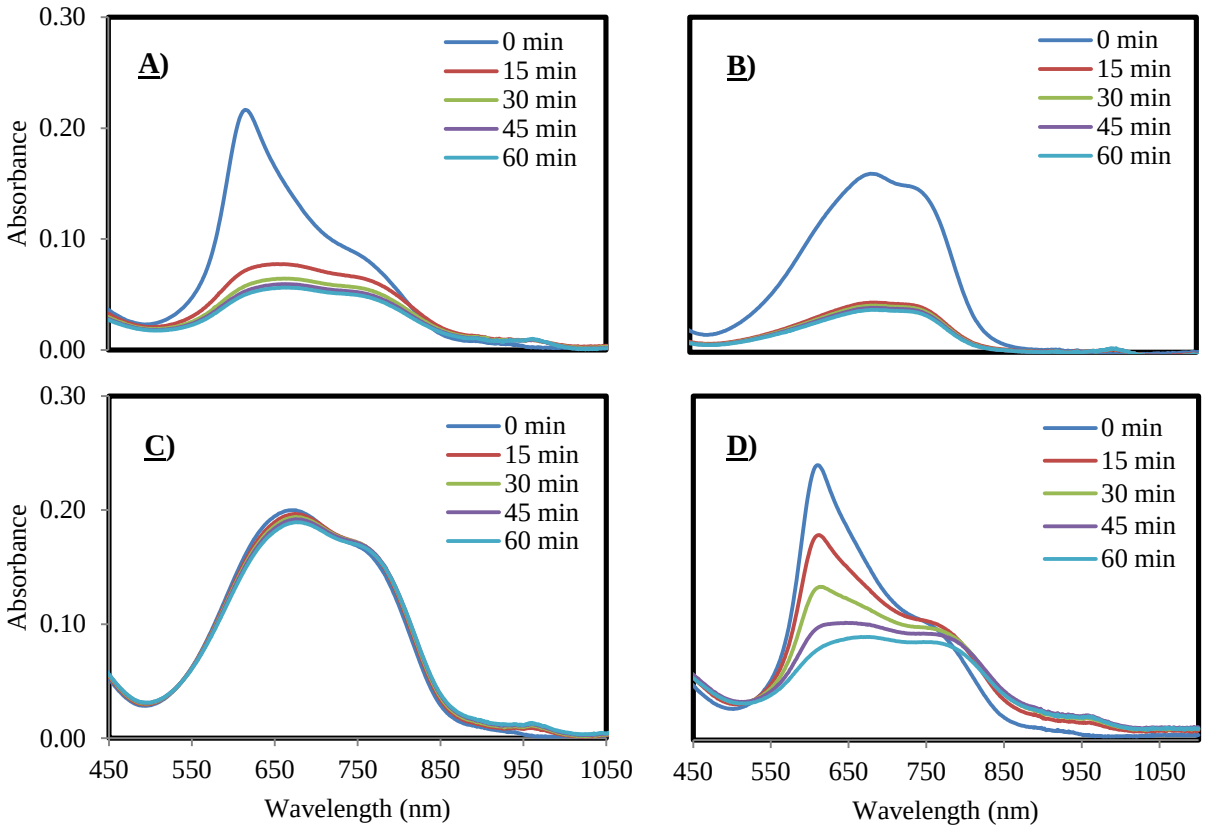

Figure 3.S7 Time course UV-vis absorption spectra of 10 μM cyanines **1** in 10 mM sodium phosphate buffer **A)** in the absence of reagents, or in the presence of **B)** 300 μM of CT DNA, **C)** 100 μM of BCS, or **D)** 50 mM of EDTA. The absorbance was recorded at intervals of 15 min up to 1 h.

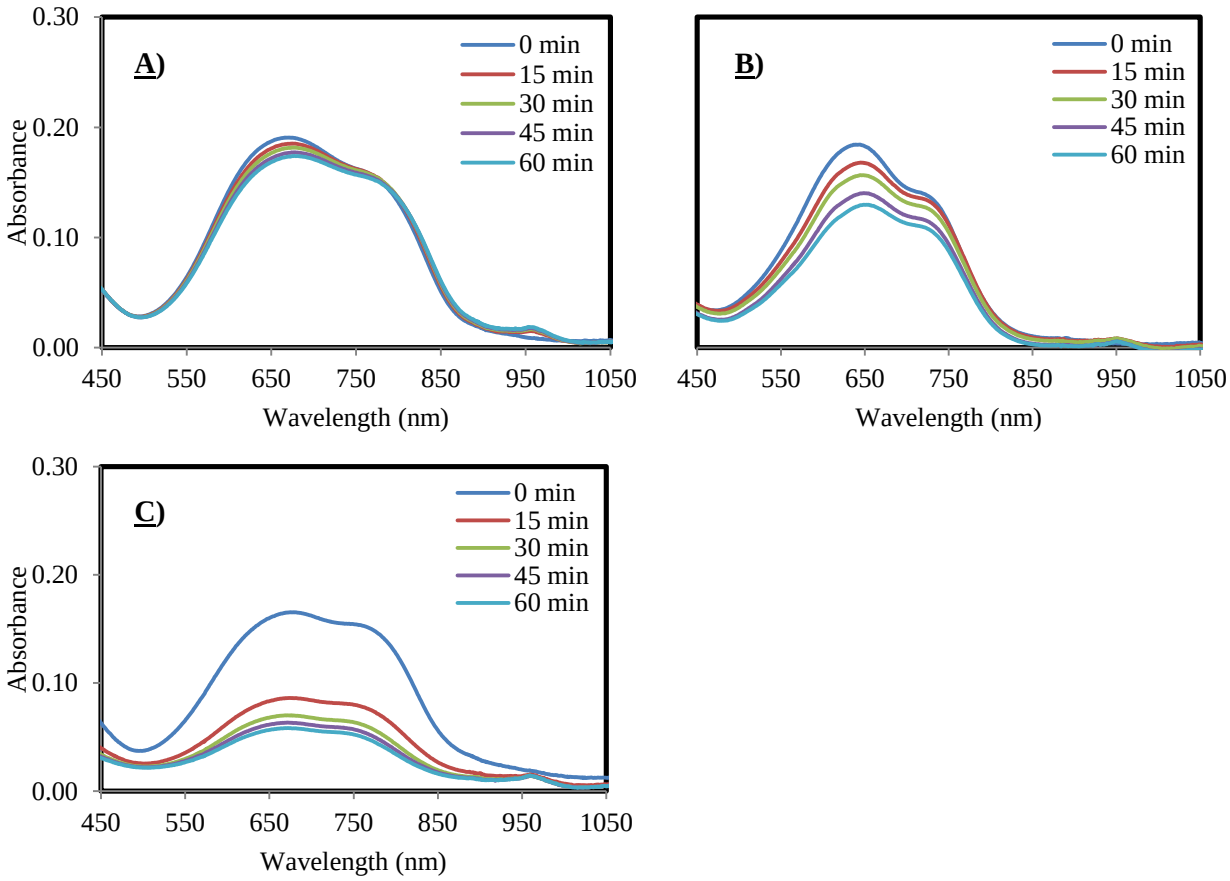

Figure 3.S8 Time course UV-vis absorption spectra of 10 μM cyanines **1** in 10 mM sodium phosphate buffer in the presence of **A)** 50 mM of KI, **B)** 25 U/μL of catalase, or **C)** 100 mM of sodium benzoate. The absorbance was recorded at intervals of 15 min up to 1 h.

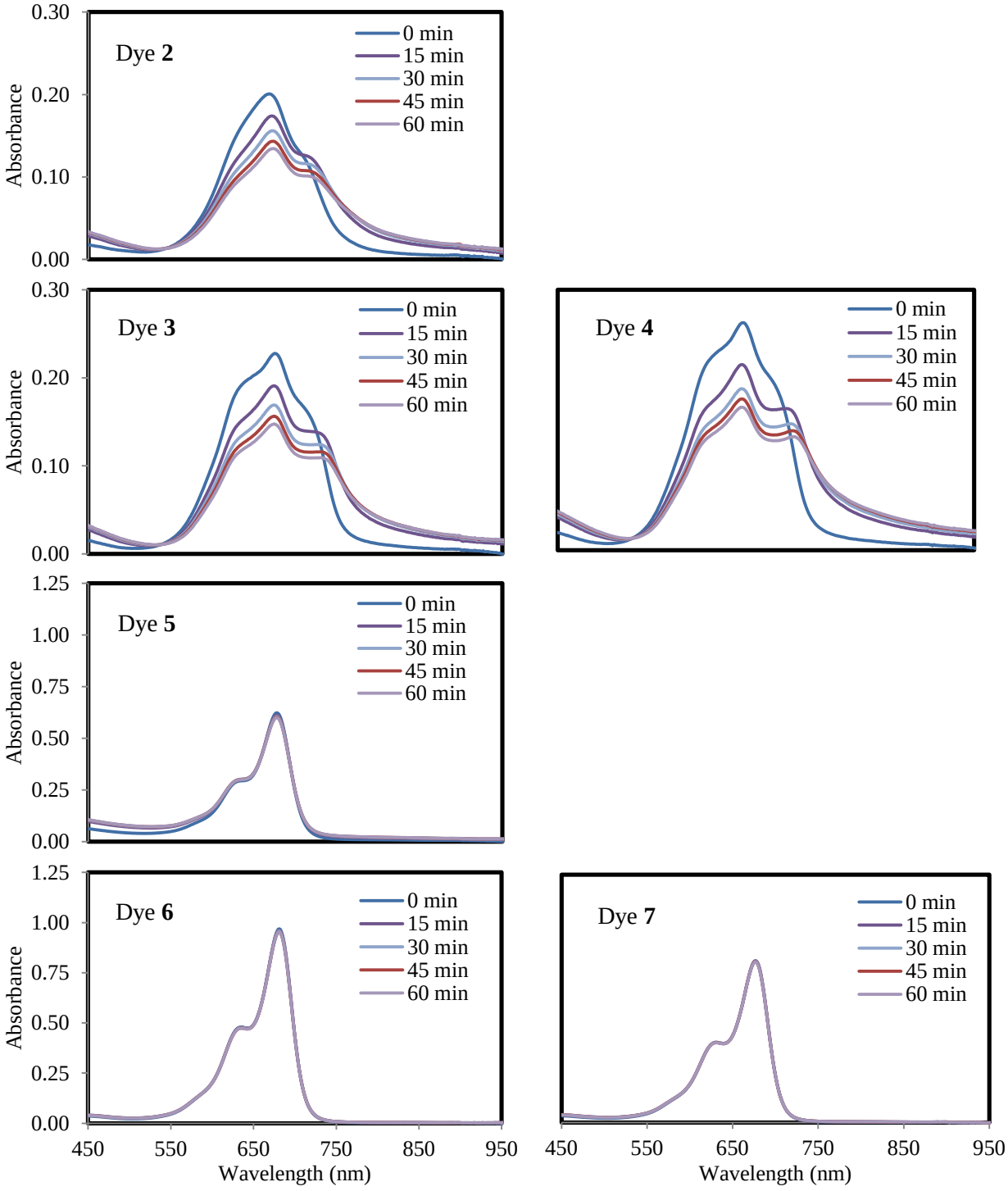

Figure 3.S9 Time course UV-vis absorption spectra of 10 μM cyanines **2-7** in 10 mM sodium phosphate buffer. The absorbance was recorded at intervals of 15 min up to 1 h.

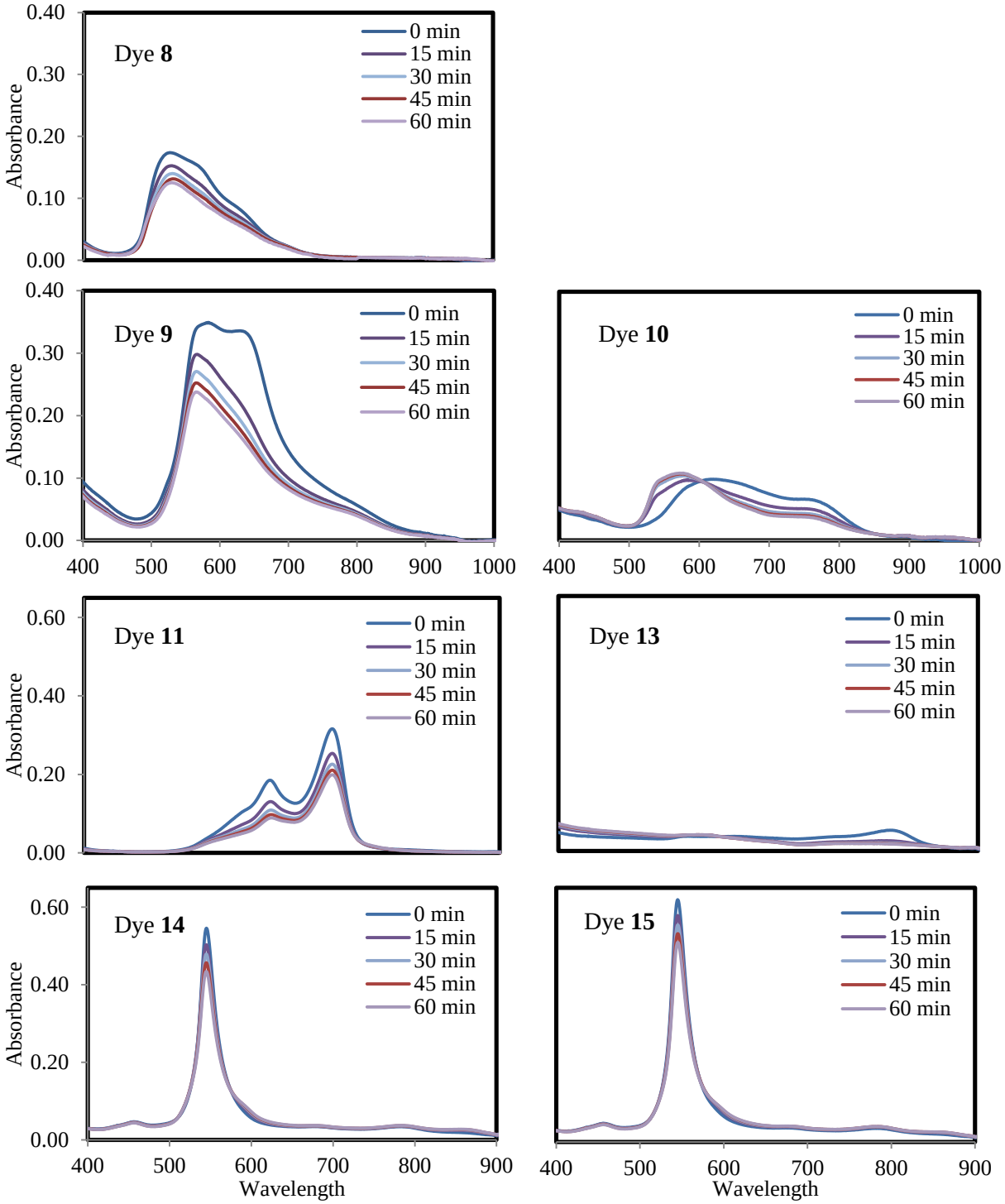

Figure 3.S10 Time course UV-vis absorption spectra of 10 μM cyanines **8-11**, **13-15** in 10 mM sodium phosphate buffer. The absorbance was recorded at intervals of 15 min up to 1 h.

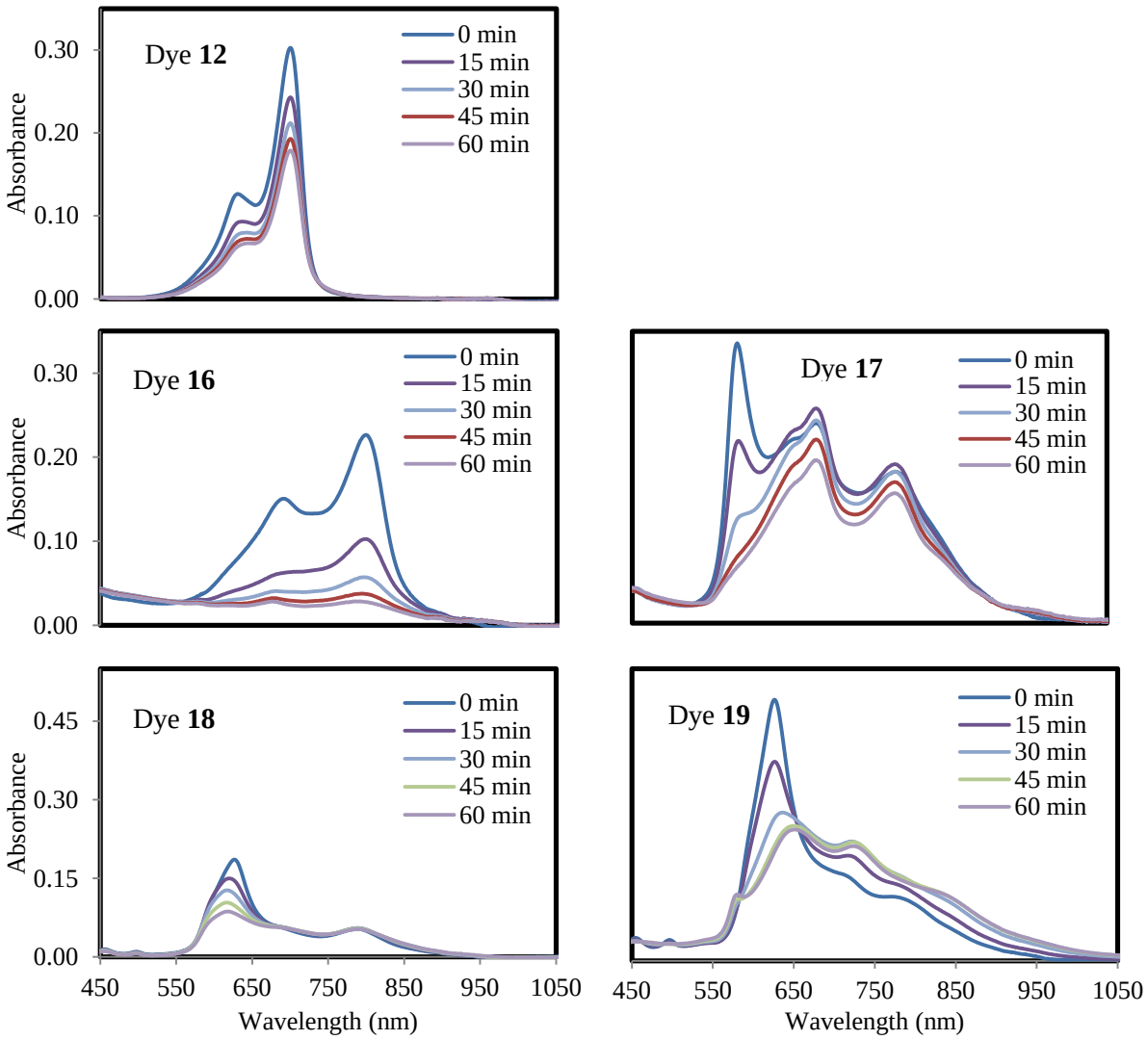

Figure 3.S11 Time course UV-vis absorption spectra of 10 µM cyanines **12**, **16-19** in 10 mM sodium phosphate buffer. The absorbance was recorded at intervals of 15 min up to 45 min or 1 h.

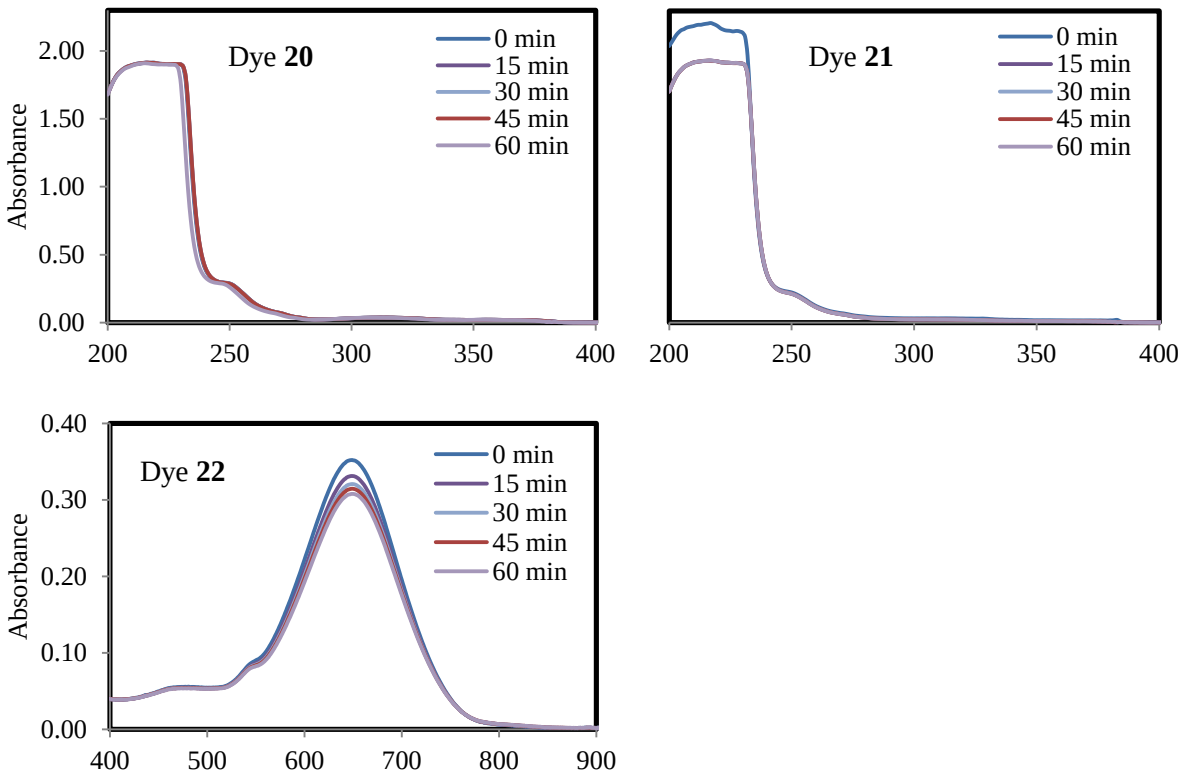

Figure 3.S12 Time course UV-vis absorption spectra of 10 μM cyanines **20-22** in 10 mM sodium phosphate buffer. The absorbance was recorded at intervals of 15 min up to 45 min or 1 h.

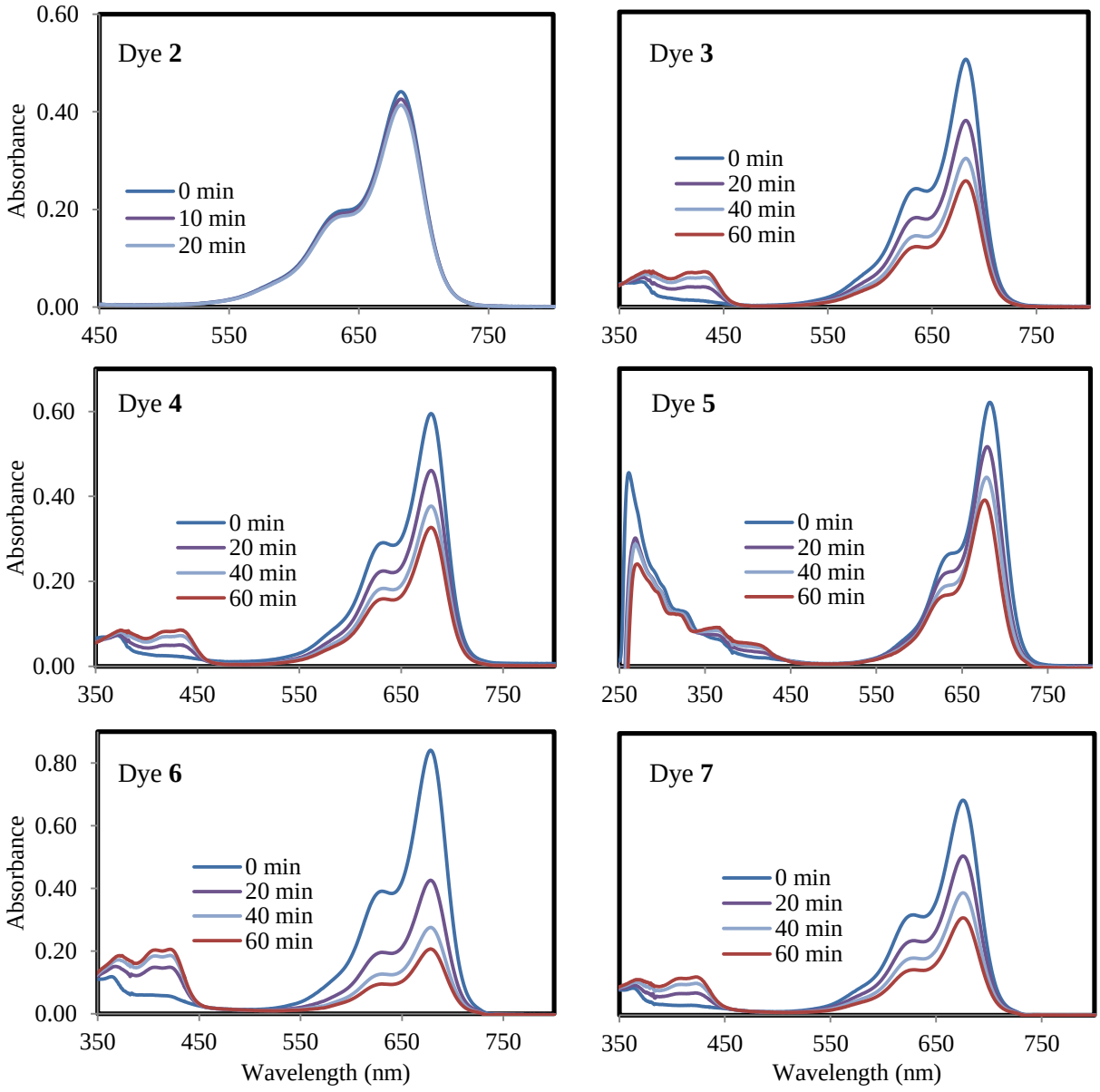

Figure 3.S13 Time course UV-visible absorption spectra of 10 μM cyanines **2-7** in DMSO. The absorbance was recorded at intervals of 10 or 20 min.

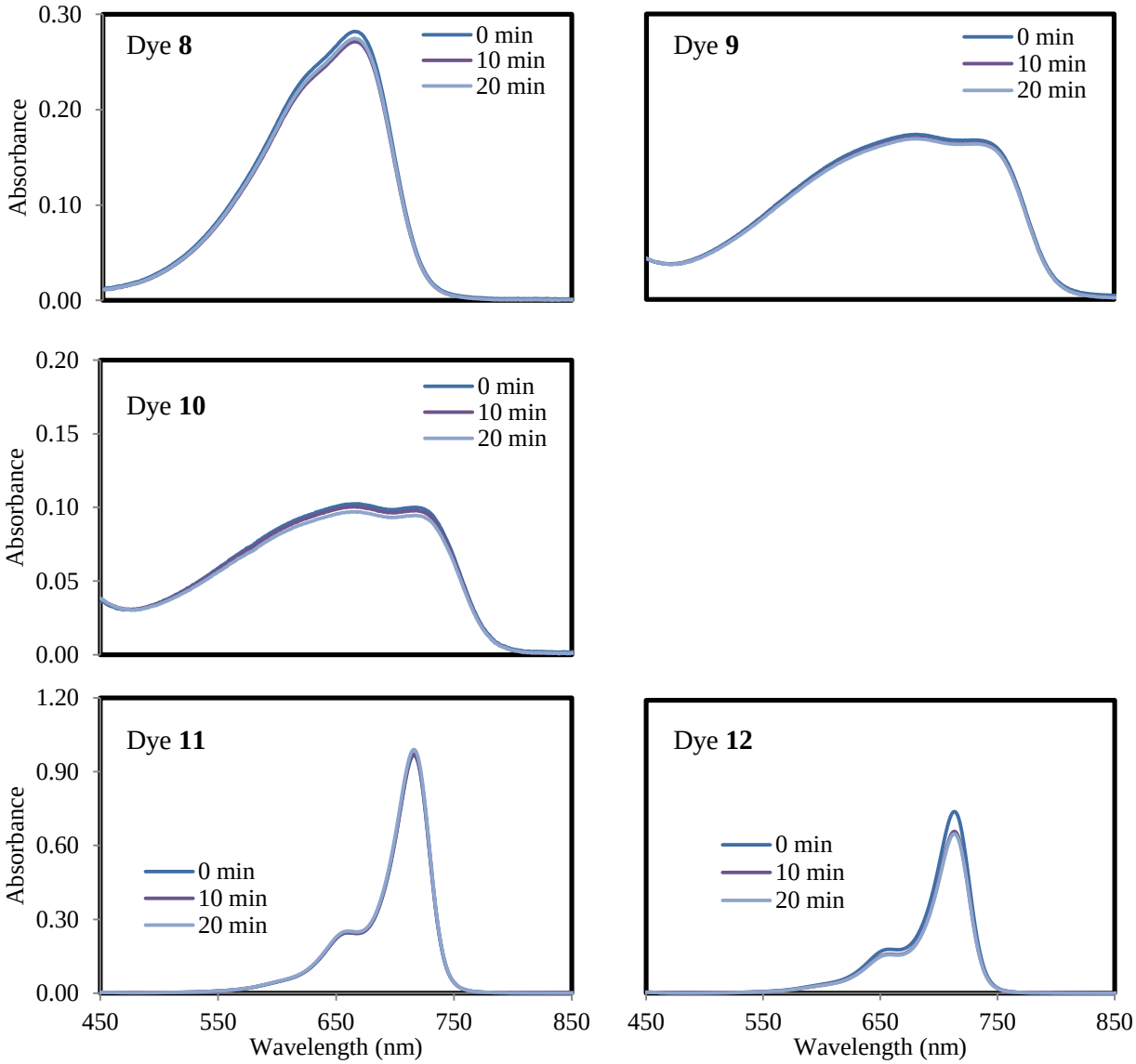

Figure 3.S14 Time course UV-visible absorption spectra of 10 μM cyanines **8-12** in DMSO. The absorbance was recorded at intervals of 10 min.

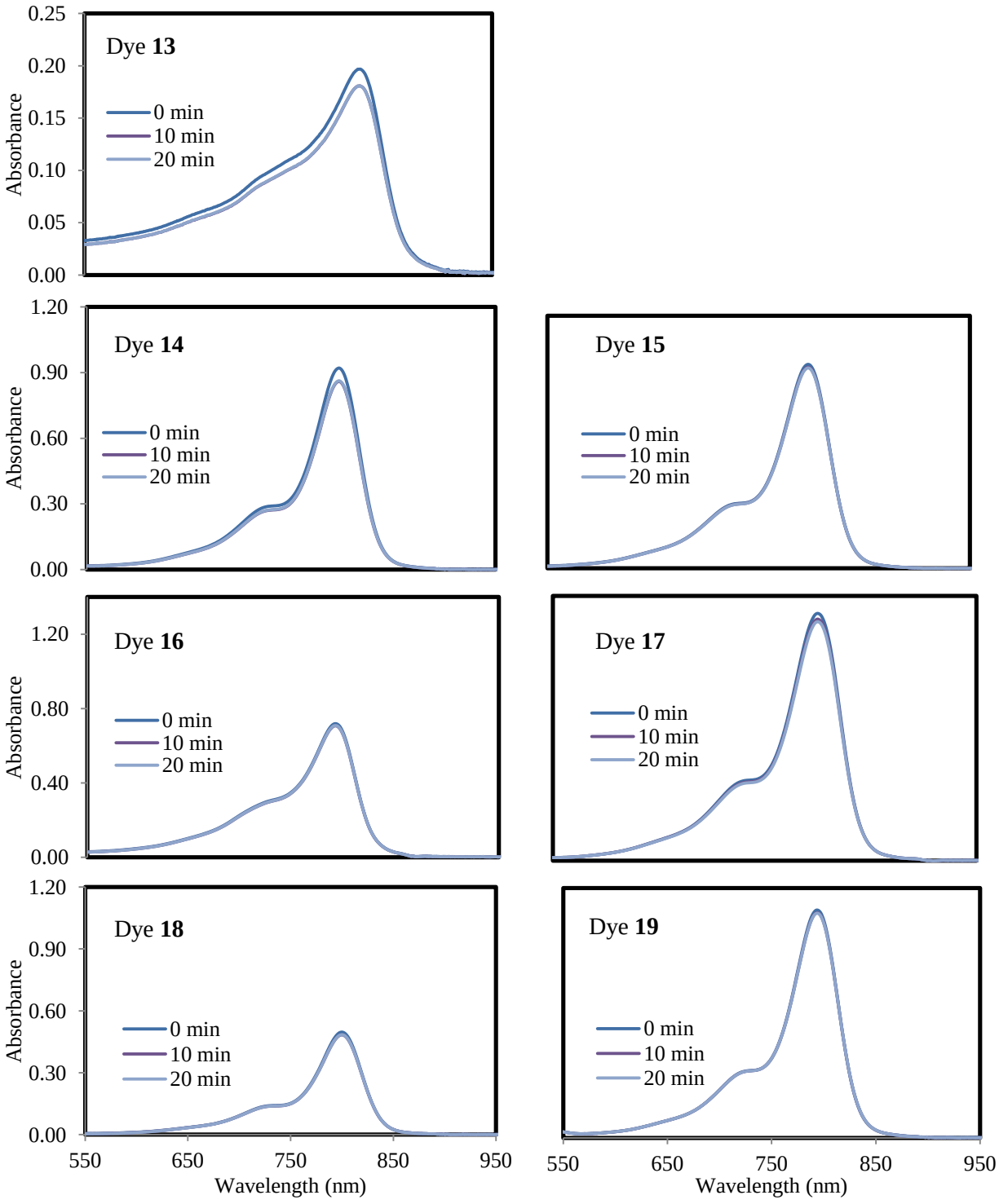

Figure 3.S15 Time course UV-visible absorption spectra of 10 μM cyanines **13-19** in DMSO. The absorbance was recorded at intervals of 10 or 20 min until the changes in absorbance were negligible.

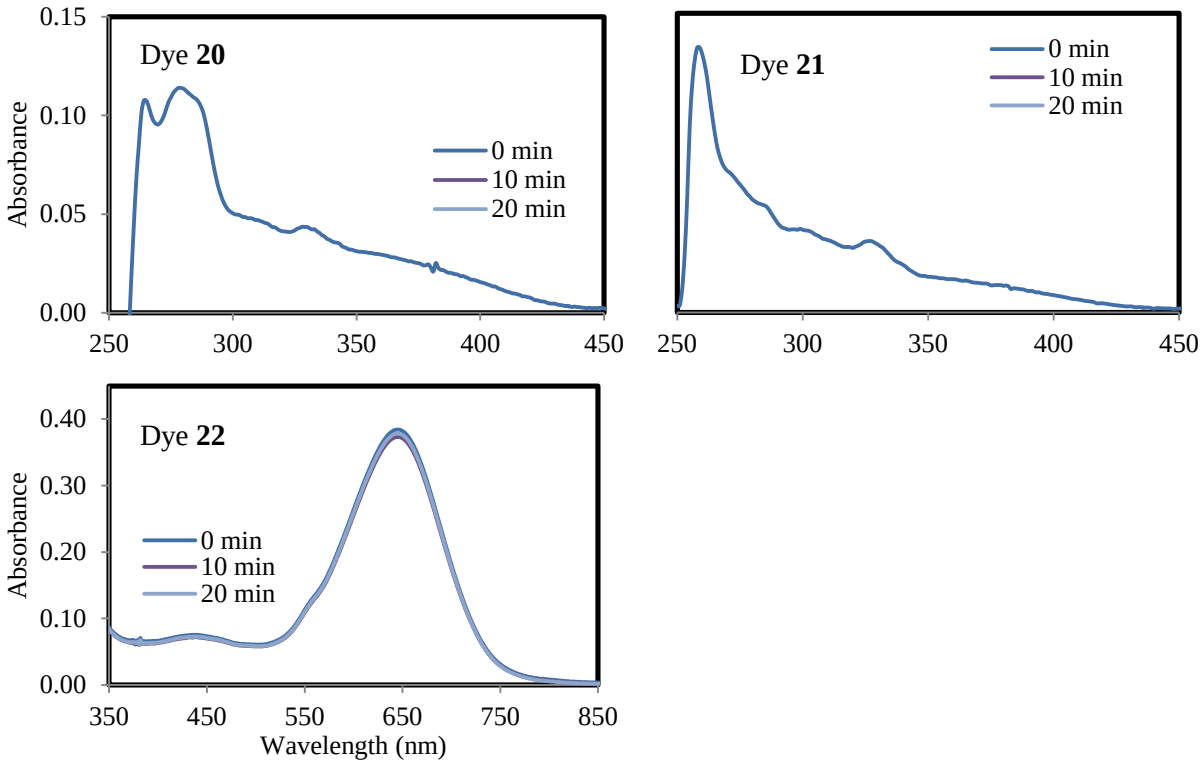

Figure 3.S16 Time course UV-visible absorption spectra of 10 μM cyanines **20-22** in DMSO. The absorbance was recorded at intervals of 10 or 20 min until the changes in absorbance were negligible.

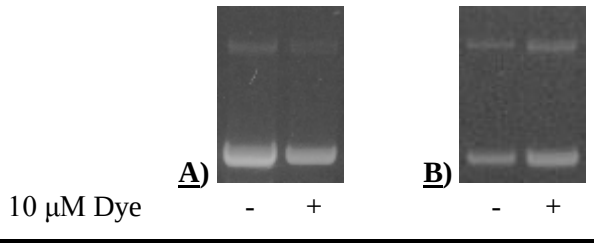

Figure 3.S17 Photographs of representative 1.5% non-denaturing agarose gels showing DNA thermal cleavage of 25 μM bp pUC19 plasmid DNA by 10 μM of **A) 23** and **B) 24**. Reactions were run in darkness for 24 h.

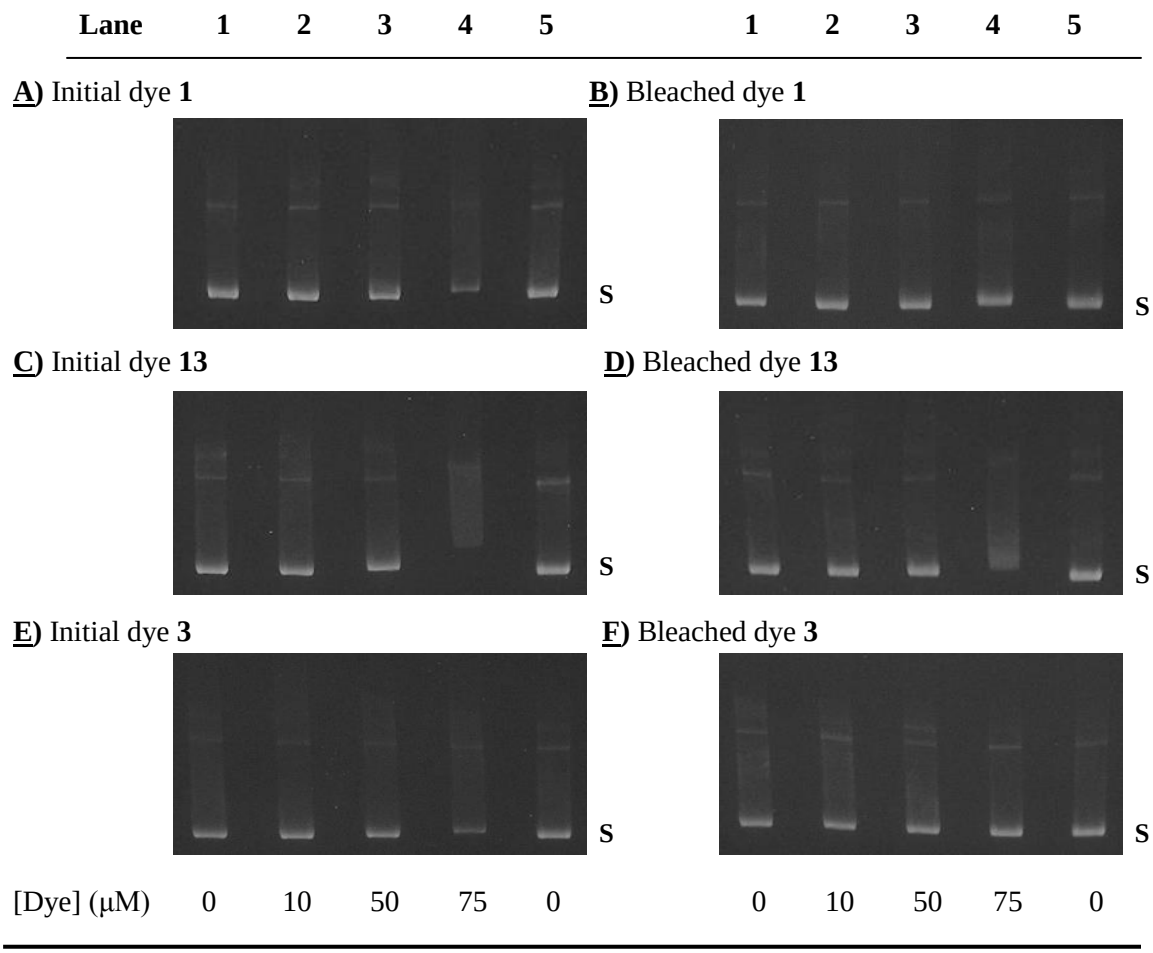

Figure 3.S18 Photographs of 1.7 % non-denaturing agarose gels showing ethidium replacement for initial **A) 1**, **C) 13**, **E) 3**, or bleached **B) 1**, **D) 13**, **F) 3** at 0, 10, 50, or 75 μM. Individual reaction was prepared in 10 mM sodium phosphate buffer (pH 7.0) and 25 μM bp pUC19 plasmid DNA and allowed to equilibrate for about 15 min. Gel electrophoresis lasted for around 3 h 30 min. The 1.7% non-denaturing agarose gels were stained in 0.5 μg/mL concentrated ethidium bromide buffer for 30 min and de-stained in 1× TAE for 10-15 min. Abbreviations: S = supercoiled.

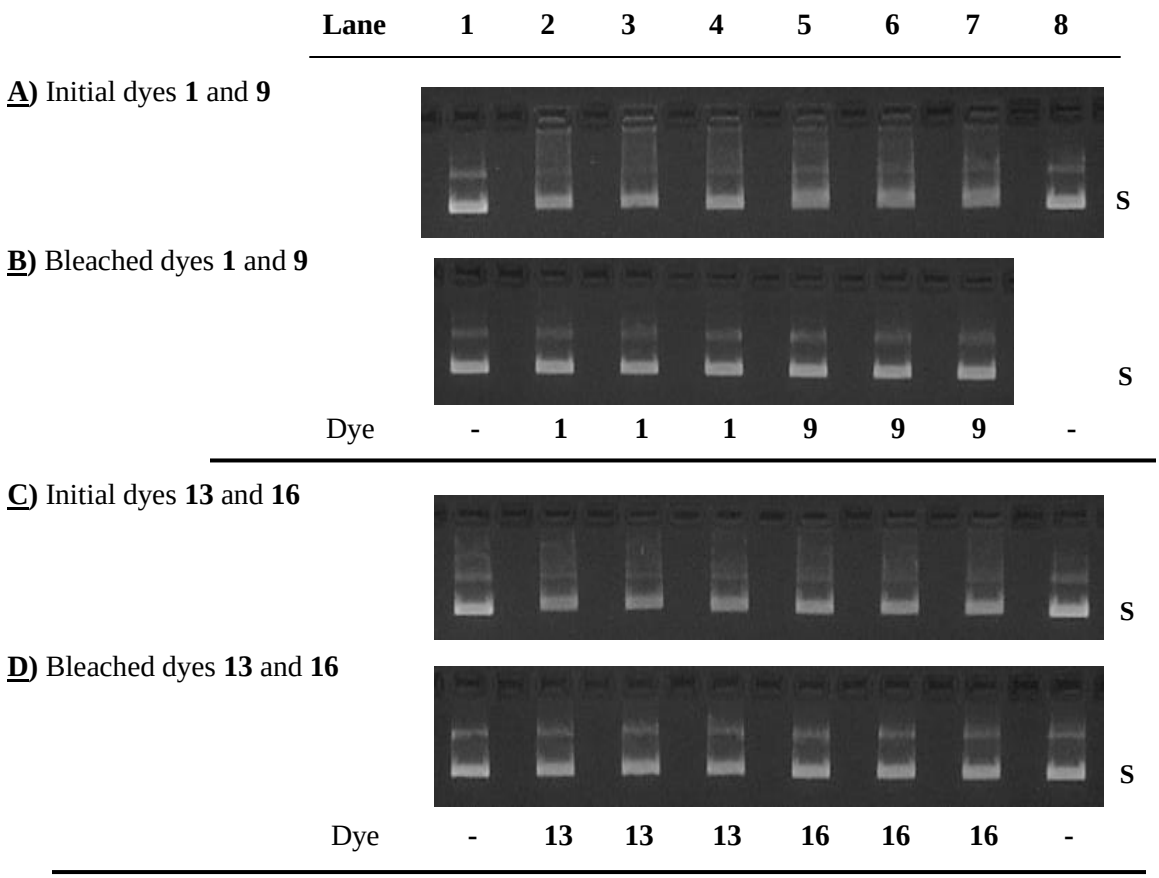

Figure 3.S19 Photographs of 1.7 % non-denaturing agarose gel showing ethidium replacement for initial dyes **A) 1** and **9**, **C) 13** and **16** and bleached dyes **B) 1** and **9**, **D) 13** and **16** at 50 μM. Reactions were run over three trials. Each sample consisting of 10 mM sodium phosphate buffer pH 7.0 and 25 μM bp pUC19 plasmid DNA in the presence of dye was allowed to equilibrate for about 15 min. Gel electrophoresis lasted for 30 min. The 1.7% non-denaturing agarose gels were stained in 0.5 μg/mL concentrated ethidium bromide buffer for 30 min and de-stained in 1× TAE for 10-15 min. Abbreviations: S = supercoiled.

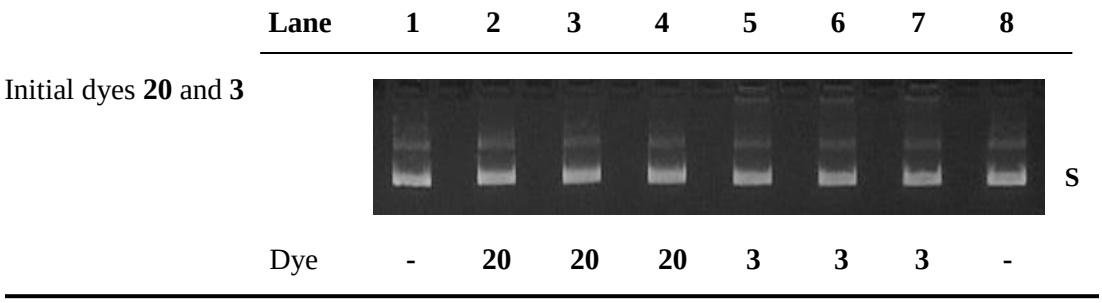

Figure 3.S20 Photographs of 1.7 % non-denaturing agarose gel showing ethidium replacement for initial dyes **20** and **13** at 50 μM. Each sample consisting of 10 mM sodium phosphate buffer (pH 7.0) and 25 μM bp pUC19 plasmid DNA in the presence of dye was allowed to equilibrate for about 15 min. Gel electrophoresis lasted for 30 min. The 1.7% non-denaturing agarose gels were stained in 0.5 μg/mL concentrated ethidium bromide buffer for 30 min and de-stained in 1× TAE for 10-15 min. Abbreviations: S = supercoiled.

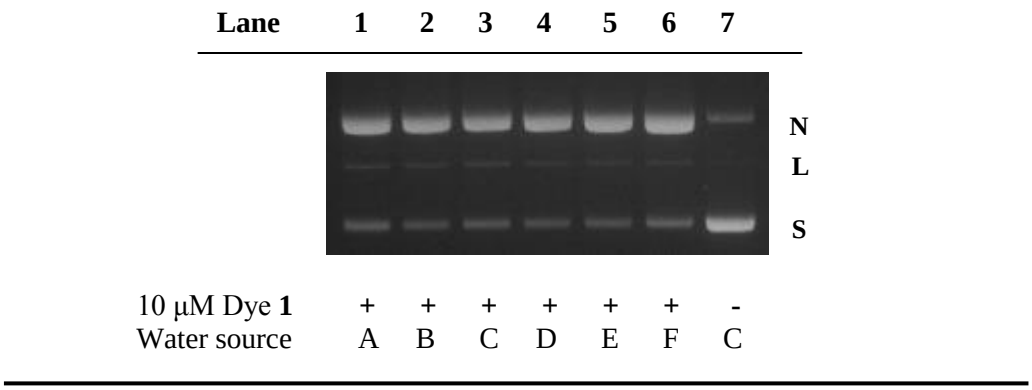

Figure 3.S21 Photographs of representative 1.5% non-denaturing agarose gels showing DNA thermal cleavage of 25 μM bp pUC19 plasmid DNA by 10 μM of **1**. Individual samples were prepared with 10 mM sodium phosphate buffer and 81.5% (v/v) of **A)** tap water, or water purified by **B)** Chelex 100 chelating ion exchange resin (Bio-Rad), **C)** Solution 2000 (Aqua solutions), **D)** PURELAB Classic DI (ELGA), **E)** Barnstead NANOpure Diamond (Thermo Scientific), and **F)** Milli-Q Advantage A10 (EMD Millipore) water purification systems. Reactions were run in darkness at 37℃ for 24 h. Abbreviations: N = nicked; L = linear; S = supercoiled.